The Pennsylvania State University

The Graduate School

College of Engineering

AN ULTRA-COMPACT AND LOW-POWER OVEN CONTROLLED CRYSTAL OSCILLATOR DESIGN FOR PRECISION-TIMING APPLICATIONS

A Dissertation in

Computer Science and Engineering

by

Jaehyun Lim

© 2009 Jaehyun Lim

Submitted in Partial Fulfillment
of the Requirements
for the Degree of

Doctor of Philosophy

August 2009

The dissertation of Jaehyun Lim was reviewed and approved* by the following:

Kyusun Choi
Assistant Professor of Computer Science and Engineering
Dissertation Advisor
Chair of Committee

Lee Coraor
Associate Professor of Computer Science and Engineering

Yuan Xie
Associate Professor of Computer Science and Engineering

Thomas Jackson
Robert E. Kirby Chair Professor of Electrical Engineering

John Mitchell
Professor of Electrical Engineering

Raj Acharya
Professor of Computer Science and Engineering
Head of the Department of Computer Science and Engineering

*Signatures are on file in the Graduate School

ABSTRACT

This thesis proposes and demonstrates an ultra-compact and low-power oven controlled crystal oscillator (OCXO) design for use in precision-timing applications. In the last decade, the rapid growth of wireless applications has led to an increasing demand for highly accurate and stable reference clock sources for data communication. Quartz crystal resonators are the most common devices used to generate frequencies in order to control and manage the systems. Among the various types of crystal oscillators, OCXOs have superior frequency stability. However, a typical OCXO package includes not only a metal block, but also multiple PCBs for the resonator, oscillator circuitry, and temperature sensitive components, the combination of which results in a large package size and a long warm-up time. An SC-cut crystal, which is considerably more expensive than an AT-cut crystal, is generally used as the resonator. In addition, power consumption of these OCXOs is very high. Despite the excellent frequency characteristics of OCXOs, these drawbacks prevent their use in small mobile or battery-powered devices.

To overcome the limitations of conventional OCXOs, we present a new design of miniature OCXO on a single CMOS chip. The object of this project is to design an ultra-compact and low-power precision OCXO. All the main components of an OCXO such as an oscillator, a temperature sensor, a heater, and temperature-control circuitry are integrated on a single CMOS chip. The OCXO package size can be reduced significantly with this design, since the resonator does not require a separate package and most of the circuitry is integrated on a single CMOS chip. Other characteristics such as power consumption and warm-up time are also improved.

Two different types of quartz resonators, an AT-cut Tab Mesa type quartz crystal and a frame enclosed resonator (FER) allowed the miniaturization of the OCXO structure. Neither of these two quartz resonator types requires a separate package inside the oven structure; therefore,

they can each be directly integrated with the custom-designed CMOS chip. The miniature OCXO achieved a frequency stability of ±0.35 ppm with an AT-cut Tab Mesa type quartz crystal in the temperature range of 0 °C to 60 °C. The maximum power consumption of this miniature OCXO was 1.2 W at start-up and 303 mW at steady state. The warm-up time to reach the steady state was 190 seconds. These results of the proposed design are better than or comparable to high-frequency commercial OCXOs. Polyimide flexible circuit boards and anisotropic conductive film bonding techniques were also investigated for further optimization.

TABLE OF CONTENTS

LIST OF FIGURES vii

LIST OF TABLES xi

ACKNOWLEDGMENTS xii

Chapter 1 Introduction 1

- 1.1 Crystal Oscillators 1
- 1.2 MEMS Resonators 5
- 1.3 Motivation 8
- 1.4 Thesis Overview 9

Chapter 2 Oven Controlled Crystal Oscillator Background 10

- 2.1 An Overview of the Oven Controlled Crystal Oscillator 10
- 2.2 Oven Temperature Control 11
  - 2.2.1 Temperature Sensor 13
  - 2.2.2 Heater 15
- 2.3 Performance Evaluation of OCXO 17
  - 2.3.1 Frequency Stability 17
  - 2.3.2 Warm-up Time and Power Consumption 18
  - 2.3.3 Cost 19
- 2.4 Previous Work 20

Chapter 3 Miniature OCXO Design on a CMOS Chip 26

- 3.1 Design of a One-chip Temperature-control Circuit 26
  - 3.1.1 Temperature Sensor 27
  - 3.1.2 On-chip Heater 33
  - 3.1.3 Temperature-control Circuit 35
  - 3.1.4 Quartz Crystal Resonators 38
    - 3.1.4.1 On-chip Quartz Crystal 38
    - 3.1.4.2 Frame Enclosed Resonator (FER) 43
    - 3.1.4.3 Conventional Quartz Crystal Package 47
- 3.2 IC Layout and PCB Design 48

Chapter 4 Experiment Results 50

- 4.1 Testing and Measurements 50
  - 4.1.1 Chip-scale OCXO with On-chip Resonator 50
  - 4.1.2 Chip-scale OCXO with FER 58

Chapter 5 Further Optimization 60

- 5.1 Cubic Compensation 60

5.2 Embedded Microprocessor and ADC 66
5.2.1 On-chip Microprocessor 67
5.2.2 Power Management Method for Low-power ADC.......................................71
5.3 Size Optimization 77
5.3.1 Polyimide Flexible Circuit Board 77
5.3.2 Anisotropic Conductive Film...79

Chapter 6 Conclusion...83

6.1 Summary 83
6.2 Future Work – Smart Clock Generating System...86
6.2.1 Frequency Compensation...87
6.2.2 Application and Operation Environment Adaptive System.........................89
6.2.3 Additional Functionalities..90
6.3 Cubic Compensation..91

Bibliography 92

Appendix A MOSIS Parametric Test Results for AMIS 0.5 µm CMOS Run 101

Appendix B MOSIS Parametric Test Results for TSMC 0.35 µm CMOS Run 107

Appendix C MOSIS Parametric Test Results for TSMC 0.18 µm CMOS Run 113

LIST OF FIGURES

Figure 1-1: f vs. T plot of an AT-cut quartz crystal resonator from -40 °C to 90 °C of ambient temperature. Note that the variation of the frequency also depends on the cut-angle of the crystal. [image courtesy of SaRonix] 2

Figure 1-2: Relative f vs. T characteristic curves of AT and SC cut crystals. 3

Figure 1-3: Plot showing various types of MEMS resonators and exponential growth in the frequency-Q product over time **[4]** 5

Figure 1-4: Image showing a MEMS resonator integrated with CMOS IC in a single package. [image from www.sitime.com] 6

Figure 1-5: Components inside a conventional OCXO package. 8

Figure 2-1: Block diagram of a typical OCXO oven. 11

Figure 2-2: Oven temperature controller. 11

Figure 2-3: Setting the oven temperature. 12

Figure 2-4: Typical RTD design. [image from www.omega.co.uk] 14

Figure 2-5: Kapton heater. [image from www.northeastflex.com] 16

Figure 2-6: OCXO oven structure with power transistors. 17

Figure 2-7: An example of an SC-cut quartz resonator frequency spectrum plot. 20

Figure 2-8: Quartz crystal resonator with thin film resistive heater deposited on its surface **[19]**. 21

Figure 2-9: Quartz crystal resonator on silicon substrate with direct-bonding technique **[22]**. 23

Figure 2-10: Schematic drawing of DOCXO **[25]**. 24

Figure 3-1: An inverter-type temperature sensor. 27

Figure 3-2: Expected sensor output from its modeling. 29

Figure 3-3: Temperature sensor test results. 30

Figure 3-4: Three different temperature sensor output measurements with same gate bias voltages. 31

Figure 3-5: CMOS PTAT temperature sensor. 32

Figure 3-6: PTAT sensor test results. 32

Figure 3-7: Heater array. 33

Figure 3-8: Heater measurement results. 34

Figure 3-9: Temperature-control circuit. 36

Figure 3-10: Control circuit Spice simulation results. 36

Figure 3-11: PID controller block diagram. 37

Figure 3-12: Spice simulation results with different control parameters. 38

Figure 3-13: (a) Illustration and (b) micrograph of the on-chip quartz resonator. 39

Figure 3-14: Spectrum analyzer plot from multiple core (155.52 MHz and 51 MHz) testing. 42

Figure 3-15: Fundamental and harmonic frequencies of the on-chip 100 MHz quartz crystal resonator. 42

Figure 3-16: Structure of the chip-on-crystal approach. 44

Figure 3-17: (a) Schematic of frame enclosed resonator (b) Fabricated frame enclosed resonator. 45

Figure 3-18: Stacked FER and CMOS OCXO chip (a) schematic (b) photo. 46

Figure 3-19: Fundamental and harmonic frequencies of 195.3 MHz FER with an OCXO chip. 47

Figure 3-20: Low-cost OCXO structure with a quartz resonator in HC49/U and a packaged temperature-control chip. 47

Figure 3-21: (a) Chip die photo (b) PCB and close-up of the chip inside the oven structure. 49

Figure 4-1: OCXO test boards. 51

Figure 4-2: The temperature sensor output plot with and without the temperature control. 52

Figure 4-3: The on-chip resonator frequency plot with and without the temperature control. 52

Figure 4-4: Heater control voltage and temperature sensor output during the temperature control process. 54

Figure 4-5: Warm-up time measurements at room temperature. 55

Figure 4-6: Femlab heat-transfer simulation plots. 56

Figure 4-7: Heat-transfer modeling of the miniature OCXO for (a) heat transfer through the mounting structure and (b) heat transfer through air. (This image is not to scale.) ...56

Figure 4-8: The FER frequency plot with and without temperature control.........................59

Figure 5-1: Flattening the f vs. T curve with cubic compensation technique. 61

Figure 5-2: f vs. T compensation in TCXO. 61

Figure 5-3: Schematic of the variable gain amplifier (VGA). 63

Figure 5-4: Block diagram of the cubic compensation voltage generator. 64

Figure 5-5: Voltage adder configuration using an operational amplifier..............................64

Figure 5-6: Core layout of the cubic compensation voltage generator. 65

Figure 5-7: Oscilloscope screen of the cubic compensation voltage generator output with different gain parameters. 66

Figure 5-8: Simple microprocessor architecture. 69

Figure 5-9: Layout of the microprocessor chip...70

Figure 5-10: Block diagram of the sampling frequency scaling power management method...73

Figure 5-11: Pulse width modulator for the frequency adaptive power management method...73

Figure 5-12: Layout of the power management circuitry with TIQ ADC. 74

Figure 5-13: Power management circuitry test results..75

Figure 5-14: Building a 3-D structure from 2-D circuitries using flexible circuit boards **[56]**. 78

Figure 5-15: Comparison of two test patterns printed with (a) laser printer and (b) phaser printer on polyimide flexible boards. 78

Figure 5-16: Schematic representation of an ACF bonding process....................................80

Figure 5-17: Photo of a flexible circuit sample ACF-bonded on chromium electrodes. 81

Figure 5-18: Miniaturizing an OCXO with a typical resonator by applying one-chip temperature control, flexible circuit, and ACF-bonding. 82

Figure 6-1: Frequency stability measurement plots of 100 MHz MEMS resonators. 85

Figure 6-2: Miniature OCXO with an on-chip microprocessor. 87

Figure 6-3: Quartz resonator f vs. T plot showing two different set temperature ranges....... 89

LIST OF TABLES

Table 1-1: Accuracy and Typical Application of Various Clock Generators. 7

Table 2-1: Temperature Sensor Comparison..15

Table 3-1: Required Amount of Current Through the Heater for Different Chip Temperatures...34

Table 3-2: Packaged Device with Crystal Mounted Outside the Package. 40

Table 3-3: Unpackaged Device with Crystal Mounted on Chip. 41

Table 4-1: Thermal Conductivity Values and Approximate Resonator Dimensions. 58

Table 5-1: Dual-port SRAM Based RISC Microprocessor Instructions. 71

Table 5-2: ADC Power Measurement Results with Sampling Frequency Scaling Method. 76

Table 5-3: ADC Power Measurement Results with and without Power Management Method. 76

Table 6-1: Comparison Table of the Miniature OCXO and Commercial OCXOs. 85

Table 6-2: Power Consumption Comparison at Different Miniature OCXO Set Temperatures...90

ACKNOWLEDGMENTS

Finishing this dissertation would not have been possible without help from numerous individuals and organizations. I want to take this opportunity to thank all who have supported me throughout the process.

My greatest thanks go to my family back in Korea, in particular my parents and my sister. They have supported and encouraged me throughout my entire education. I would also like to express my deepest gratitude to my wife Min Kyung, and my baby boy Brandon. I would not have achieved all that I have without their love and constant support during my academic career at Penn State. I am extremely fortunate to have them in my life.

I would like to thank all those who contributed to this work. Primarily, sincere appreciation is extended to my thesis advisor, Dr. Kyusun Choi, for his professional guidance and patience. I have been fortunate to work with Dr. Choi during both my M.S. and Ph.D. studies here at Penn State. I would also like to thank my committee members, Dr. Thomas Jackson, Dr. Lee Coraor, Dr. John Mitchell, and Dr. Yuan Xie, for supporting my efforts and for their valuable commentary and feedback. In particular, my thanks go to Dr. Jackson for the many insights he shared with me, his willingness to allow me access to necessary equipments, and his constant support of my research.

I must also thank Insoo Kim, Hyunsoo Kim, and Peter Cho who are my colleagues, collaborators, and most importantly, friends for their kindness and their assistance with my chip design and fabrication. I also owe a dept of gratitude to Dave Kenny at Pletronics; he provided me with both information and advice regarding quartz crystal devices. I would also like to thank all my Penn State friends for their kindness and collegiality.

I acknowledge the Pittsburgh Digital Greenhouse for providing funding for my graduate research through a grant from the Commonwealth of Pennsylvania Department of Community

and Economic Development. My thanks also go to the Department of Computer Science and Engineering at Penn State for supporting me as a graduate instructor during my doctoral studies.

Last, but by no means least, I am thankful to all the members of the Mixed Signal Chip Design Group for their friendship and advice.

Chapter 1

Introduction

This chapter introduces precise reference clock sources and discusses their importance. Various technologies used as clock sources, such as quartz resonators and MEMS resonators, are introduced. The motivation for this project is also discussed.

1.1 Crystal Oscillators

In the last decade, the rapid growth of wireless applications has led to increasing demand for highly accurate and stable reference clock sources for data communication. The applications for which wireless communication devices can be used include pagers, cordless phones, cellular phones, global positioning systems (GPS), and wireless local area networks (WLAN) transmitting either voice or data. All these systems require precise reference clocks. For example, the accuracy and speed of a GPS receiver in locking on to a satellite's signal heavily depends on whether the former's internal clock is synchronized to that of the satellite or not.

Quartz crystal resonators are the most commonly used devices for generating frequencies to control and manage the systems. A blank crystal wafer is obtained by cutting the quartz bar at specific angles to the various axes. The properties of a quartz crystal unit – the physical and electrical parameters of the resonator – depend strongly on the axis and cut angles of the crystal plate. There are various types of crystal cuts, such as AT, BT, and SC – cuts **[1]**. The most commonly used resonator type is an AT-cut crystal, which has a very high Q. SC-cut crystals are often used in high-stability devices due to the former's better stability, faster warm-up time, and wider operating temperature range. However, the SC-cut crystal is significantly more expensive

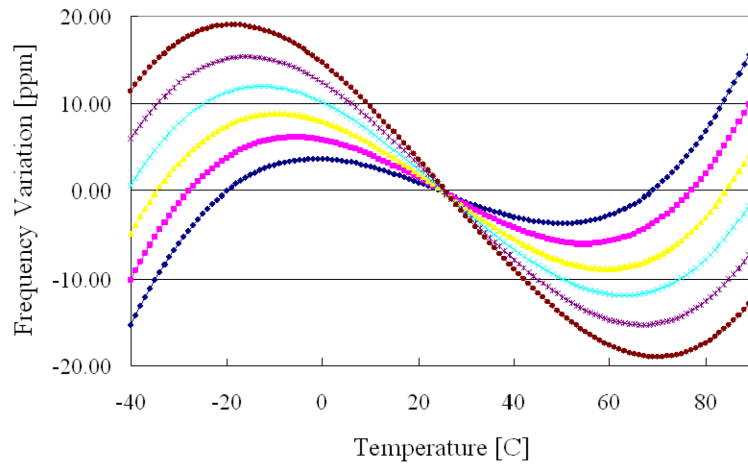

Figure 1-1: f vs. T plot of an AT-cut quartz crystal resonator from -40 °C to 90 °C of ambient temperature. Note that the variation of the frequency also depends on the cut-angle of the crystal. [image courtesy of SaRonix]

than that of a same frequency AT-cut crystal; this is because of difficulties in the manufacturing process of SC-cut crystals. Also, SC-cut crystals are larger than AT-cut crystals.

In spite of its abundance, diversity, and economical efficiency, a quartz resonator cannot be used alone as a high-precision reference clock since the frequency of a quartz resonator is affected by changes in ambient temperature. The frequency versus temperature (f vs. T) characteristic of an AT-cut quartz crystal is shown in **Figure 1-1**. The stability of the quartz crystal is a function of temperature and depends on the angle of the crystal cut. The f vs. T characteristic of a quartz crystal can be modeled as follows: where Δf is frequency stability, a_1 and a_3 are cut-angle dependent temperature coefficients, T_i is an inflection-point temperature, and T is an actual ambient temperature **[2]**.

$$\Delta f = a_3 \cdot (T - T_i)^3 + a_1 \cdot (T - T_i) \qquad \textbf{1.1}$$

Adding higher-order terms in **Eq. 1.1** can make the modeling more accurate.

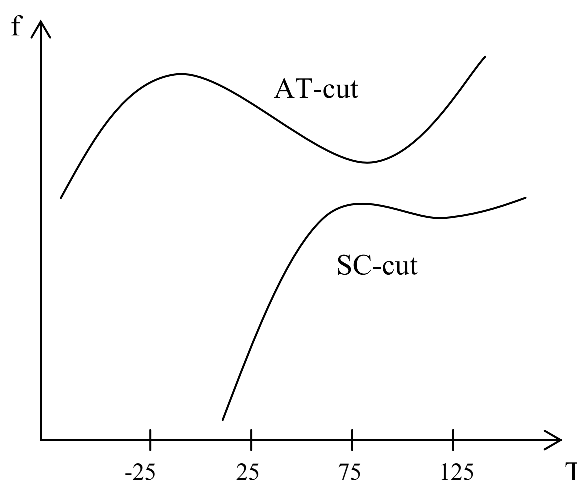

Figure 1-2: Relative f vs. T characteristic curves of AT and SC cut crystals.

Figure 1-2 shows the relative f vs. T characteristics of AT- and SC-cut crystals. The figure clearly shows that the curve of the SC-cut crystal is relatively flat at higher temperatures. This is the main reason why this type of crystal is used in many OCXOs. However, at lower temperatures its frequency falls off rapidly.

Currently, various kinds of technology are used to stabilize the resonator frequency of crystal oscillators: VCXO, TCXO, OCXO, etc **[3]**. Their basic characteristics are as follows:

- VCXO: Voltage Controlled Crystal Oscillator. The output frequency of a VCXO can change with a change of control voltage. The amount of frequency shift with a given voltage change is highly dependent on the oscillator circuit. VCXOs are widely used in telecommunications, phase locked loops, instrumentation, and other electronic equipment when a stable but electrically tunable oscillator is required. The VCXO typically employs a varactor diode to vary the frequency of oscillation by applying control voltage.

- TCXO: Temperature Compensated Crystal Oscillator. A TCXO adjusts its frequency for temperature variation. As a VCXO is an integral part of a TCXO, the general approach is to use a network of temperature sensors designed to appropriately bias the voltage control of the VCXO for a range of temperatures. The correction voltage is usually applied to a varactor diode in the crystal circuit so that the crystal frequency can be varied by a small amount.
- OCXO: Oven Controlled Crystal Oscillator. An OCXO offers higher stability and better phase noise specification than other crystal oscillators do. The crystal and other temperature-sensitive components are in a stable oven, which is adjusted to the temperature at which the crystal's frequency change is the smallest over the temperature range of the oven. Additional circuitry is required to control the oven temperature.
- MCXO: Microcomputer Compensated Crystal Oscillator. An MCXO uses a digital technique to observe the frequency drift, and compensates for this drift through digital-to-analog conversion to a tuning port in the circuit. The stability of an MCXO is generally better than that of any TCXO, but worse than that of any OCXO. In addition, the MCXO has a frequency-jumping problem.
- DCXO: Digitally Compensated Crystal Oscillator. A DCXO is a temperature-compensated oscillator that has digital compensation electronics. It offers greater frequency stability than the TCXO over a range of temperatures. However, it also has a frequency-jumping problem.

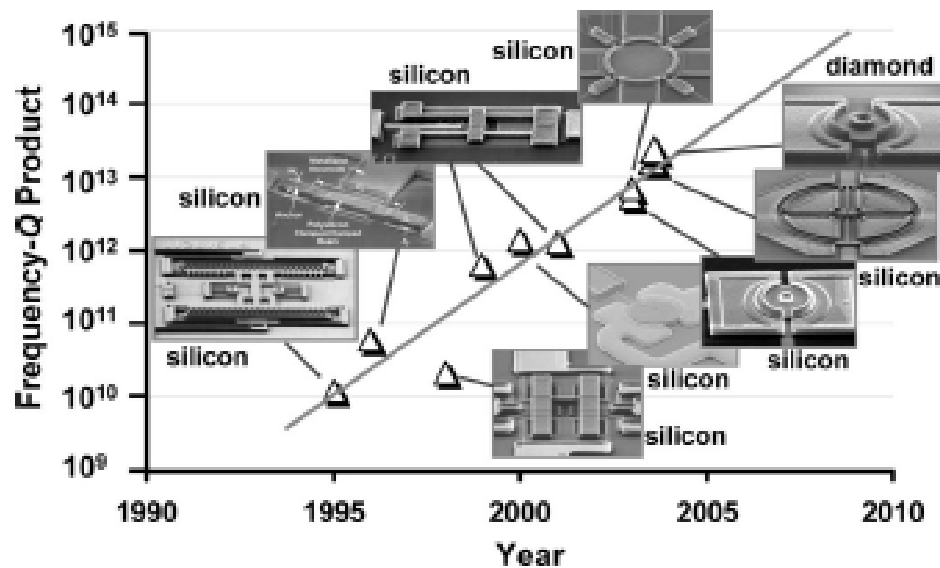

Figure 1-3: Plot showing various types of MEMS resonators and exponential growth in the frequency-Q product over time **[4]**.

1.2 MEMS Resonators

While quartz crystals have provided very accurate frequency references in timing and frequency-control systems over the past few decades, silicon micro electro mechanical systems (MEMS) technology is now able to provide reliable clock sources, as shown in **Figure 1-3 [4]**. Although quartz crystals provide good frequency selection and stability, they are generally large and difficult to batch process. Further, it is challenge to integrate a quartz crystal on a chip. In addition, unlike silicon MEMS resonators, quartz crystals become more expensive and perform worse when they are squeezed into smaller packages. These drawbacks, and the limitations they impose, are becoming more apparent in modern products. A MEMS resonator can overcome these drawbacks of quartz. This is because it is fabricated on top of silicon wafer with a standard CMOS process and materials that enable thinner, cheaper, and lower power consumption. A

complete MEMS resonator is typically a few tenths of a millimeter across; this is about a hundred times smaller than a quartz crystal. As newer CMOS technologies scale down in size, MEMS resonators can be scaled as well.

MEMS resonators are manufactured using batch-processing semiconductor technologies so that the resonators can be encapsulated at wafer level. This eliminates the need for further hermetic packaging to protect the resonator; thus manufacturing costs are reduced and a higher level of integration can be achieved **[5]**. Another significant advantage of MEMS resonators is that they are extremely tough with the highest performance ratings for shock and vibration. **Figure 1-4** illustrates a MEMS resonator integrated with a CMOS IC in a single package.

However, some issues and obstacles remain to be addressed. One of the biggest challenges in using MEMS resonators is the issue of temperature stability. The temperature coefficient of a MEMS resonator normally ranges from 20 ppm/°C to 40 ppm/°C, a much wider

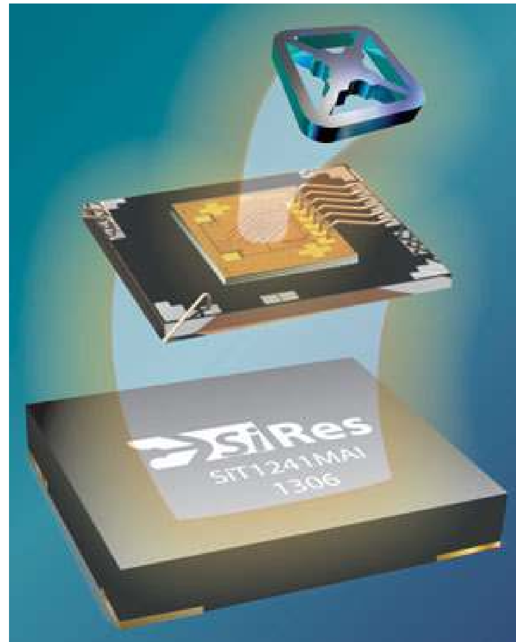

Figure 1-4: Image showing a MEMS resonator integrated with CMOS IC in a single package. [image from www.sitime.com]

range than that of quartz materials. However, the linearity of the temperature dependency of a MEMS resonator makes temperature compensation easy, and the frequency can be stabilized at less than ±5 ppm, ranging from -40 °C to 85 °C **[6]**.

The lower quality factor (Q factor) of the MEMS resonator compared to quartz resonators is another problem. A higher Q factor results in better frequency stability. Quartz crystals have a very high Q factor of 50,000 to 250,000, while MEMS resonators have a Q factor of approximately 80,000. This means that MEMS resonators are more susceptible to aging error in 10's to 100's ppm per year. **Table 1-1** summarizes the relative accuracy and typical applications of various clock sources.

Table 1-1: Accuracy and Typical Application of Various Clock Generators.

Clock Generator Type	Accuracy	Applications
Crystal oscillator (XO)	10 ~ 100 ppm	Computer timing, consumer electronics
Temperature compensated crystal oscillator (TCXO)	0.5 ~ 5 ppm	Mobile phones, GPS satellite navigation
Microcomputer compensated crystal oscillator (MCXO)	0.1 ~ 1 ppm	Spread spectrum system clock
Oven controlled crystal oscillator (OCXO)	~ 0.1 ppm	Measurement device, navigation system clock, frequency standard
MEMS oscillator	5 ~ 200 ppm	Consumer electronics, computer timing, USB devices

1.3 Motivation

The frequency stability of OCXOs is superior to that of other crystal oscillators. They are very popular in synchronous optical networking (SONET) and the measurement equipment such as frequency counters, spectrum analyzers, network analyzers, etc. However, in a typical OCXO package, in addition to a metal enclosure, there are multiple printed circuit boards (PCBs) for the resonator, oscillator circuitry, and temperature-sensitive components that result in a large package size and long warm-up time [**Figure 1-5**]. An SC-cut crystal, which is much more expensive than an AT-cut crystal, is generally used for a resonator. In addition, power consumption of these OCXOs is very high. Despite their excellent frequency characteristics, OCXOs are prevented by these drawbacks from being used for small mobile or battery-powered devices.

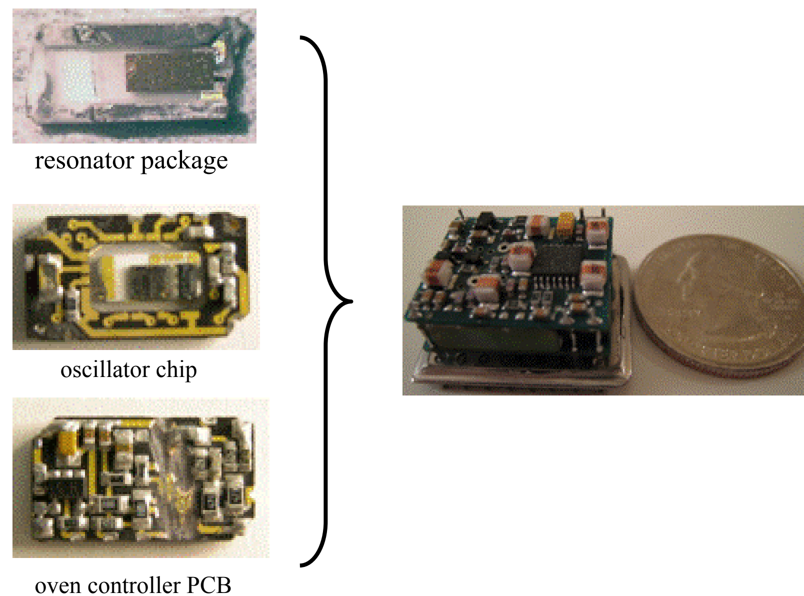

Figure 1-5: Components inside a conventional OCXO package.

To overcome the limitations of conventional OCXOs, we present a new design of miniature OCXOs on a single CMOS chip. The object of this project is to design an ultra-compact and low-power precision OCXO. All the main components of an OCXO, such as an oscillator, temperature sensor, heater, and temperature-control circuitry, are integrated on a single CMOS chip. Three different types of quartz resonators are used: an AT-cut Tab Mesa type quartz crystal, frame enclosed resonator, and conventional AT-cut quartz in an HC49/U package. The OCXO package size can be reduced significantly with this design, since the resonator does not require a separate package and most of the circuitry is integrated on a single CMOS chip. Other characteristics such as power consumption and warm-up time can also be improved.

1.4 Thesis Overview

In Chapter 2, the general concepts of OCXO, architecture, components, implementation, and methods to evaluate its performance are presented. Other related previous works are also discussed. In Chapter 3, the design of the miniature OCXO is presented as well as details of each component and its specifications. The experiments and test methods are described in Chapter 4, which also discusses the performance of the miniature OCXO in terms of frequency stability, power consumption, and warm-up time. Chapter 5 focuses on additional works conducted with a view to further optimizing performance. Evaluation of the miniature OCXO performance and discussions about cost and size reduction are presented in Chapter 6. Comparisons between other commercial OCXOs and MEMS oscillators are also shown. In addition, future research plans are described.

Chapter 2

Oven Controlled Crystal Oscillator Background

In this chapter, the general concepts and background of OCXOs, OCXO architecture, implementation, and methods for evaluating its performance are presented. Previous works related to OCXOs are also discussed.

2.1 An Overview of the Oven Controlled Crystal Oscillator

The key to an effective OCXO performance is to maintain the crystal and other oscillator components at a constant temperature as the outside ambient temperature changes. If a basic crystal oscillator or TCXO is to meet very high stability requirements, the crystal and critical circuits may be temperature controlled inside a package by a structure called an oven.

Figure 2-1 shows a block diagram of a typical OCXO oven structure. Its main components are an oscillator, crystal resonator, temperature sensor, controller circuitry, and heat source. Usually, thermistors are used as the temperature-sensing device. The thermistors sense an ambient temperature variation by a change to a slightly different resistance value. The controller circuitry consists of differential op-amps and other passive components, and it controls the amount of power generated in the heat source. The heat source is usually either a power transistor or a power resistor.

The following sections describe in greater detail the oven controller circuitry in a typical OCXO and some techniques to improve its performance and characteristics.

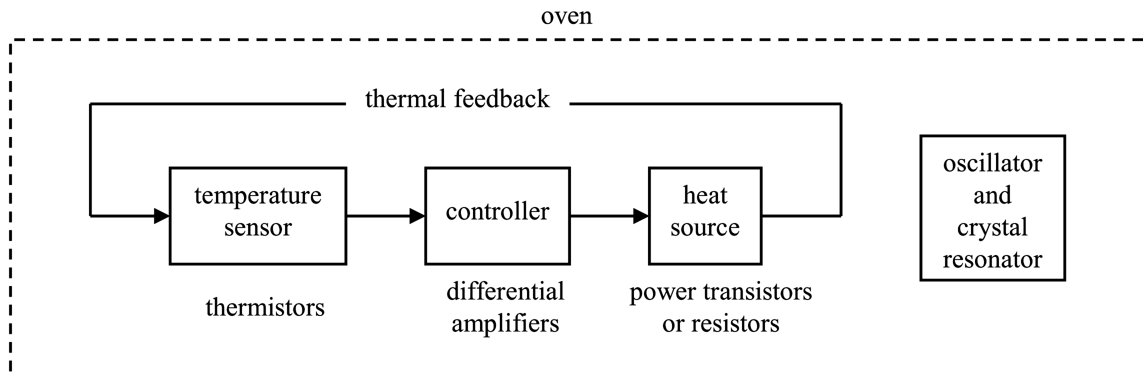

Figure 2-1: Block diagram of a typical OCXO oven.

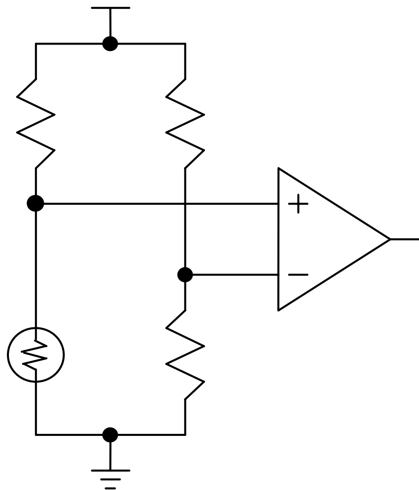

Figure 2-2: Oven temperature controller.

2.2 Oven Temperature Control

The most cost-efficient way to keep a crystal resonator at a constant temperature in an oscillator assembly is not heating and cooling it, but raising its temperature above any expected ambient temperature. **Figure 2-2** shows a simplified schematic of an oven controller as used in an OCXO **[7]**. At the lower left is a thermistor, a passive device that exhibits a resistance curve

inversely proportional to its temperature. This resistor and thermistor bridge senses the temperature variation of the oven, and the output of this circuit drives a heater.

Setting the oven temperature is critical to minimize the effect of ambient temperature change. As shown in **Figure 2-3**, if the oven temperature were set to point (1), and a change in ambient temperature caused a change in oven temperature from A to B, there would be a frequency change of magnitude X. However, if the oven temperature were set to the upper turning point (2), an equal amount of temperature change C to D would result in a significantly reduced change in frequency.

If ambient temperatures exceed the oven set point, the oven temperature will rise as well. The controller will then try to decrease the temperature of the oven. However, without any cooling mechanism, this cannot be done. Even if the oven controller shuts down the main heater completely, heat is still added by the oscillator circuitry. The heat generated by the oscillator is very small compared to that generated by the heater, but it is still sufficient to cause the heater to

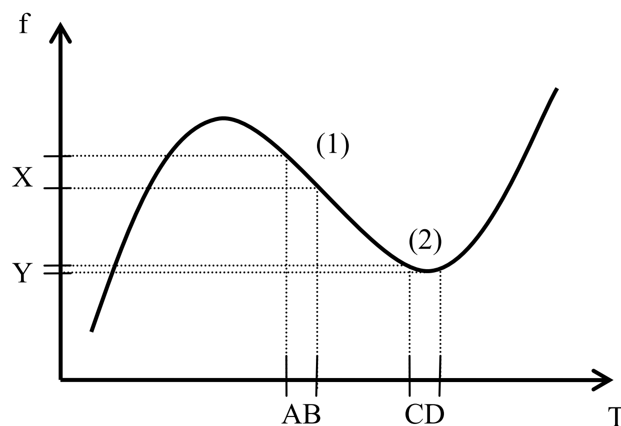

Figure 2-3: Setting the oven temperature.

shut down even before ambient temperatures reach the oven set point. Thus, the oven set point should be a few degrees higher than the highest expected ambient temperature.

A lower-most limit for the ambient temperature should also be anticipated. As the ambient temperature drops, more and more power is required to keep the oven warm; hence, there will be a point at which the power required to keep the oven at the set point will be higher than the power limit of the heater. This limit also keeps the heater circuit from being damaged by a constant and huge amount of power draw.

The following sections describe in detail the temperature sensor and heater and the interaction between them.

2.2.1 Temperature Sensor

The most common temperature-sensing devices are thermocouples, resistance temperature detectors (RTD), thermistors, and integrated circuit (IC) sensors **[8]**. The thermocouple converts temperature difference from two different metals into a voltage difference. Its main advantages are low cost, wide operating temperature range, simple structure, and no self-heating. However, it produces small output voltages that limit its accuracy, and it cannot be scaled down sufficiently to be integrated with ICs. Thermocouples are widely used for measuring gas temperature and measuring the temperature inside a vacuum or pressure chamber, as well as for many other industrial processes in harsh environments.

Resistance temperature detectors (RTD) employ a specific property of metals in order to operate; that is, they use the fact that the electrical resistance of metals increases at about 0.3 %/°C over a wide temperature range **[9, 10]**. To obtain a significant amount of resistance, the thin-film metal wire is patterned on a substrate, as shown in **Figure 2-4**. While almost any kind of metal can be used for a RTD, platinum is the most widely used since it is stable over a wide

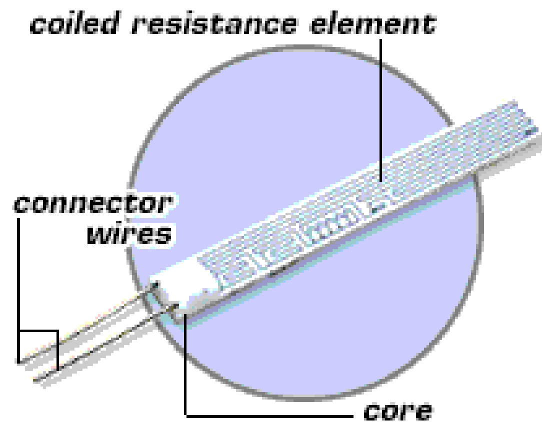

Figure 2-4: Typical RTD design. [image from www.omega.co.uk]

temperature range and it can be refined to high purity level. The RTD is the most accurate temperature-sensing device. It is capable of resolving temperature changes to at least 0.001 °C over a temperature range of -200 °C to 400 °C. Its disadvantages are that it is expensive and cannot be integrated with ICs.

The thermistor is a type of resistor made from ceramic or polymer whose resistance normally decreases with increasing temperature. If a resistance curve is inversely proportional to its temperature, the thermistor is called a negative temperature coefficient (NTC) device. If the opposite is the case, the thermistor is said to be a positive temperature coefficient (PTC) device. The thermistor is highly sensitive to temperatures, a property that makes it easy to measure temperature changes. However, relatively poor linearity limits its useful temperature span to about 100 °C. The small form factor of the thermistor, though, is another of its most important advantages. Thermistors are used inside many devices including temperature-sensing units, and they can easily be integrated with ICs. Also, the controlling resistance and thermal properties of thermistor can be achieved easily by the fabrication process **[11, 12]**. In addition, a thermistor is usually used as the temperature-sensing device inside most OCXO packages.

Various IC temperature-sensor designs are available **[13–15]**. As the I-V characteristics of semiconductor devices vary greatly with temperature, integrating temperature-sensing circuitry on silicon is an effective method for achieving a low-power and high-speed operation. A proportional-to-absolute-temperature (PTAT) circuit is the best candidate for a fully integrated temperature sensor with a linear temperature characteristic **[16]**. Its operation principle is based on the phenomenon that the voltage difference between two transistors that have different sizes but the same amount of current conduction is proportional to absolute temperature. The on-chip temperature sensor embedded within an IC is an efficient device for low-power and high-speed temperature management. **Table 2-1** summarizes the comparisons among different temperature-sensing techniques described above.

Table 2-1: Temperature Sensor Comparison.

Type	Cost	Linearity	Temperature Range	Integration with IC
Thermocouple	low	bad	wide	no
RTD	high	good	wide	no
Thermistor	low	bad	~ 100 °C	yes
IC sensor	low	good	~ 150 °C	yes

2.2.2 Heater

Resistors or power transistors can be used as the heat source **[17]**. A resistor heat source is generally formed by wrapping resistance wire around the oven structure. In general, nichrome wire or a flexible heater such as a Kapton heater shown in **Figure 2-5** is used. These materials are wound around the oven or crystal package to form the resistor heat source.

Another common device for the heating element is a power transistor. Advantages of power transistor as a heat source include ease of manufacture and power that is proportional to

the current rather than the square of the current. Also, most of the power is dissipated in the heater rather than in the control amplifier, a feature that improves power efficiency. **Figure 2-6** is an example of a typical OCXO with a metal oven block and power transistor heaters. Two power transistors that are controlled by the circuitry on the same PCB are the heat source. The heat generated from the power transistors is then transferred through the thermal contact to the metal block surrounding a crystal resonator package that eventually heat up the crystal resonator.

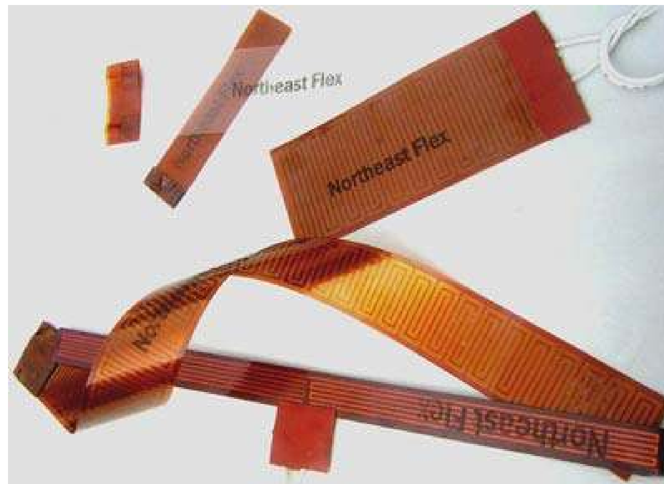

Figure 2-5: Kapton heater. [image from www.northeastflex.com]

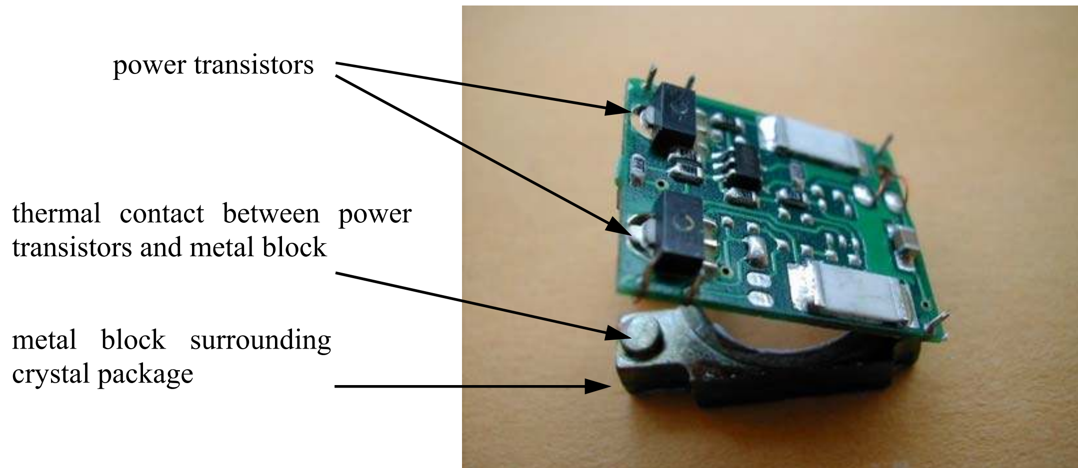

Figure 2-6: OCXO oven structure with power transistors.

2.3 Performance Evaluation of OCXO

Various factors should be taken into account when evaluating an OCXO. The most important factor is frequency stability, which can be categorized into short-term and long-term stability. Closely related to warm-up time and package size, level of power consumption is another key factor. Cost should also be considered for the device's marketability. This section describes these factors in greater detail.

2.3.1 Frequency Stability

Short-term stability is usually caused by changes in components due to circuit heating, temperature fluctuations, warm-up, mechanical shock, and vibration, and so forth. Generally time periods here are minutes to an hour. Electrical noise caused by the amplifier, power supply, and circuit components, and thermal noise generated in the resistors, together with mechanical factors can cause even shorter-term frequency fluctuation in periods consisting of a few seconds down to

microsecond intervals. This type of noise is called phase noise; it is measured in a given bandwidth at some specified frequency away from the main carrier. Low phase noise is a critical factor in both RF and synchronous digital systems, since timing uncertainty affects system performance by, for example, increasing the required channel separation in RF systems, and reducing timing margins in digital systems.

Long-term stability is caused by component aging due to electrical, thermal, physical, and chemical changes in components over a relatively long time period. Some of the most common causes are internal contamination, crystal surface changes, wire fatigue, out gassing of the materials, thermal effects, mounting stress, and over-driving the crystal **[3, 18]**. This frequency drift is generally permanent and can be compensated for by readjusting circuit parameters either manually or automatically. Typical aging figures for crystal resonators are between 0.1 ppm to 5.0 ppm per year.

An OCXO exhibits superior performance in terms of frequency stability. The frequency stability for a typical OCXO ranges from ±0.5 ppm to ±0.01 ppm over an operating temperature range of -20 °C to 75 °C, while that of a typical TCXO ranges from ±1 ppm to ±0.1 ppm.

2.3.2 Warm-up Time and Power Consumption

Power consumption is also an important performance factor. Typical OCXOs have power requirements that range from less than 1 W to more than 10 W. Maximum current draw is experienced during initial turn on and operation at low ambient temperatures. At room temperature, once the oven has warmed up, the power draw drops to some lower steady-state value.

Another performance issue is the warm-up time required for the oven. Because of the mass of the oven and the finite amount of power used to heat it, there will be some delay after

initial power up until the frequency is stabilized. The warm-up time of an oscillator is a function of the thermal properties of the resonator, the oscillator circuit and oven construction, the input power, and the oscillator's temperature prior to turn on **[18]**. The typical warm-up time of OCXOs ranges from 3 minutes to 10 minutes.

Power consumption and warm-up time are both closely related to the size of the entire OCXO package. A bulky package enclosing a separate vacuum-sealed crystal soldered on a PCB with discrete components and a metal block yields ample current, but also necessitates a long time to heat the entire structure to the certain temperature. Although, reducing the size of the entire structure can be a solution to these drawbacks, there are tradeoffs. For instance, making the oven smaller in order to effect a quicker warm-up will reduce ambient frequency stability, as the smaller mass is more responsive to ambient temperature fluctuations. However, making the oven larger for better frequency stability will raise the amount of power required to maintain oven temperature.

2.3.3 Cost

OCXOs are generally much more expensive than other crystal oscillators **[3]**. One of the main reasons is the high manufacturing cost of SC-cut quartz resonators. Since the SC resonator cut is a double rotation, the cutting operation is labor-intensive and difficult to control. Moreover, cut-angle tolerance for SC-cut resonators is much tighter than AT-cut resonators, causing a lower yield. The high sensitivity of SC-cut resonators to pressure also increases their manufacturing cost. Unlike AT-cut resonators, most SC-cut resonators require vacuum sealing to prevent Q degradation due to pressure. This can be done with coldweld or glass seal, both of which are expensive packages. Some other reasons include the extra calibration process and additional circuitry in oscillator. Each OCXO needs to be calibrated either automatically or manually before

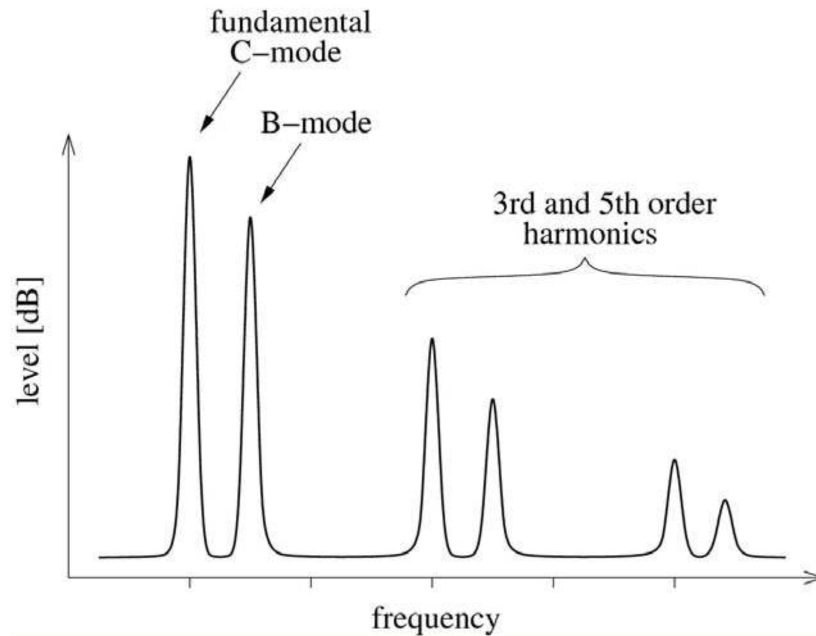

Figure 2-7: An example of an SC-cut quartz resonator frequency spectrum plot.

it is enclosed in the final package. Further, the spurious mode (B-mode) in the SC-cut resonator, that is almost as strong as its fundamental mode (C-mode) and 10% higher in frequency than the fundamental mode, must be trapped to prevent the oscillator from running on the wrong frequency. This requires extra circuitry that, in turn, raises costs. A frequency spectrum example of an SC-cut quartz resonator showing its fundamental C-mode, B-mode and their harmonics is shown in **Figure 2-7**.

2.4 Previous Work

Many studies have been published on improving OCXOs in terms of frequency stability, power consumption, packaging, and so on. To reduce the warm-up time and package size of OCXOs, the directly heated resonator (DHR) technology was introduced and studied **[19, 20]**. In

this technology, a thin-film resistive is deposited on the crystal surface inside a standard evacuated resonator package, as shown in **Figure 2-8**, so that the crystal can be heated directly. The heating element runs along the resonator edge, and it is divided into two sections to avoid shorting the resonator electrodes. The heating elements are deposited by the same process used to deposit the resonator electrodes but with reduced thickness in order to increase electrical resistance. This is an effective technique to miniaturize an OCXO because using a metallic enclosure as a heating element is not necessary. Reducing the warm-up time and power consumption can also be achieved since the resonator is the only component to be heated. However, the frequency stability of this type of resonator is low due to a considerable heat flow through the crystal. The intensive heat from the heating elements causes an inhomogeneous thermal field on the resonator plate that influences resonator frequency. Significant mechanical stress coming from underneath the thin film heater is another problem as a quartz resonator reacts to stress by changing its frequency. It is also difficult to control the resonator temperature because placing a temperature sensor on the resonator might load and damp the quartz crystal, thus expediting the aging process.

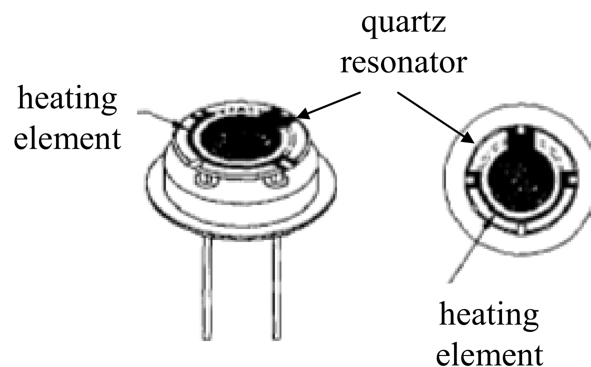

Figure 2-8: Quartz crystal resonator with thin film resistive heater deposited on its surface **[19]**.

Igor Abramson has proposed a composite-heated crystal resonator design to resolve the problems described above **[21]**. In this design, both the DHR technique and the conventional heating method are used. At start-up, the temperature controller turns on the power to the resistive film heater. This heats the resonator to a given set temperature as in the DHR technique and so effects a fast warm-up of the resonator plate. Then, when the resonator temperature reaches the steady-state condition, the temperature controller redistributes the heat power to the power transistor, thus heating up the metal enclosure to sustain the set temperature as in the conventional OCXO. This technique reduces warm-up time as in the DHR, while improving frequency stability compared to **[19]** and **[20]**. However, the package size cannot be reduced as it requires a separate heater, as in a conventional OCXO.

Kazuo Eda et al. have proposed a one-chip crystal oscillator **[22]**. A direct bonding technique was developed to integrate the quartz crystal onto the silicon substrate with an oscillator circuit in a single chip. Since a quartz crystal resonator is greatly sensitive to its supporting structure, direct bonding by a heat treatment without any adhesive is the most desirable method for integrating a quartz resonator into a silicon chip. Although quartz crystal consists of a single SiO_2 crystal, it has a large expansion coefficient compared to that of silicon (quartz crystal: $14.5 \sim 16.9 \times 10^{-6}$, silicon: 4.9×10^{-6} at 300 °C). Thus, to find the proper heat treatment temperature for direct bonding that will not damage either the quartz resonator or the silicon chip is the key issue. In addition, the silicon substrate under the bonded quartz resonator needs to be etched off in all but the region supporting the quartz resonator. A concept of the design is schematically shown in **Figure 2-9**. Applying this method to the miniature OCXO design may help remove the separate PCB and package for the resonator. However, the Q value reported in this work is only 7,000, which is not sufficient for high-precision applications.

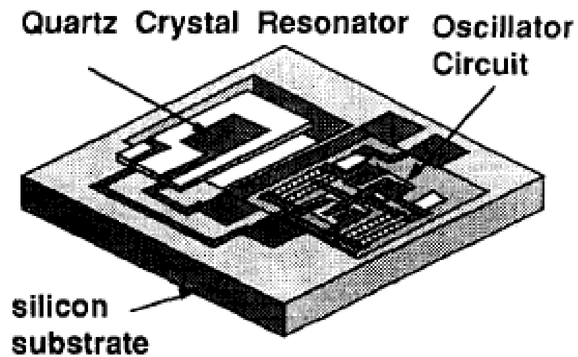

Figure 2-9: Quartz crystal resonator on silicon substrate with direct-bonding technique **[22]**.

To minimize the temperature gradients over the crystal resonator in order to improve their frequency stability, Anastasyev et al. designed an OCXO that placed the crystal resonator symmetrically in relation to the heaters **[23]**. This design minimizes the temperature gradients over the quartz crystal plate, thereby preventing heat flow through the resonator and so improving frequency stability. Although the heat flow through the resonator plate can be minimized in this structure, there is still a static temperature difference between the resonator and the electronic parts. This is due to the temperature difference between the resonator and the temperature sensor and it causes a static error in the oven set temperature. To avoid the static error, the author used a dual-mode crystal oscillator technique. However, this design does not reduce the package size, power consumption, or warm-up time at all.

In the dual-mode crystal oscillator technique **[24, 25]**, both the B-mode and C-mode are simultaneously excited. Thus, the dual-mode crystal oscillator needs two oscillator circuits with different bands connected in parallel at a common resonator. Since the B-mode has a large first-order temperature coefficient, its resonant frequency changes linearly with the temperature variation. Due to this characteristic, the B-mode frequency can be used as a temperature sensor while the C-mode frequency is the OCXO output frequency. Since the temperature sensor is the

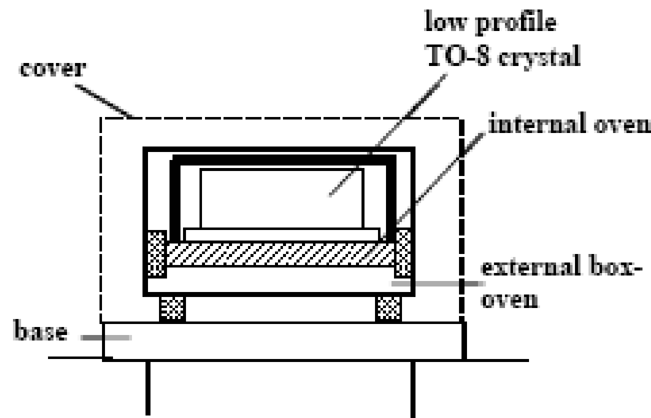

Figure 2-10: Schematic drawing of DOCXO **[25]**.

resonator itself, there is no static error in the oven set temperature. However, the dual-mode OCXO must be digitally controlled, and the additional B-mode degrades the phase noise of the output frequency **[26]**.

For ultimate performance in retaining a stable frequency over temperature, typically less than 0.1 ppb, double oven crystal oscillators (DOCXO) were developed **[27, 28]**. In a DOCXO, the crystal resonator is encased in an inner oven with temperature-control circuitry, and then the inner oven is again placed in the second outer oven as shown in **Figure 2-10**. The outer oven affords the DOCXO an additional layer of insulation. Most DOCXOs use higher temperature set points, which increases the size of DOCXOs, which, in turn, causes them to require more power in order to operate.

Bogomolov proposed a two-crystal technique for phase noise improvement **[29]**. Two identical AT-cut crystals are connected in a series within the feedback loop of the oscillator circuit in order to improve phase noise and maximize the Q factor. Two crystals allow the power

of a signal in the feedback loop to be doubled, thus leading to phase noise improvement. However, exactly matching two distinct quartz resonators can be difficult.

Chapter 3

Miniature OCXO Design on a CMOS Chip

This chapter presents a new design for an OCXO, specifically a miniature precision OCXO that is ultra compact and consumes low power. The details of implementing temperature sensors, on-chip heaters, controller circuitries, and quartz resonators are given. In addition, the test structure of the miniature OCXO is discussed and methods for further optimization are offered.

3.1 Design of a One-chip Temperature-control Circuit

In this project we attempt a new design: a one-chip temperature-control circuit with an AT-cut Tab Mesa type quartz crystal **[30]** directly mounted on the chip. The proposed design allows the size of the OCXO package to be reduced dramatically. As the resonator is not in a metal enclosure, and the control circuitry, including a heater and temperature sensor, is placed directly below the resonator, the warm-up time is considerably reduced. A reduction in package size can lead to less power consumption because a smaller volume needs to be heated. Thus, the small package size and correspondingly lower power consumption of the new design makes for the production of OCXOs that are suitable for battery-powered mobile devices.

The temperature-control circuit is designed to keep the chip temperature at the set point where the upper turning point of the resonator's f vs. T curve is located through thermal feedback control. The upper turning point of the quartz resonator used in this work was at 60 °C. When the temperature sensor detects the temperature variation of the chip, the control circuit responds by

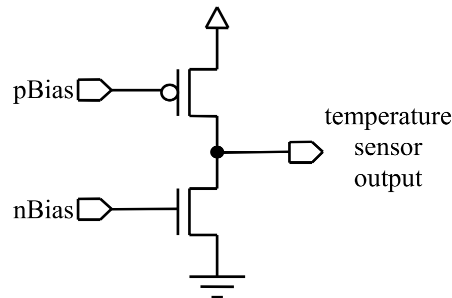

Figure 3-1: An inverter-type temperature sensor.

increasing or decreasing the amount of current flow through the heater to maintain the chip temperature. All the main components such as the temperature sensor, heater, op-amps, and oscillator are implemented on a single CMOS chip. The chip was fabricated in AMI 0.5 μm technology, and the chip area is 5.0 mm^2.

3.1.1 Temperature Sensor

Almost all the devices available in a CMOS process have temperature-dependant characteristics. The threshold voltages of MOS transistors have negative temperature dependencies, while integrated resistors have positive temperature dependencies. Due to these temperature dependencies, many different types of integrated CMOS temperature sensors are available **[31–37]**. Also, since the cost of CMOS temperature sensors is low, they are used for many applications, such as on-chip and on-board temperature stabilization.

Two different types of CMOS temperature sensors are implemented for the one-chip temperature-control circuitry. The first temperature sensor has an inverter-like structure composed of one PMOS and one NMOS transistors [**Figure 3-1**]. Its advantage is that the operating range of the sensor can be controlled easily by adjusting its gate voltages at pBias and

nBias. Further, it has the simplest structure and the minimum number of transistors. The operation of the sensor can be modeled as follows **[38, 39]**.

Two variables that change with temperature in the MOS transistor drain current expression are the threshold voltage and the mobility. The threshold voltage at temperature T can be written as a function of temperature:

$$V_{TH}(T) = V_{TH}(T_0) \cdot \{1 + TCV_{TH}(T - T_0)\} \quad \textbf{3.1}$$

where $V_{TH}(T_0)$ is the threshold voltage measured at temperature T_0, and TCV_{TH} is the temperature coefficient of the threshold voltage. The units for the temperature can be Kelvin or Celsius since the difference of the temperature is used in the equation. The reduction in mobility with increasing temperature can be modeled using

$$\mu(T) = \mu(T_0) \cdot \left(\frac{T_0}{T}\right)^{\alpha} \quad \textbf{3.2}$$

where α is the process-dependent parameter that usually ranges between 1 and 2, and the unit for the temperature in this equation is Kelvin. If we assume that the short channel effect is negligible and apply **Eq. 3.1** and **Eq. 3.2** to the expression for the NMOS transistor drain current

$$I_{DSn} = \frac{1}{2}\mu_n C_{oxn} \frac{W_n}{L_n}(V_{GSn} - V_{THn})^2 \cdot (1 + \lambda_n \cdot V_{DSn}) \quad \textbf{3.3}$$

and PMOS transistor drain current

$$I_{DSp} = -\frac{1}{2}\mu_p C_{oxp} \frac{W_p}{L_p}(V_{GSp} - V_{THp})^2 \cdot (1 + \lambda_p \cdot V_{DSp}) \quad \textbf{3.4}$$

the voltage at the temperature sensor output can be derived with the expression

$$I_{DSn} = -I_{DSp} \quad \textbf{3.5}$$

with the parameter values of

$$\frac{1}{2}\mu_n(T_0)\cdot C_{oxn} = 57.4\,\mu A/V^2$$
$$\frac{1}{2}\mu_p(T_0)\cdot C_{oxp} = -18.5\,\mu A/V^2$$
$$T_0 = 300\,K$$
$$TCV_{TH} = 1{,}250\ ppm/^{\circ}C \qquad \textbf{3.6}$$
$$\lambda_n = 0.01$$
$$\lambda_p = 0.05$$

More specific parameter values can be found in **[38]**, **[40]**, and Appendix A.

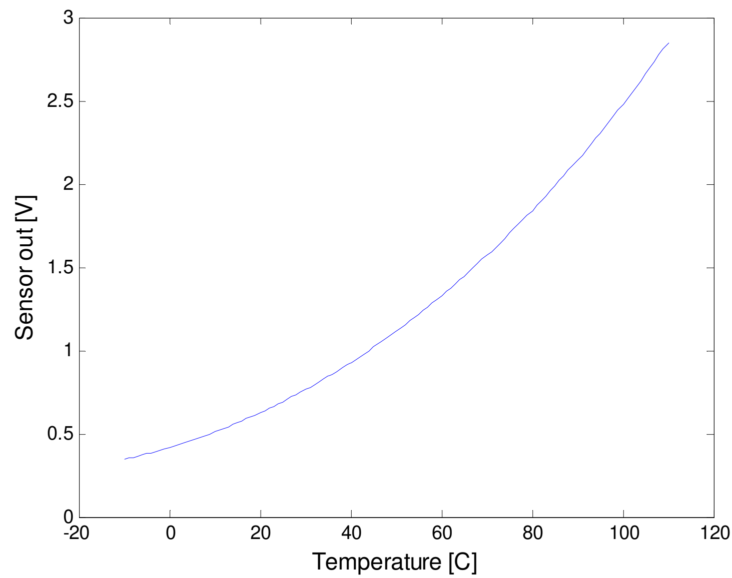

Figure 3-2: Expected sensor output from its modeling.

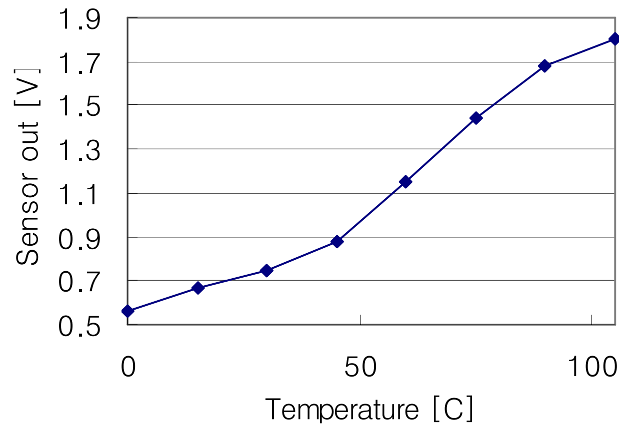

Figure 3-3: Temperature sensor test results.

Figure 3-2 is the plot of the output voltage derived from the first temperature sensor modeling described above; **Figure 3-3** shows the actual measurement result at various temperatures. The behavior of the sensor generally matches the result from the modeling and its sensitivity is measured to be 18 mV/°C.

Due to the simplicity of its structure, the temperature sensor is vulnerable to process variation. Therefore, its output voltage can vary in response to even a small mismatch in transistor width or length. To verify the effect of the process variation, output voltages of three different temperature sensors with the same gate bias voltages (nBias and pBias) were measured simultaneously inside the temperature chamber at every 15 °C from 0 °C to 105 °C. The measurement results are shown in **Figure 3-4**. The maximum output voltage divergence was 282 mV at 75 °C. It is not necessary for all the sensors to produce identical output voltages at the operating temperature range. However, it is desirable to get a matching output at the oven set temperature. Thus, for a proper sensor output voltage at the oven set temperature, the gate bias voltages need to be fine tuned.

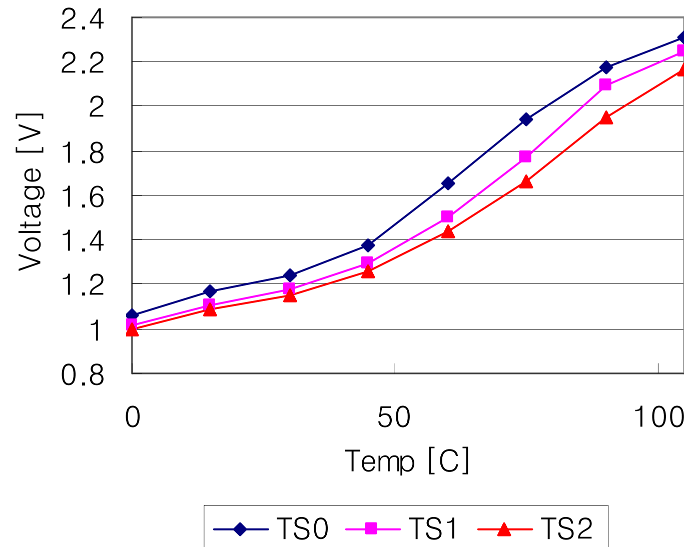

Figure 3-4: Three different temperature sensor output measurements with same gate bias voltages.

Another type of temperature sensor implemented for this project is the CMOS PTAT circuit **[41]**. The structure of the sensor is shown in **Figure 3-5**, and it was implemented in 0.18 μm technology. The output voltage can be described by the following formula:

$$Sensor\,output = T \cdot \frac{k}{q} \cdot \ln\left(1 + \frac{I_{M1} + I_{M2}}{I_{M1}} \cdot \frac{\left(\frac{W}{L}\right)_{M1}}{\left(\frac{W}{L}\right)_{M2}}\right) \quad \textbf{3.7}$$

where T is the temperature, k is the Boltzman constant $(1.38 \times 10^{-23}\ J/K)$, and q is the electronic charge $(1.6 \times 10^{-19}\ C)$. Based on the **Eq. 3.7**, it is clear that the sensor output voltage is proportional to the temperature. The measurement result of the PTAT sensor is shown in

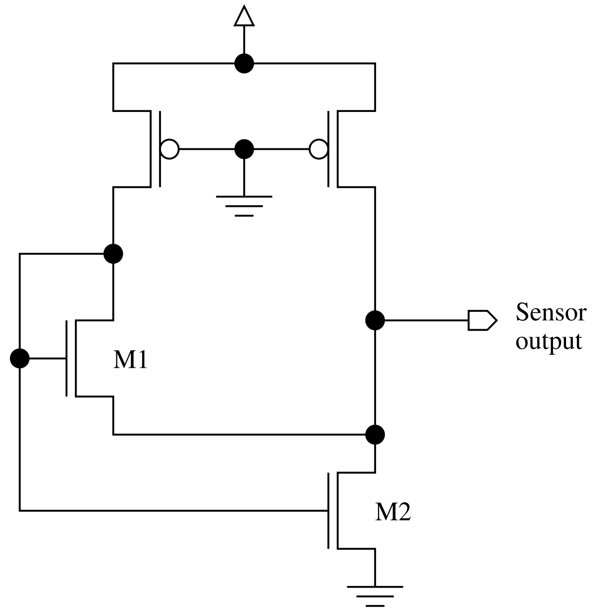

Figure 3-5: CMOS PTAT temperature sensor.

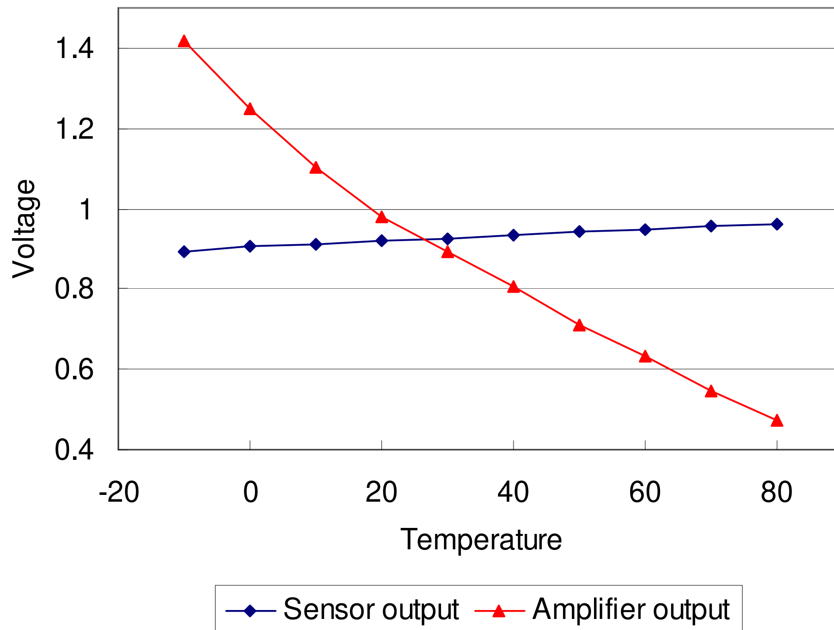

Figure 3-6: PTAT sensor test results.

Figure 3-6. It is clear from the measurement result that the PTAT circuit output has a better linearity against the temperature variation. However, the linearity of a temperature sensor is not critical in OCXO; this is because once the temperature inside the oven is raised to the set point, no significant temperature change occurs.

3.1.2 On-chip Heater

Poly resistors and NMOS transistors are used to build the heater array [**Figure 3-7**]. The heater warms up the chip by increasing the current through the structure, which is controlled by its gate voltage of V_{hc}. It conducts a maximum current of 350 mA when V_{hc} = 3.3 V, and it is disabled when V_{hc} < 0.7 V. Thus, the maximum power consumption at the heater is 1.16 W with a 3.3 V supply. **Figure 3-8** shows the measurement results of the heater. From the HSpice simulation, it was verified that half the heater power is consumed at the resistors, and the half the heater power is consumed at the transistors. Since all the components are implemented in the standard design rule, the reliable operation of the heater is guaranteed to have a large amount of current flow **[42]**.

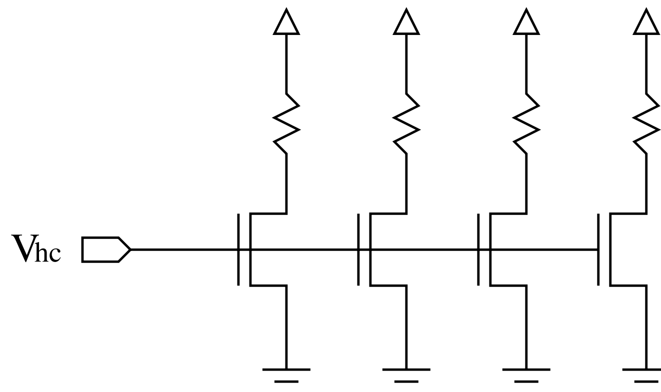

Figure 3-7: Heater array.

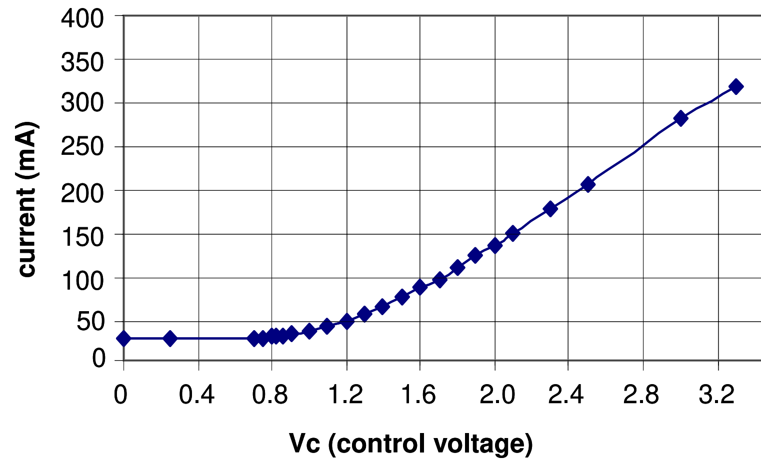

Figure 3-8: Heater measurement results.

To verify the relationship between the heater current and the chip temperature, required amount of current through the on-chip heater necessary to maintain the chip temperature at different set temperatures was measured. The measurement was taken at room temperature by manually adjusting the heater control voltage while monitoring the on-chip temperature sensor output. **Table 3-1** summarizes the measurement results.

Table 3-1: Required Amount of Current Through the Heater for Different Chip Temperatures.

Chip Temperature [°C]	Required Current Through the Heater [mA]
40	50
50	62
60	73
70	86
80	99
90	111

3.1.3 Temperature-control Circuit

Figure 3-9 is a control-circuit schematic diagram. The amp at the first stage of the control circuitry compares the sensor output with the reference voltage (V_{ref}), which is set to the sensor output when the chip temperature is 60 °C. Reference voltages V_{r1} and V_{r2} for amps at the next stage determine the control range of the circuit ($V_{r1} < V_{ref} < V_{r2}$). When the output voltage of the amplifier at the first stage is lower then V_{r1}, the temperature-control circuit increases the heater control voltage, V_{hc}, and the current through the heater. On the other hand, if the first-stage amplifier output voltage is higher than V_{r2}, the opposite occurs: the current through the heater decreases. **Figure 3-10** shows the Spice simulation result. The resistors and capacitors used to build the complete control circuit are off-chip components. This controller circuit can be categorized as a bang-bang controller with a dead-zone between V_{r1} and V_{r2}. Due to the nature of the bang-bang controller, the heater control voltage can oscillate during the control process. The effect of the oscillation is described in Chapter 4.

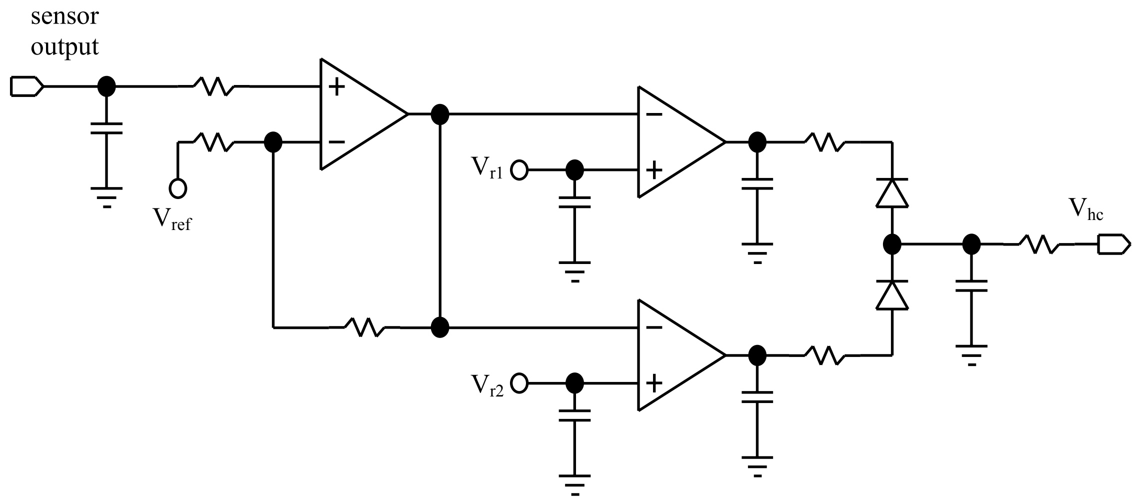

Figure 3-9: Temperature-control circuit.

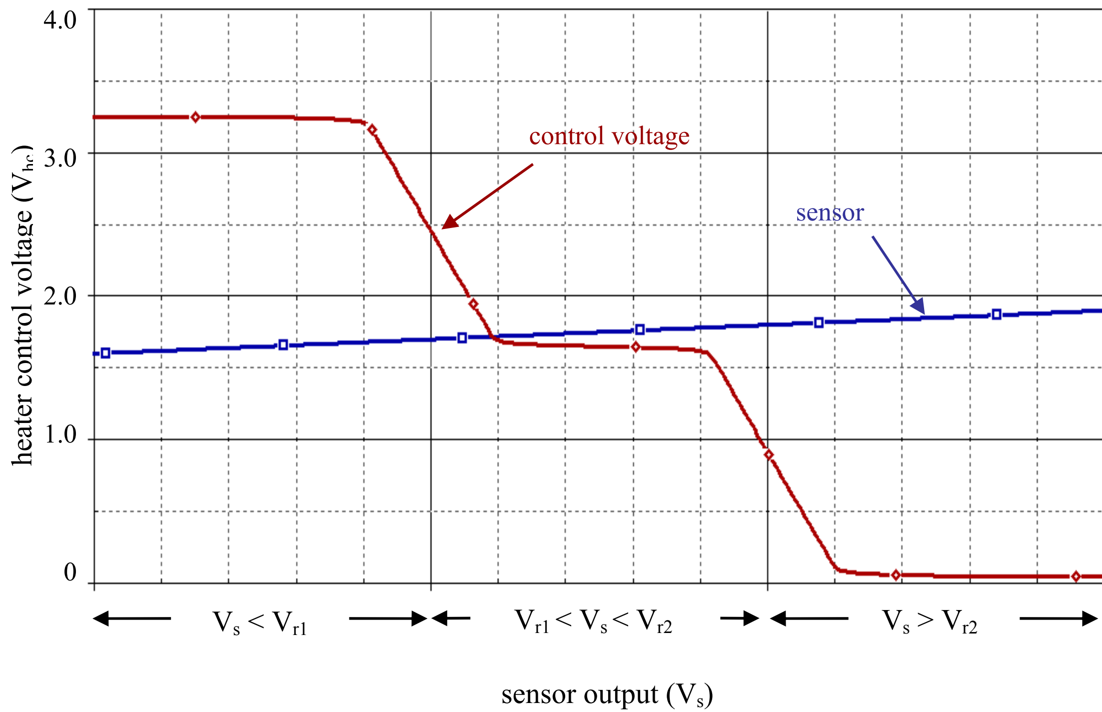

Figure 3-10: Control circuit Spice simulation results.

Another type of controller used in this project is the proportional-integral-derivative (PID) controller. A PID controller is a feedback-control system that is very effective for continuous process. A PID controller consists of three control components: proportional, integral, and derivative. The PID is a control system that generates the correction voltage proportional to the current amount of error. The proportional controller is not effective by itself as it retains the steady-state offset error. An integral controller is added in order to avoid the offset error, thus improving long-term precision. The integral controller accumulates the amount of error that should have been eliminated; this allows the accumulated error to be multiplied by the integral gain and added to the PID controller output. The derivative controller is added to the proportional-integral system to speed up the control process. It generates a correction voltage according to the rate of error variation. Thus, the steeper the slope of the error over time, the larger the correction voltage generated. **Figure 3-11** and **Figure 3-12** show a PID block diagram and the Spice simulation results of the PID controller, respectively.

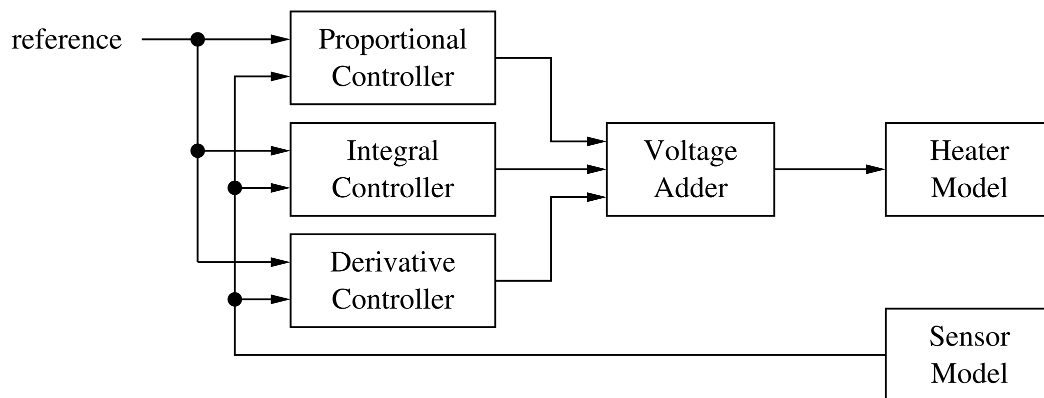

Figure 3-11: PID controller block diagram.

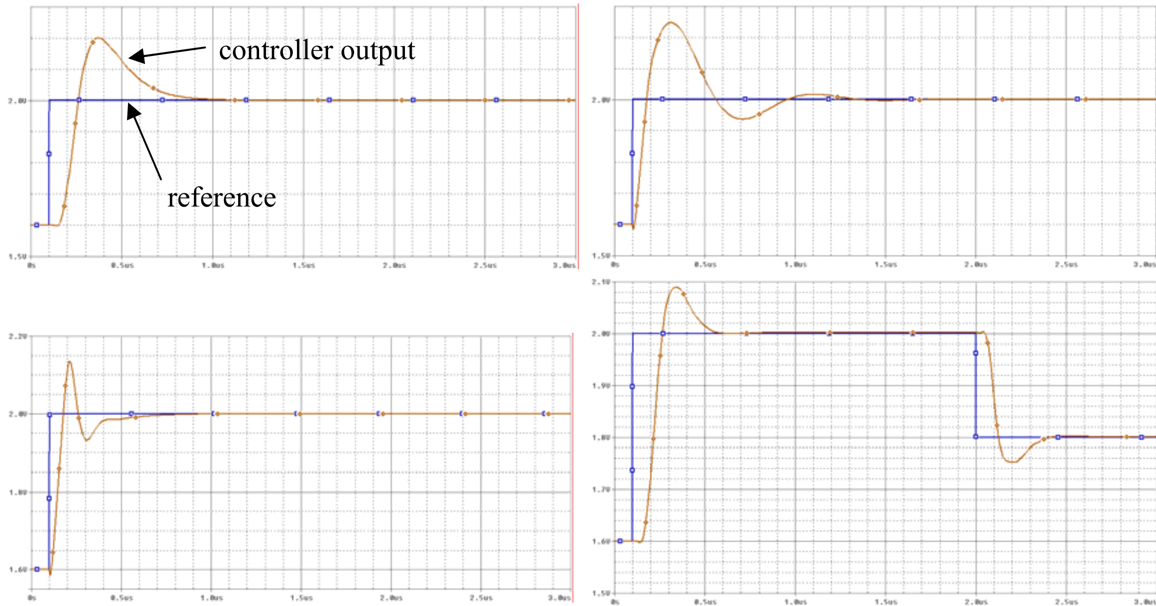

Figure 3-12: Spice simulation results with different control parameters.

3.1.4 Quartz Crystal Resonators

Three different types of quartz crystal resonators were used in this project. A Tab mesa type quartz crystal and frame enclosed resonator (FER) were used for minimal package size, and a conventional quartz crystal in an HC49/U package was used to reduce costs.

3.1.4.1 On-chip Quartz Crystal

As shown in **Figure 3-13**, a 100 MHz AT-cut Tab Mesa type quartz crystal resonator is directly mounted on the chip **[43]**. The quartz resonators were provided by SaRonix, a corporation that supported this research. Mounting a high-precision quartz crystal directly onto a CMOS chip enables the closest coupling of the crystal with the oscillator circuit. Due to the close proximity of the crystal and the circuits, the temperature compensation or stabilization will

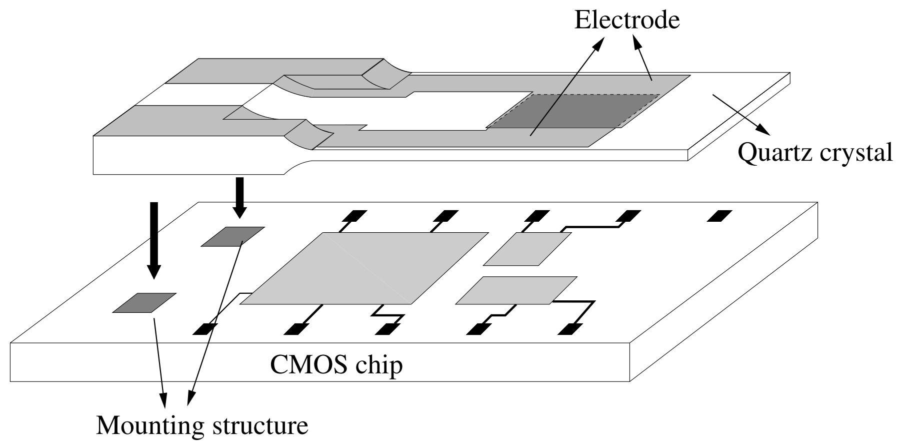

(a)

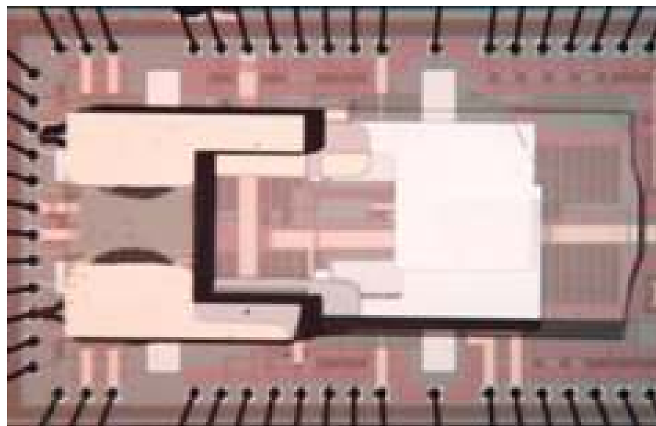

(b)

Figure 3-13: (a) Illustration and (b) micrograph of the on-chip quartz resonator.

improve. The reliability of the system, frequency stability, and precision will also improve. The elimination of an off-chip interface for the crystal and separate crystal packaging will reduce the size of the entire clock generation system, which also reduces the final system-on-chip product cost.

Two thin gold electrodes are located on both sides of the resonator that eventually form the resonator support structure. Electrodes on a thicker U-shaped crystal support structure are

mounted on a chip with conductive epoxy and cured in a vacuum oven at 150 °C for 40 minutes. Mounting a quartz resonator on a chip for mass manufacturing can be achieved inexpensively using pick-and-place equipment. Also, the on-chip resonators are already commercialized, thus an additional resonator design cost will not be incurred.

The performance of the on-chip resonator was verified by integrating the resonator on a CMOS PLL chip **[44]**. The integration process was carried out by Dr. Jackson's electronics research group (JERG), Department of Electrical Engineering, Pennsylvania State University. In this project, a 155.52 MHz AT-cut Tab Mesa type quartz crystal resonator was directly mounted on a CMOS PLL chip to eliminate both the off-chip interface and the separate crystal packaging.

To provide perspective for the test results, a standard 155.52 MHz stand-alone quartz oscillator product with a fundamental mode was used as a reference. The jitter measured on this oscillator was 3.5 ps rms. For the on-chip crystal chip, we measured several circuit setups to understand both the chip function and the effects of crystal integration. These measurements can be divided into two groups: (1) the packaged chip test with the crystal mounted outside the package, and (2) the unpackaged chip test with the crystal mounted on the chip. These test measurements included the oscillator output with all circuits running, and with the digital circuits off. All measurements were done under the same conditions with the same test equipment. **Table 3-2** and **Table 3-3** show the results of the jitter measurement.

Table 3-2: Packaged Device with Crystal Mounted Outside the Package.

Condition	Jitter Measurements (rms)
Output with PLL locked	35 ps
Output with digital circuits off	3.5 ps

Table 3-3: Unpackaged Device with Crystal Mounted on Chip.

Condition	Jitter Measurements (rms)
Output with PLL locked	15 ps
Output with digital circuits off	1.9 ps

To verify if frequency degradation has occurred due to the close mounting of the electronic chip and the quartz crystal, oscillator coupling tests were conducted with the on-chip quartz crystal with an additional oscillator core running. The primary core oscillator frequency was 155.52 MHz and the secondary core oscillators were run at 51 MHz. **Figure 3-14** shows a spectrum analyzer plot of the 155.52 MHz oscillator output with the 51 MHz secondary core also running. Significant coupling between the two cores is clearly evident. To ascertain if this was related to coupling between the integrated quartz crystal resonator and the oscillator chip, we removed the crystal resonator from the chip and used an external crystal instead. The coupling was essentially unchanged indicting that it is related to on-chip coupling and not coupling to the direct mounted resonator.

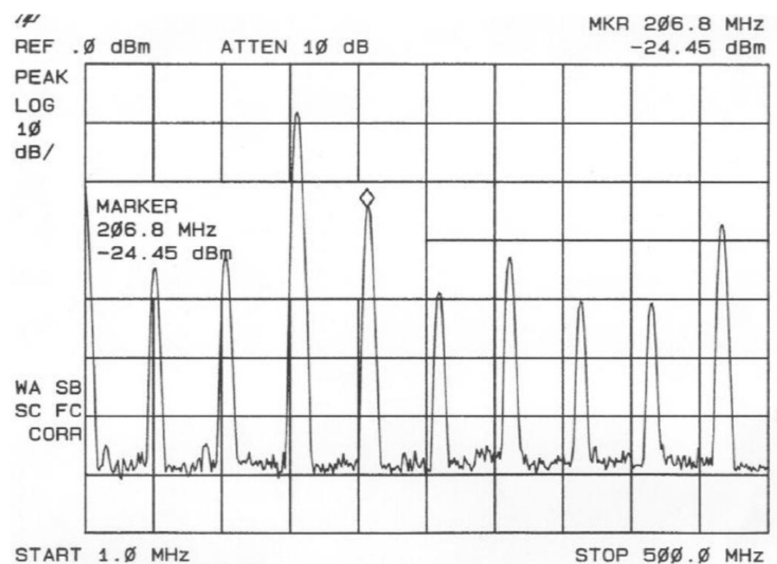

Figure 3-14: Spectrum analyzer plot from multiple core (155.52 MHz and 51 MHz) testing.

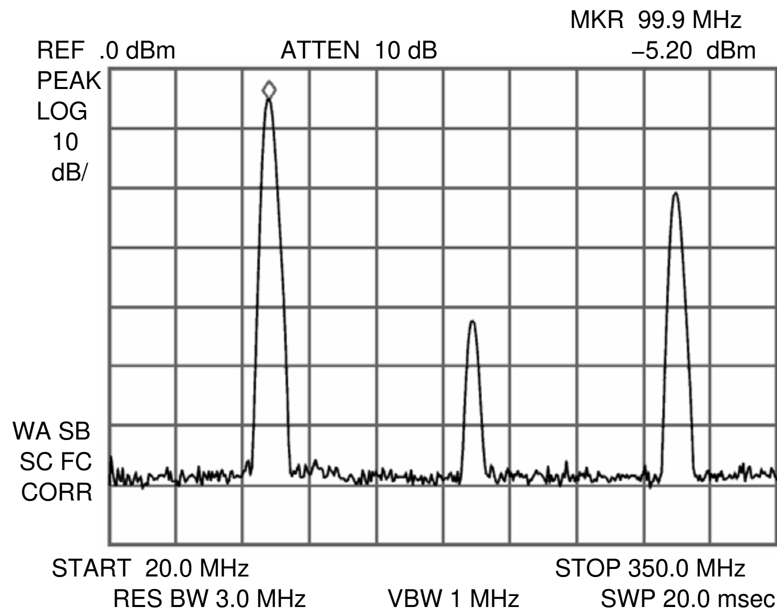

Figure 3-15: Fundamental and harmonic frequencies of the on-chip 100 MHz quartz crystal resonator.

Figure 3-15 shows the spectrum analyzer plot of the 100 MHz on-chip quartz resonator. The crystal oscillator has normal output with the second harmonic peak at 40 dB below the fundamental frequency and the RMS jitter at 2.2 ps. Further, the shock and vibration test (MIL-STD-883 method 2002 condition B and MIL-STD-883 method 2007 condition A) for the on-chip resonator proved the robustness of the structure.

3.1.4.2 Frame Enclosed Resonator (FER)

The on-chip crystal resonator approach can be extended to a chip-on-crystal structure for extremely compact oven controlled crystal oscillators. For this concept, a frame enclosed resonator (FER) was fabricated and integrated with a CMOS OCXO chip by the JERG group **[45]**. In **Figure 3-16**, the structure of the chip-on-crystal concept is shown. The quartz resonator element (FER) is enclosed by base and cap material. For OCXOs, there may be advantages for a material with low thermal conductive like quartz. The active area of FER is naturally sealed with these base and cap materials. These also help to minimize stress between the silicon chip and FER due to a difference of thermal expansion coefficient. A variety of bonding techniques are possible including epoxy or solder. Especially for OCXOs, low-contamination bonds that also form high-reliability seals, for example eutectic bonding or diffusion bonding, will be particularly useful.

Figure 3-17(a) shows a schematic of the FER. The dimension of the frame enclosed resonator is 2.4 mm by 3 mm. The fabrication process begins with a double-side polished AT-cut quartz blank. A high-quality AT-cut quartz blank of 80 μm-thickness and 2 inch by 1 inch is used. Cr (100 Å) / Au (1500 Å) is deposited on the quartz surface for a mask layer, and pattered photolithographically for 1.5 mm by 1.8 mm recess. Patterned quartz blanks are dipped in the ammonium biflouride solution at 80 °C and etched until the active area is 8 μm thick. Cr (70 Å) /

Au (800 Å) electrodes are formed on both sides of the active area. This resonator used a 600 μm by 600 μm electrode. **Figure 3-17(b)** shows a picture of the fabricated frame enclosed resonator.

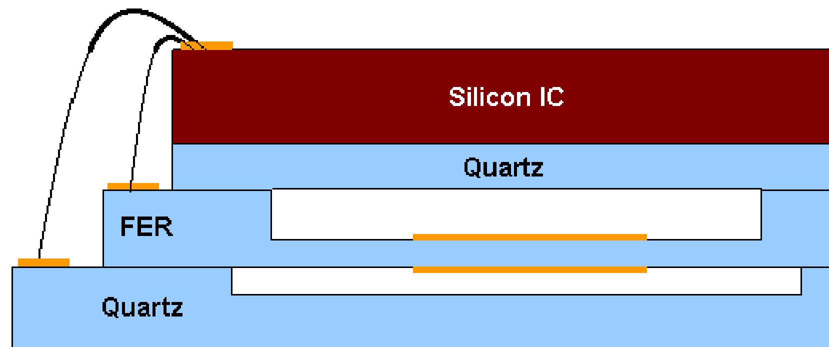

Figure 3-16: Structure of the chip-on-crystal approach.

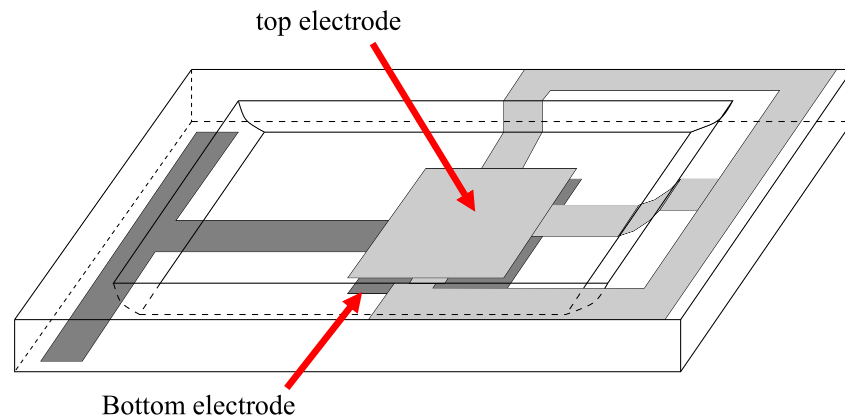

(a)

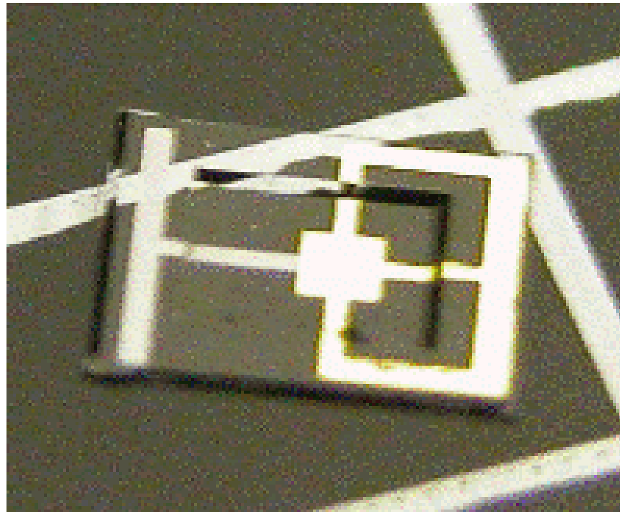

(b)

Figure 3-17: (a) Schematic of frame enclosed resonator (b) Fabricated frame enclosed resonator.

A test structure was built to verify the crystal-on-chip concept. As shown in **Figure 3-18**, a printed circuit board (PCB) was prepared to test the structure. The PCB itself is already a big heat sink so the copper area around the structure was minimized. A quartz substrate was inserted between the CMOS chip and FER to electrically isolate the IC and resonator top contact. This will help to reduce the thermal expansion difference between IC and FER. Conductive epoxy and

wire bonding were used for the electrical connection. A photo of the actual structure is also shown in the figure. **Figure 3-19** is the spectrum analyzer plot of the fundamental and harmonic frequencies of the 159.3 MHz FER with the OCXO chip.

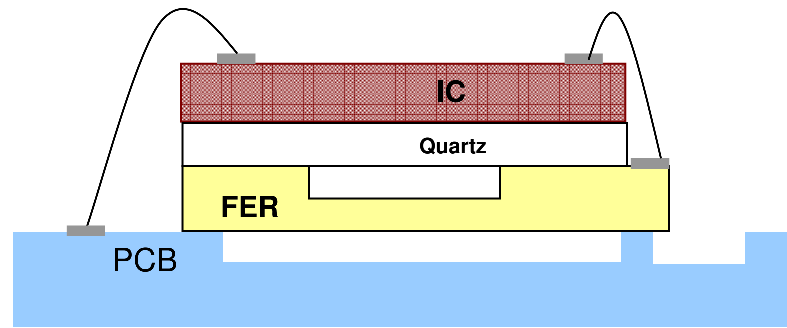

(a)

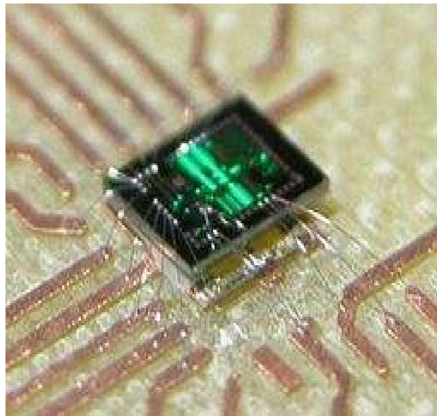

(b)

Figure 3-18: Stacked FER and CMOS OCXO chip (a) schematic (b) photo.

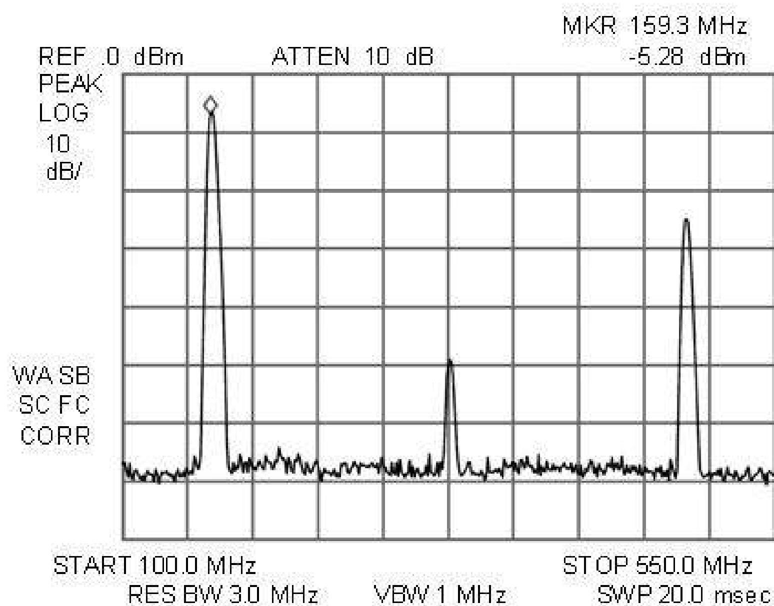

Figure 3-19: Fundamental and harmonic frequencies of 195.3 MHz FER with an OCXO chip

Figure 3-20: Low-cost OCXO structure with a quartz resonator in HC49/U and a packaged temperature-control chip.

3.1.4.3 Conventional Quartz Crystal Package

A low-cost OCXO structure can be built with the one-chip temperature-control circuit proposed in this study. A packaged chip was bonded on a quartz resonator in an HC49/U package with thermally conductive epoxy. In this structure, the heat generated at the on-chip heater flows through the thermally conductive epoxy to warm up the crystal package. **Figure 3-20** is a

photograph of the OCXO structure. An unpackaged chip can be used to reduce the volume of the structure.

With this method, frequency stability can be improved by a factor of 18 in the temperature range of 20 °C to 70 °C. The cost of the structure is low since a very cheap HC49/U-packaged AT-cut resonator is used. However, the warm-up time of this structure can be longer than that of the chip-scale OCXO due to the former's larger resonator package size, and the heat loss from its chip and resonator packages.

3.2 IC Layout and PCB Design

Figure 3-21(a) is a die photo of the fabricated chip. The heater is located at the center and the sensors are at the top, middle, and bottom of the chip. Multiple numbers of sensors are integrated for testing purpose; however, the top one is mainly used for this project since it is placed right below the resonator active area. Five op-amps are integrated for the control circuit. The mounting structures for quartz crystal resonators are also shown in the figure.

A PCB with an unpackaged chip bonded on it and sealed is shown in **Figure 3-21(b)**. The chip is sealed to build a temporary oven structure. The material of the structure is FR4, and it is covered with a glass cap on top. The structure protects the chip and the mounted quartz crystal from humidity or external damage.

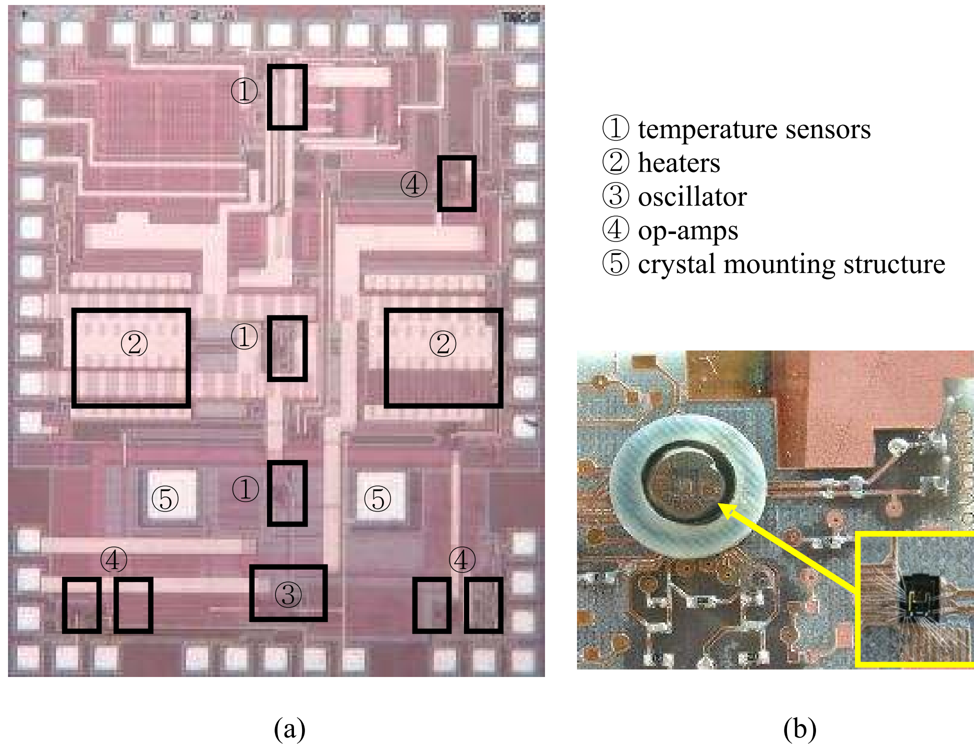

Figure 3-21: (a) Chip die photo (b) PCB and close-up of the chip inside the oven structure.

Chapter 4

Experiment Results

Experiment results and test methods are described in this chapter.

4.1 Testing and Measurements

The testing and measurement results of the miniature OCXO with the on-chip resonator and the FER are discussed in following sections.

4.1.1 Chip-scale OCXO with On-chip Resonator

The test board for the miniature OCXO with the on-chip quartz resonator was covered with styrofoam to reduce heat loss and tested in a temperature chamber (EC10, Sun Electronic Systems). The temperature sweep testing range was from 0 °C to 100 °C. Test boards are shown in **Figure 4-1** and steps for the chip testing were as follows.

The sensor output voltages are measured at different temperatures while the heater is disabled (grounded V_{hc}). Based on these temperature measurements, the sensor bias voltages are determined. Next, at room temperature (25 °C), while monitoring the sensor output, the heater control voltage (V_{hc}) is adjusted from outside the chip. Through this process, the proper value of V_{hc} and the amount of current flow are found. These values are the voltages from the control

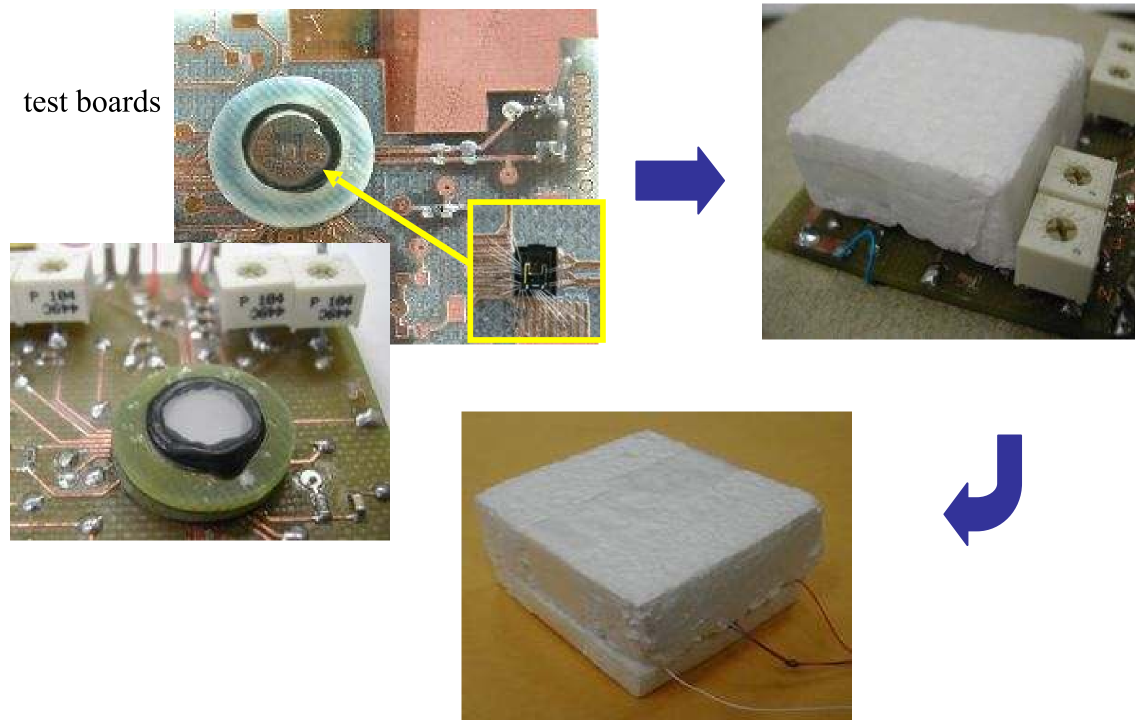

Figure 4-1: OCXO test boards.

circuit and current through the heater that are required to maintain 60 °C inside the chip at room temperature. After V_{r1} and V_{r2} have been set, the control-circuit output voltage is tuned to the V_{hc} value, which was established via the previous process. With all the parts connected together and tuned, the sensor output voltage, total current flow, and frequency of the quartz resonator are measured and recorded during temperature sweep inside the chamber.

Figure 4-2 and **Figure 4-3** are the plots of the sensor output and crystal frequency stability with and without the temperature control respectively. Each measurement was taken at 10 °C intervals from 0 °C to 80 °C. Two points are clear: (1) the frequency of the crystal changes as the temperature changes without the temperature control; and (2) the frequency is stabilized against the temperature change with the temperature control. The chip temperature was controlled

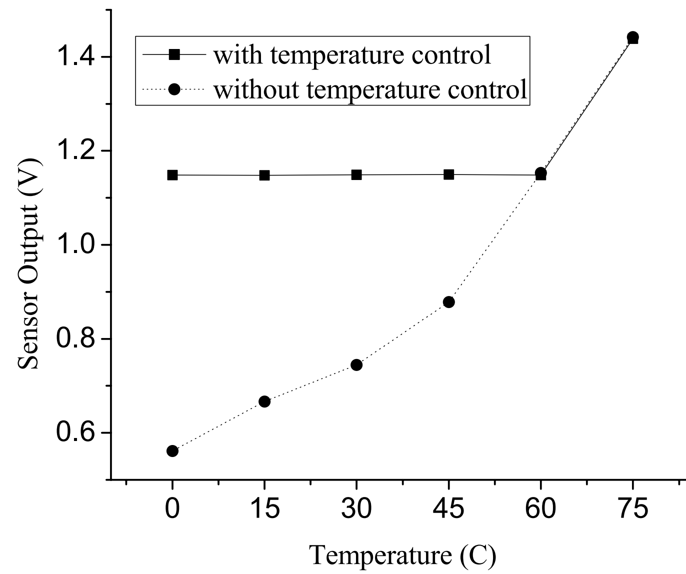

Figure 4-2: The temperature sensor output plot with and without the temperature control.

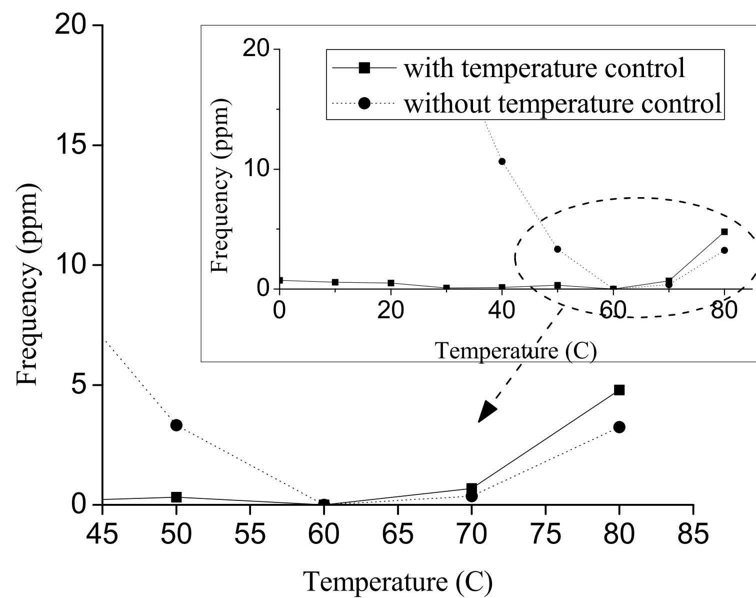

Figure 4-3: The on-chip resonator frequency plot with and without the temperature control.

and stabilized while the chamber temperature sweep was between 0 °C and 60 °C. The frequency stability measurement was ±0.35 ppm in the same temperature range. However, when the chamber temperature exceeds the temperature controller set point, which is 60 °C, the crystal frequency is no longer stabilized.

In the event of an initial power-up or a sudden ambient temperature change, the heater control voltage from the temperature-control circuit oscillates. The oscillation at the heater control voltage and its effect on the temperature sensor output are shown in **Figure 4-4**. At earlier stages of the temperature-control process, the temperature-control circuit raises the temperature inside the miniature OCXO by rapidly turning the on-chip heater on and off. This causes a voltage fluctuation at the temperature sensor output. The amount of the fluctuation can be managed by adjusting the reference voltages V_{r1} and V_{r2}, as shown in **Figure 3-9**. However, if the voltage difference between the references becomes smaller, the oscillation frequency of the heater control voltage will increase. As the temperature inside the oven reaches the steady state, the oscillation frequency goes down as shown in **Figure 4-4(b)**, and the oscillation eventually stops in order to maintain the set temperature.

According to the measurement results, if it is assumed that the temperature inside the oven is the only factor that affects frequency stability, the ±0.35 ppm variation corresponds to a 5 °C to 6 °C temperature fluctuation. Therefore, if the oven set temperature is changed from 60 °C to 40 °C where the f vs. T slope of the resonator is significantly steeper, the frequency stability will degrade to the range of ±2 ppm to ±3 ppm variation with the same temperature controllability.

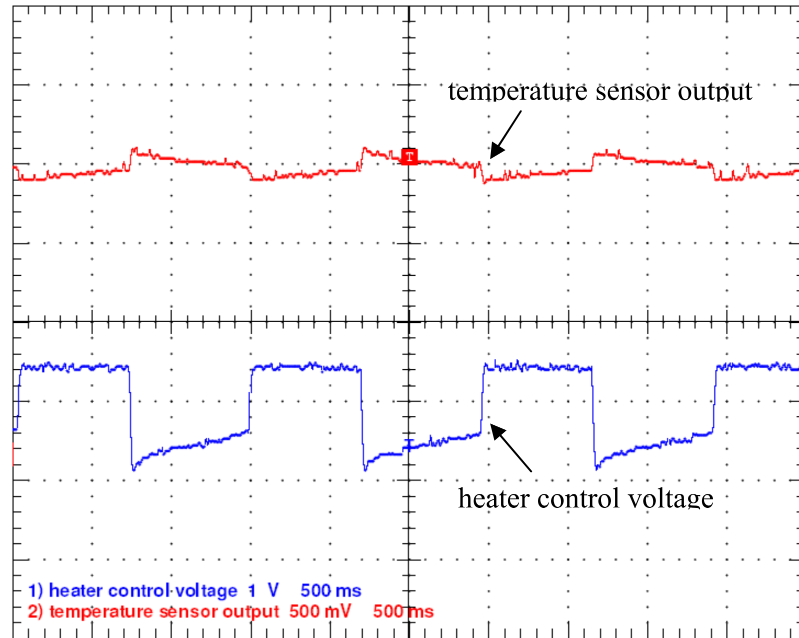

(a) earlier stage of the temperature control process

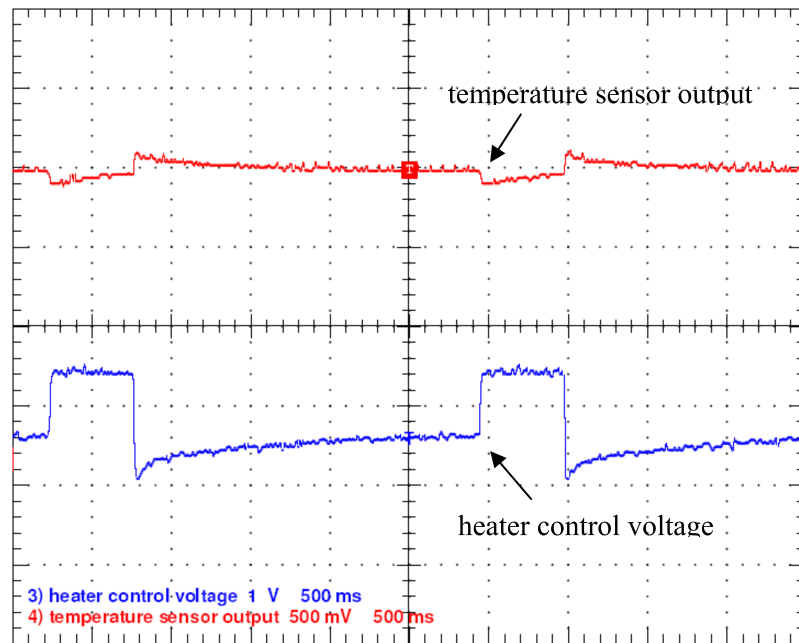

(b) getting close to the steady state

Figure 4-4: Heater control voltage and temperature sensor output during the temperature control process.

The current through the heater was 73 mA at room temperature to keep the chip temperature at 60 °C. The maximum power consumption of this miniature OCXO was 1.2 W at start-up. This is because the on-chip heater drives its maximum current to bring up the chip temperature to the set point. The point at which the chip temperature reaches the temperature controller set point and the controller tries to maintain that temperature is referred to as "steady-state". In this instance, the steady-state power consumption was 303 mW. The warm up time required to reach ±1.0 and ±0.1 ppm stability was 100 seconds and 190 seconds, respectively [**Figure 4-5**].

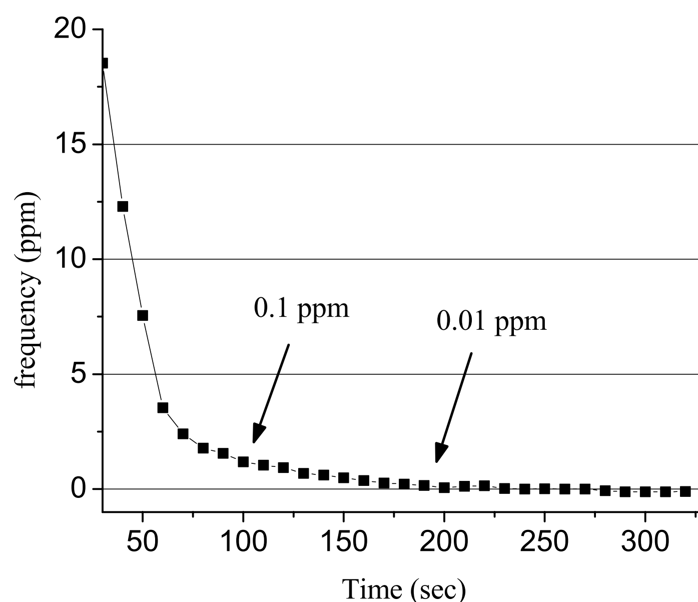

Figure 4-5: Warm-up time measurements at room temperature.

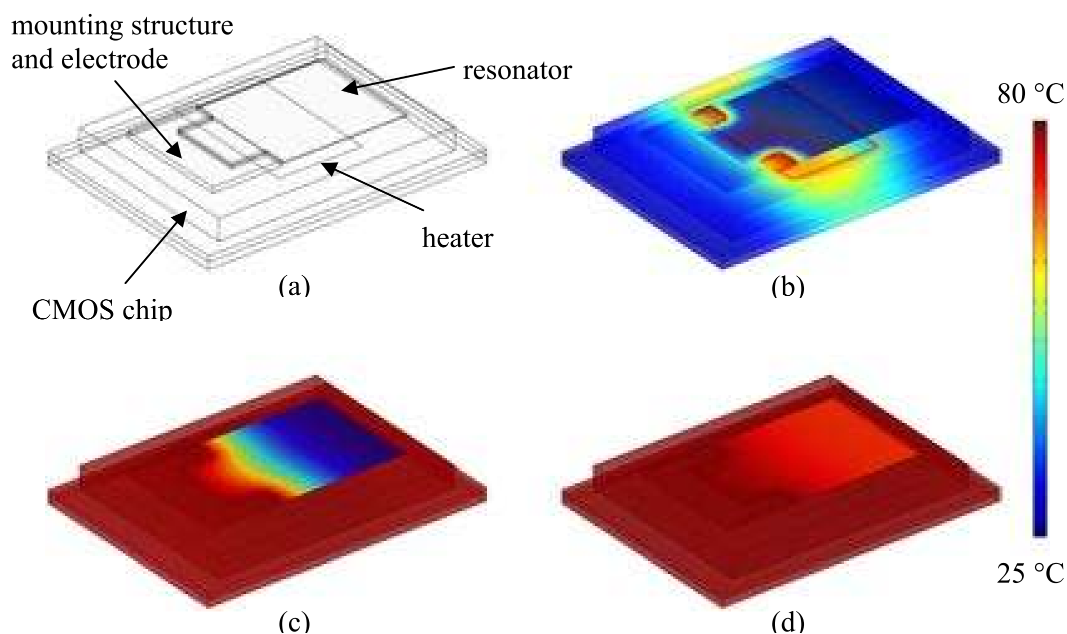

Figure 4-6: Femlab heat-transfer simulation plots.

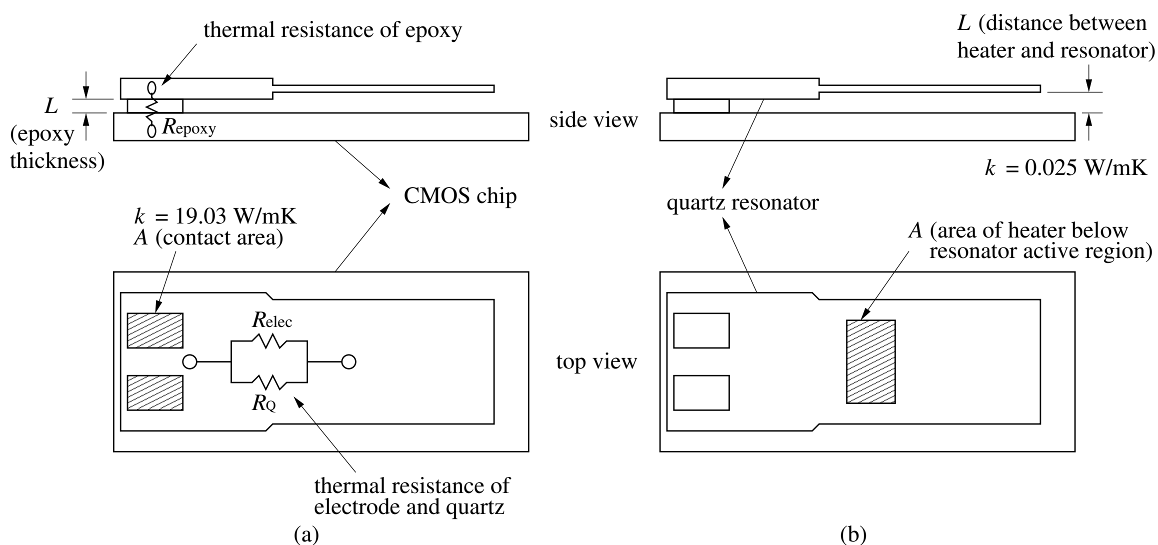

Figure 4-7: Heat-transfer modeling of the miniature OCXO for (a) heat transfer through the mounting structure and (b) heat transfer through air. (This image is not to scale.)

Figure 4-6 shows Femlab heat-transfer simulation results for an OCXO model. In this figure, (a) is the OCXO modeling, (b) shows the heater beginning to warm up at start-up, (c) is the stage when the resonator gets heated, and (d) shows the entire structure at steady-state. **Figure 4-6(c)** shows that the quartz resonator is heated mostly by conduction through the mounting structure rather than convection or radiation. This simulation result agrees with the conjecture from following simple analytical method. Modeling for the analytical method is shown in **Figure 4-7**.

If we assume that the initial temperatures of the on-chip heater and the quartz resonator are 80 °C and 25 °C respectively, the heat transfer rate $Q_{conduction}$ through the mounting structure can be defined as

$$Q_{conduction} = \frac{80-25}{R_{tot}} \text{ [W]} \quad \textbf{4.1}$$

where R_{tot} is the equivalent thermal resistance between the heater and the resonator active area. Thus, if we assume that the thermal contact resistance is negligible, R_{tot} can be computed by

$$R_{tot} = R_{epoxy} + \left(\frac{R_{elec} \cdot R_Q}{R_{elec} + R_Q} \right) \text{ [°C/W]} \quad \textbf{4.2}$$

where R_{epoxy}, R_{elec}, and R_Q are the thermal resistances of the epoxy, the electrode, and the quartz respectively. The thermal resistance R is defined as

$$R = \frac{L}{k \cdot A} \text{ [°C/W]} \quad \textbf{4.3}$$

where k is heat conductivity, A is the area, and L is the distance or thickness. Therefore, the heat transfer rate by conduction can be calculated to be $Q_{conduction}$ = 29.4 mW. The thermal conductivities and the approximate resonator dimensions used in this calculation are shown in **Table 4-1**.

Table 4-1: Thermal Conductivity Values and Approximate Resonator Dimensions.

	Epoxy	Electrodes	Quartz
k [W/mK]	19.03	237	1.3
L [m]	10×10^{-6}	0.5×10^{-3}	0.5×10^{-3}
A [m^2]	80×10^{-9}	1×10^{-9}	24×10^{-9}

On the other hand, the heat-transfer rate $Q_{convection}$ from the heater to the resonator through the air is $Q_{convection}$ = 10 mW by the same method where the heat conductivity of air is k = 0.025 W/mK, the area of the heater below the resonator active region is A = 0.365×10^{-6} m^2, and the distance between the on-chip heater and the resonator is L = 50 μm. This analysis shows that the amount of heat transferred from the on-chip heater to the resonator is dominated by the conduction through the mounting structure. Also, in **Figure 4-6(d)** it can be seen that the entire structure is evenly heated once it reaches the steady state.

4.1.2 Chip-scale OCXO with FER

A 159.3 MHz FER was fabricated for the chip-on-crystal structure. Since the FER with its cap and base material and the OCXO chip form a naturally sealed structure, the size of the OCXO package can be reduced significantly. In addition, the miniature OCXO with the FER was covered with styrofoam in order to reduce heat loss and tested in a temperature chamber in the same way as the OCXO with the on-chip resonator. With temperature control, frequency was stabilized within a ±0.6 ppm variation. The measurement results are shown in **Figure 4-8**. Frequency stability may be improved by further package and wire-bonding optimizations.

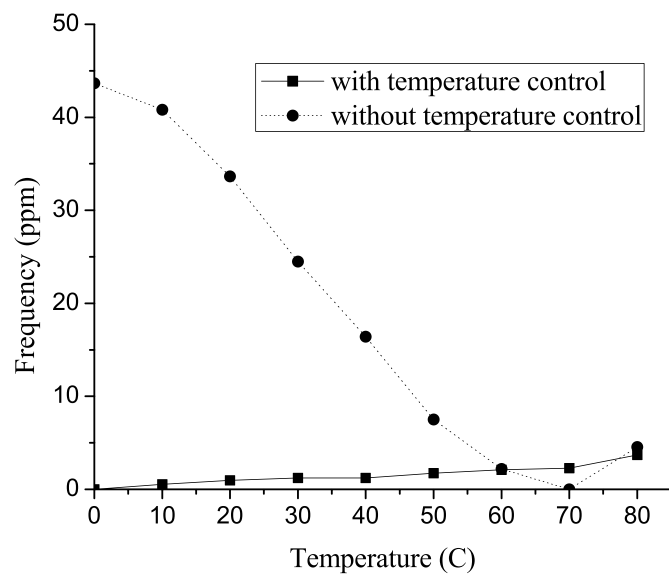

Figure 4-8: The FER frequency plot with and without temperature control.

Chapter 5

Further Optimization

Additional work for further miniature OCXO optimization is discussed in this chapter. The work includes applying the cubic compensation technique, integrating the on-chip microprocessor with its peripherals, using polyimide flexible circuit boards, and applying the anisotropic conductive film (ACF) bonding technique.

5.1 Cubic Compensation

While the temperature inside an oven is locked at a set temperature where the upper turning point of the f vs. T curve is located, there still exists a small amount of frequency variation as shown in **Figure 2-3**. This causes the frequency instability even when the temperature inside the oven is stabilized. To overcome this problem and achieve better frequency stability, the cubic frequency compensation technique can be applied to flatten the f vs. T curve at the set point area as shown in **Figure 5-1**.

Cubic frequency compensation is the main idea in a temperature compensated crystal oscillator (TCXO). A typical TCXO consists of a temperature sensor, a cubic compensation voltage generator, and a voltage controlled crystal oscillator (VCXO). The principle of the TCXO is to stabilize the frequency variation of the quartz resonators against ambient temperature variation as shown in **Figure 5-2**. Because the frequency of the VCXO can be changed linearly by its control voltage, the compensation voltage of the TCXO must also be a cubic function of the temperature.

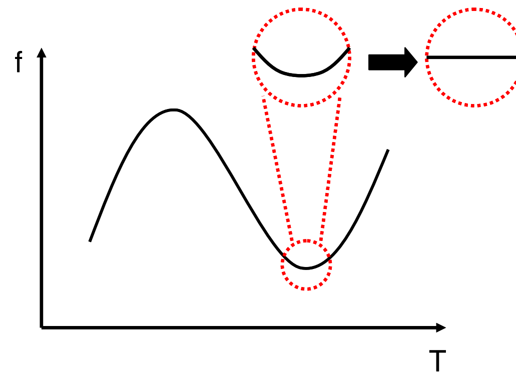

Figure 5-1: Flattening the f vs. T curve with cubic compensation technique.

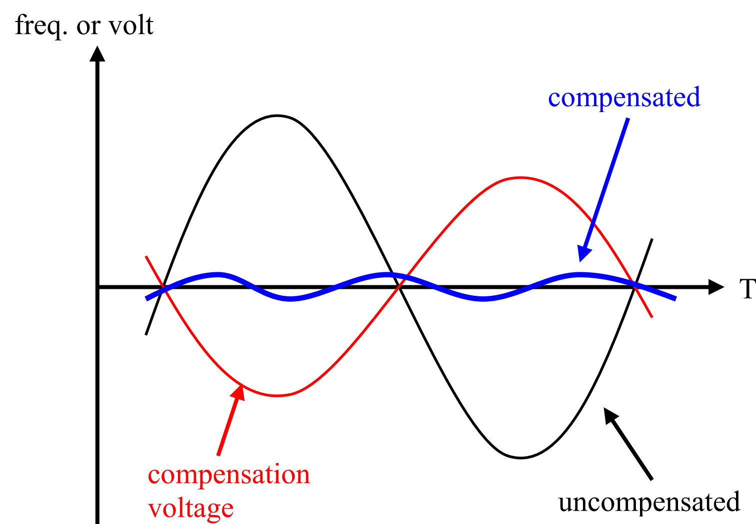

Figure 5-2: f vs. T compensation in TCXO.

There are many techniques to generate the cubic compensation voltage for TCXO applications. One common method is to store the compensation voltages for certain temperature range digitally on an on-chip memory **[46]**. This type of TCXO is called a digital-TCXO (DTCXO). It is easy to trim the compensation voltage values in DTCXOs, and it is suitable for one-chip implementation. However, due to the nature of the digital signals, the compensation

voltages are not continuous, and this causes phase-jumping at the output frequency. This phenomenon makes DTCXOs inappropriate for phase modulation schemes in communications. To resolve these problems, a number of analog TCXO designs were presented. In most of these designs, compensation voltages are generated for lower, middle, and higher temperature ranges separately and summed together to build a cubic-like compensation voltage **[47]**, **[48]**. This is sometimes called a pseudo cubic wave since it only approximates a cubic wave. Thus the compensation voltages here cannot follow **Eq. 1.1**, and adjusting the wave parameters may not be straightforward.

We designed a CMOS true-cubic compensation voltage generator by using analog variable gain amplifiers and a voltage adder **[67]**. The design is a fully analog circuit that does not cause phase-jumping when applied to a crystal oscillator. The output of the proposed circuit can be described by **Eq. 1.1** which exactly matches the quartz resonator's f vs. T characteristic. The design is completely suitable for standard CMOS process and appropriate for compact and low power TCXO applications. Also, the wave parameters of **Eq. 1.1** with higher order terms can be adjusted easily by controlling the output gain of each term in the design.

Variable gain amplifiers (VGAs) [**Figure 5-3**] are used to build the cubic function generator in this design. The circuit is a modification of the design from **[68]**. It is based on a Gilbert cell which is widely used for mixer and modulator applications. The resistors R_1 and R_2 are added to apply common mode feedback to improve the linearity of the circuit. These also make it easy to control the voltage gain.

The input-output relationship of the multiplier can be described with the following equation:

$$V_o^+ - V_o^- = K \cdot (V_1^+ - V_1^-) \cdot (V_2^+ - V_2^-) \quad \textbf{5.1}$$

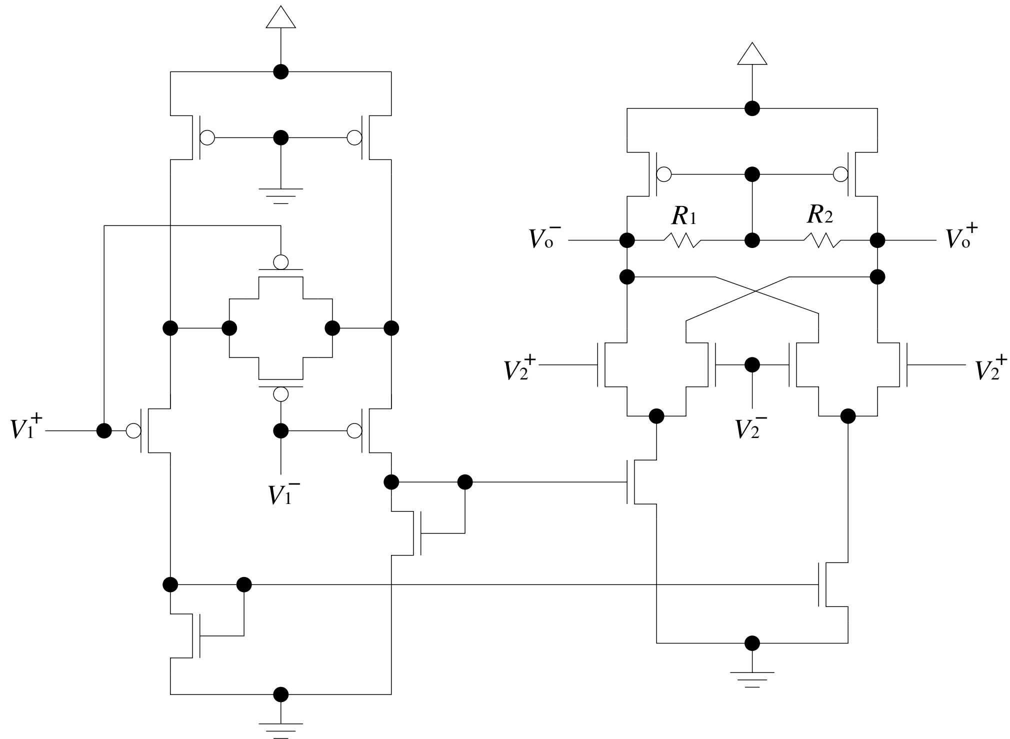

Figure 5-3: Schematic of the variable gain amplifier (VGA).

where V_o^+ and V_o^- are differential voltage outputs, V_1^+, V_1^-, V_2^+, and V_2^- are two pairs of differential voltage inputs, and K is a constant value. This equation clearly shows that the circuit can be used as an analog voltage multiplier with the constant scaling factor K.

The proposed design of the cubic compensation voltage generator is shown in **Figure 5-4**. It is composed of two variable gain amplifiers, two voltage amplifiers, and a voltage adder. The circuit input should be a linear signal which would be an output from a temperature sensor. The voltage adder can be configured as in **Figure 5-5**. It has the input-output relationship as described below:

$$V_{out} = -R_f \cdot (V_1 / R_1 + V_2 / R_2 + \cdots + V_n / R_n) \qquad \textbf{5.2}$$

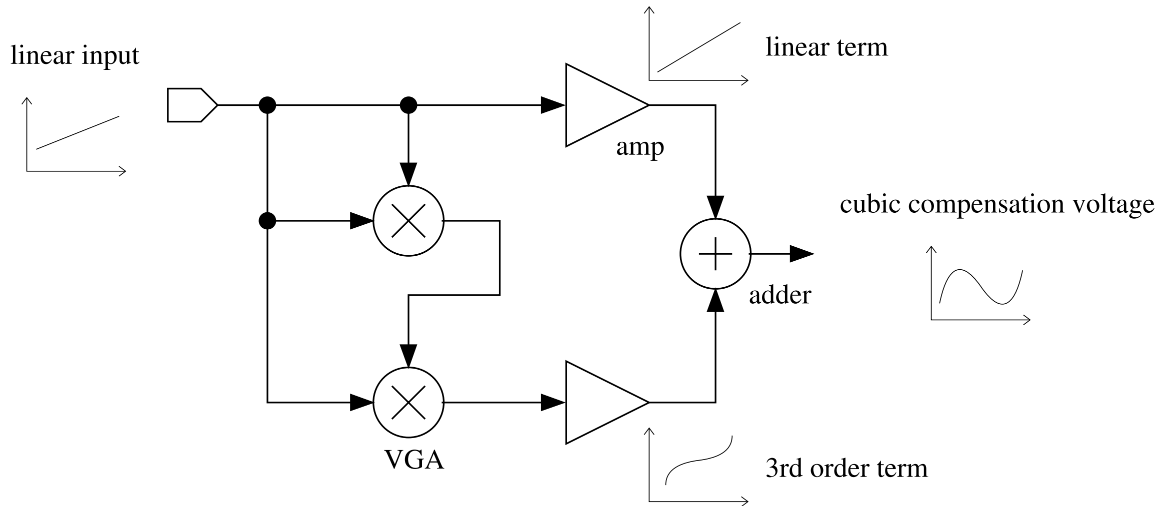

Figure 5-4: Block diagram of the cubic compensation voltage generator.

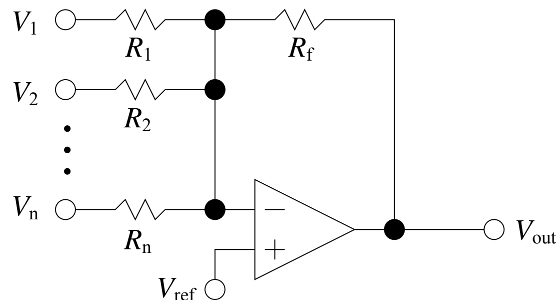

Figure 5-5: Voltage adder configuration using an operational amplifier.

Since the gain for each input to the adder can be controlled by the ratio of the resistors in the adder, the amplifier stage between the voltage multiplier and the voltage adder in **Figure 5-4** can be eliminated.

By combining **Eq. 5.1** and **Eq. 5.2**, the overall relationship between input and output can be derived as:

$$V_{cubic} = -K^2 \frac{R_f}{R_2} \cdot V_{in}^3 - K \frac{R_f}{R_1} \cdot V_{in} \qquad \textbf{5.3}$$

where V_{in} is a linear input and V_{cubic} is a cubic output of the compensation voltage generator. Note that the f vs. T characteristic of the quartz resonator in **Eq. 1.1** and the input-output relationship of the compensation voltage generator in **Eq. 5.3** are identical. Thus, in the ideal case, this design can perfectly compensate for the frequency drift of the quartz resonator against the temperature variation. Adding higher order terms to the output for more accurate modeling of the frequency variation or compensation voltage can be done by simply adding more multipliers in the design.

The design was implemented in TSMC 0.35 μm and Hynix 0.18 μm technology. The layout dimension of the core is 97.3 μm by 111.6 μm [**Figure 5-6**]. The test result of the design in **Figure 5-7** shows the design matches the quartz resonator's f vs. T characteristics at different cut angles.

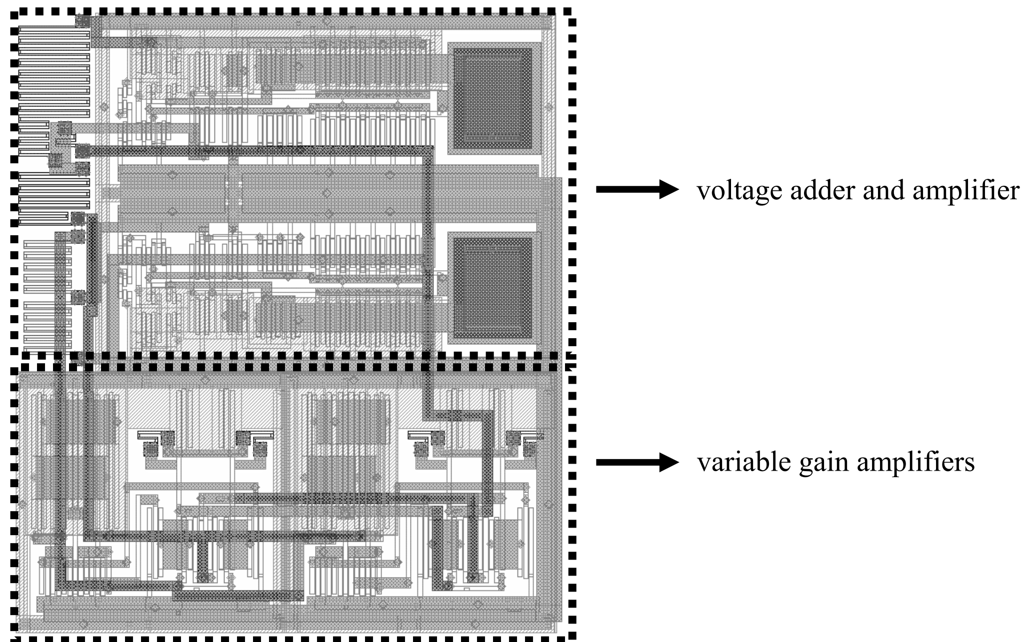

Figure 5-6: Core layout of the cubic compensation voltage generator.

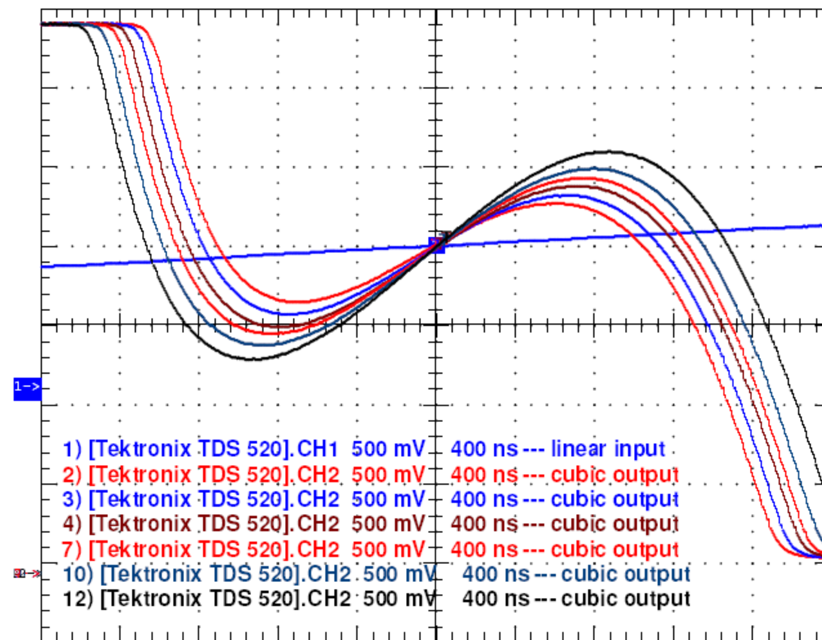

Figure 5-7: Oscilloscope screen of the cubic compensation voltage generator output with different gain parameters.

5.2 Embedded Microprocessor and ADC

Integrating a microprocessor and its peripheral components, such as an analog-to-digital converter (ADC), can improve performance as well as provide additional functionalities to the miniature OCXO. This section describes the design of a simple microprocessor and power-management methods for low power ADC that can be integrated into the miniature OCXO. Expected performance improvements and additional functionalities are described in Chapter 6.

5.2.1 On-chip Microprocessor

Microprocessors constitute one of the most important classes of VLSI chips. Over the last few decades their architecture and capabilities have evolved rapidly so that they now pack enormous computing power. The capabilities of any given system may be enhanced in many ways by a microprocessor. For example, a microprocessor-based measuring device may achieve high accuracy via repetitive measurements and averaging of the results; an automatic calibration, which is a valuable feature, can be performed; sophisticated control of a device can be accomplished more easily in a microprocessor-based system. Moreover, a flexible design with more functionality and reduced system costs is possible.

We have designed a simple dual-port SRAM-based RISC microprocessor for various applications. The simple RISC microprocessor features are an on-chip 128×24 program read only memory (ROM), an on-chip 128×8 data dual-port random access memory (RAM), a full-function 8-bit arithmetic logic unit (ALU), and four 8-bit I/O ports. **Figure 5-8** shows the architecture of the microprocessor, which consists of four main blocks: a programming unit, a control unit, a datapath unit, and an I/O unit.

The program unit maintains and controls the program clock. The program clock is an 8-bit output that determines which number instruction of the program ROM should be fetched and executed. The program clock is reset when the SJP signal is low and the SRE signal is high. It increments when both SJP and SRE are low. To retrieve an entry in the stack (RPC instruction), SJP is set high and SRE low. To jump to a certain instruction address (jump instructions), both SRE and SJP are set high. The ADD2 component adds two to the current instruction before an instruction address is saved to the stack, resulting in the next instruction, not the current instruction, being saved into the stack. This protocol is utilized when calling a subroutine. For the first-generation design, the stack is an 8-bit register that allows one subroutine depth.

The control unit produces the control signals going out to various components depending on the current instruction. Depending on the op-code fetched for the current instruction, the instruction decoder issues the appropriate control signals that allow the components in the system to execute the instruction correctly.

The datapath unit consists of a dual-port RAM and an ALU. The instructions are processed in the datapath unit according to the address data from the ROM and required operations from the ID. The ALU is responsible for computing results from input data. The computation executed by the ALU depends on the instruction op-code. The control signals issued by the control unit reach the ALU, which is then able to produce the correct output. The ALU is capable of arithmetic, logic and shift computations.

The I/O unit is designed to select a proper I/O port among four 8-bit ports. The number of instructions is 21, and there are 5 addressing modes. The target speed is 50 MHz. **Figure 5-9** is the layout screenshot of the microprocessor chip, and **Table 5-1** summarizes the microprocessor instructions. The design is taped out for fabrication in AMI 0.5 μm technology.

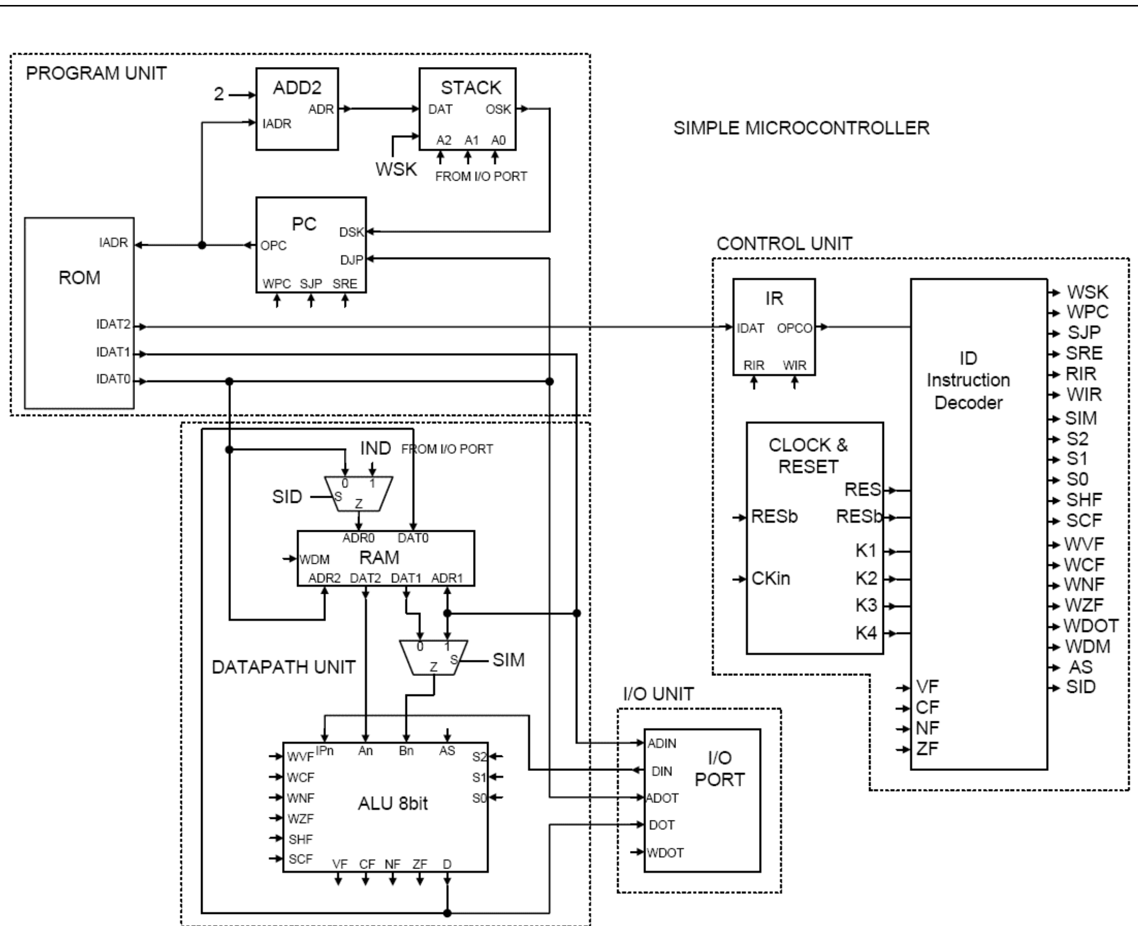

Figure 5-8: Simple microprocessor architecture.

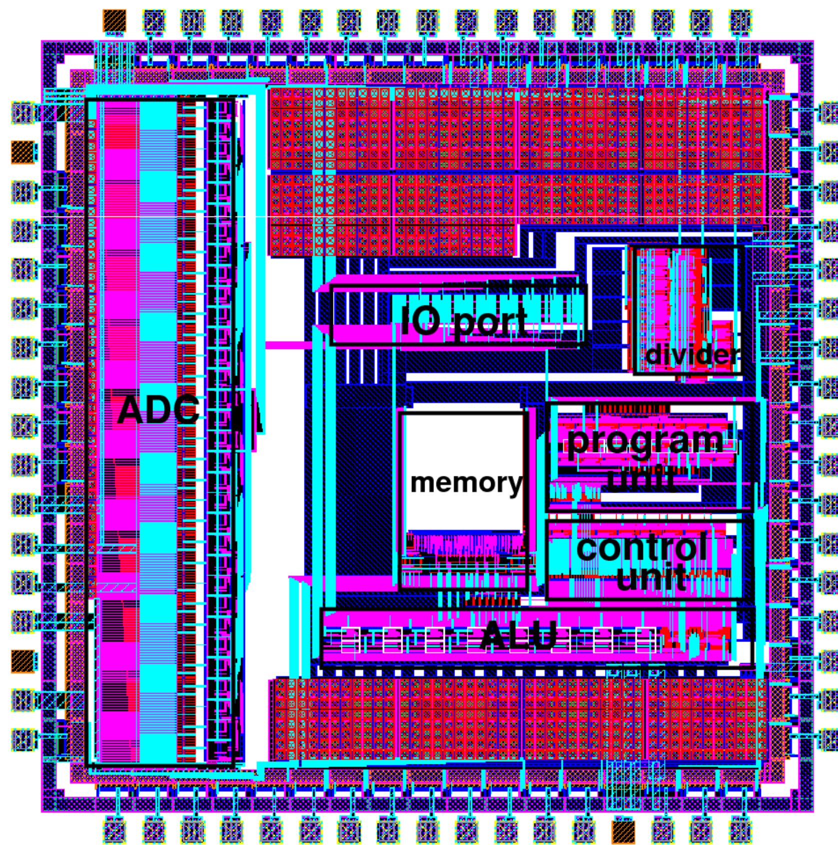

Figure 5-9: Layout of the microprocessor chip.

Table 5-1: Dual-port SRAM Based RISC Microprocessor Instructions.

MV	*Move data from source to destination*
IN	*Move data from Input port to destination*
OUT	*Move data from source to Output port*
SL	*Shift left source data, save to destination*
SR	*Shift right source data, save to destination*
ADD	*Add data from source to destination and save the result in destination*
SUB	*Subtract source from destination and save the result in destination*
AND	*AND data from source to destination and save the result in destination*
OR	*OR source from destination and save the result in destination*
XOR	*XOR data from source to destination and save the result in destination*
JMP	*Jump to destination; ie. move destination address to PC*
JNE	*Jump to destination if not equal; ie. jump if ZF=0*
JEQ	*Jump to destination if equal; ie. jump if ZF=1*
JCC	*Jump to destination if carry is clear; ie. jump if CF=0*
JCS	*Jump to destination if carry is set; ie. jump if CF=1*
JPL	*Jump to destination if minus; ie. jump if NF=0*
JMI	*Jump to destination if plus; ie. jump if NF=1*
JVC	*Jump to destination if overflow clear; ie. jump if VF=0*
JVS	*Jump to destination if overflow set; ie. jump if VF=1*
SPC	*Save PC to stack for later return; ie. PC + 2 => stack*
RPC	*Recall PC from stack to return from subroutine; ie. stack => PC*

5.2.2 Power Management Method for Low-power ADC

Flash architecture ADC is known for its fast data conversion rate. However, a typical flash ADC consumes more power than other architectures, such as pipelined, successive approximation, and sigma-delta ADCs **[51–53]**. It also requires a large silicon area. Moreover, reconfiguring the structure is difficult. These drawbacks are not acceptable for the miniature OCXO targeting for mobile device applications. The threshold inverter quantization (TIQ) technique has been proposed by **[54]** and **[60]** as an effective way to overcome both the speed and power problem. The main advantage of the TIQ comparator is the simplicity of its voltage comparison circuit, which uses CMOS digital inverters as analog voltage comparators. The TIQ-based flash-type A/D converter (TIQ ADC) eliminates the need for reference voltages that require

a resistor ladder circuit. This simplicity in the comparator circuit provides both high speed and lower power consumption.

In addition to the TIQ ADC, we have designed two power management methods in Hynix 0.18 μm CMOS technology. The first, the sampling frequency scaling method, is used to provide the comparators with minimum conversion time regardless of the sampling frequency. Assuming that the maximum conversion speed of the TIQ ADC is significantly faster than the sampling frequency required for its application, the TIQ ADC consumes more power than it really needs. Power consumption can be reduced if the comparators operate during the minimum conversion period and are turned off for the remainder of the period. Power consumption by the inverters in the TIQ comparator can be completely avoided by applying supply voltage or GND to its input. To implement the sampling frequency scaling method, an AND gate and a switch are added to the ADC front end. **Figure 5-10** shows the block diagram of the proposed power management method. The "CLK" input represents the system clock, while the "Sample" input controls sampling intervals. The AND gate ensures that the analog input voltage (V_{in}) is sampled only when both "CLK" and "Sample" are high. When the output of the AND gate is "0", the S/H circuit is disabled, and a switch connects VDD to the input of ADC to force it to "1". Therefore, there is no power consumption at the ADC during this idle period.

The "CLK" input is fixed at or below the highest ADC conversion rate, while the "Sample" signal is variable depending on the desired sampling rate. The highest sampling rate can be achieved when the "Sample" signal is fixed at VDD. Maximum power consumption will occur under this condition. By controlling the sample signal depending on a specific application's requirements, the ADC's power consumption can be reduced significantly.

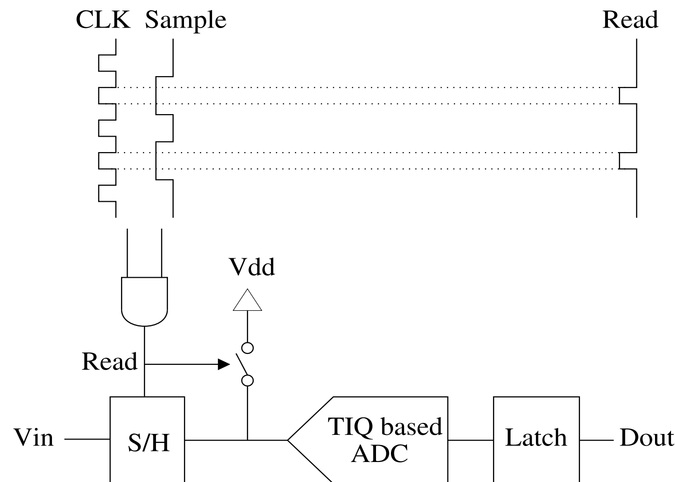

Figure 5-10: Block diagram of the sampling frequency scaling power management method.

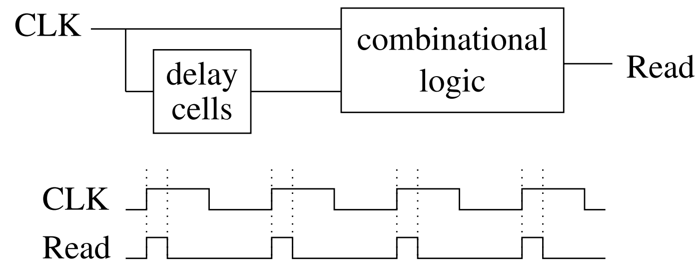

Figure 5-11: Pulse width modulator for the frequency adaptive power management method.

The principle of the second method, known as the frequency adaptive power management method, is similar to that of the previous method. However, in this method, the system clock is adaptive to any frequency up to the ADC maximum conversion speed. To implement the frequency adaptive power management method, the AND gate in **Figure 5-10** is replaced with the pulse width modulator in **Figure 5-11**. The pulse width modulator converts the system clock into the “Read” signal that has the same frequency as the system clock, but with a reduced clock pulse width. Since the data conversion speed of the TIQ ADC is very fast, the “Read” signal doesn’t have to be at “1” for a long period when the system clock frequency is low. Thus, at low

frequencies, the ADC has a long idle period and a short sampling period that together reduce its power consumption.

The pulse width is determined by the maximum ADC conversion rate. The pulse at the "Read" signal needs to stay at "1" only until the ADC completes the data conversion. For example, if the ADC speed is 2 GS/s, the pulse width has to be 500 ps at any frequency. With this method, a single high-speed ADC can be used universally and consume low amounts of power with any system clock.

The layout of the design is shown in **Figure 5-12**. **Figure 5-13** shows test result plots from the power management circuitry. **Figure 5-13(a)** shows that with the sampling frequency scaling method, the clock to the ADC ("Read" signal) can be adjusted depending on its application's requirements. **Figure 5-13(b)** shows that the frequency adaptive power

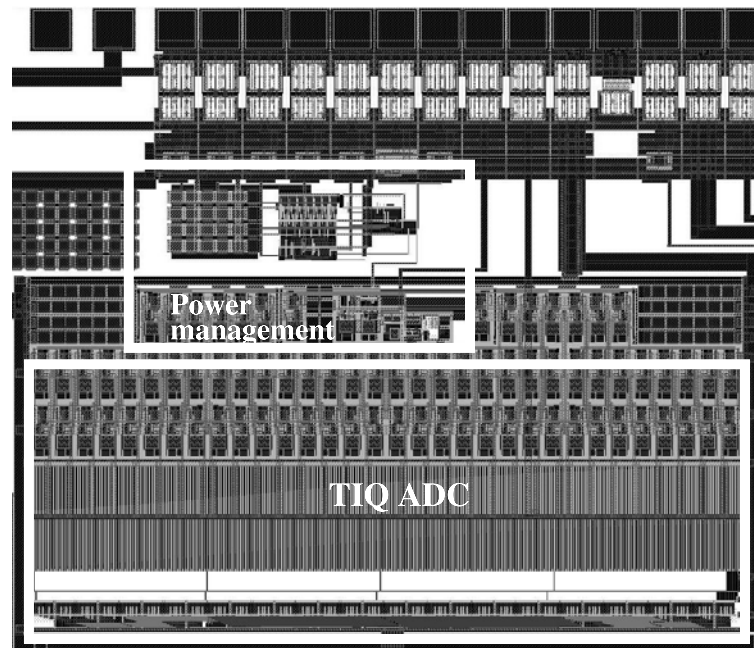

Figure 5-12: Layout of the power management circuitry with TIQ ADC.

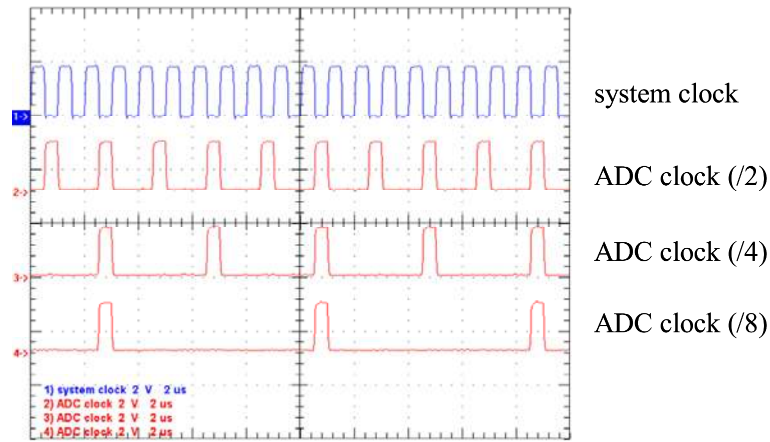

(a) sampling frequency scaling method.

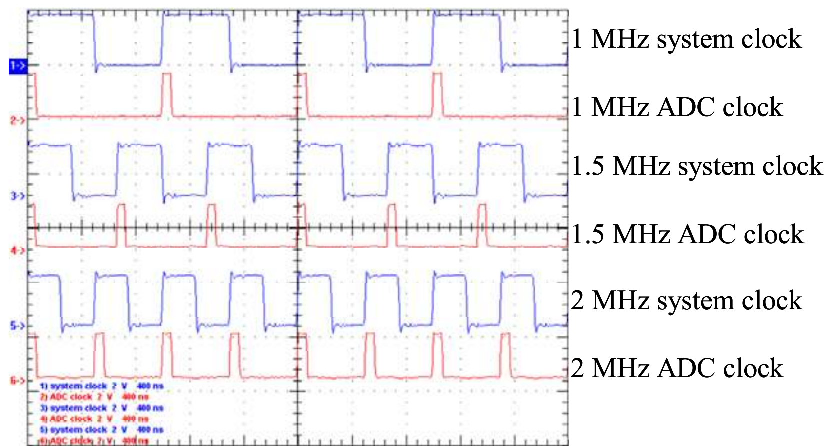

(b) frequency adaptive power management

Figure 5-13: Power management circuitry test results.

management method reduces the pulse width of the ADC clock, while the frequency remains the same. The summarized measurement results are shown in **Table 5-2** and **Table 5-3**. **Table 5-2** shows results from the sampling period scaling method and **Table 5-3** shows results from the frequency adaptive power management method. In the sampling period scaling method, we measured the power consumption at the ADC with different sampling frequencies, while in the

frequency adaptive power management method, the system clock frequency was varied. Both results show that power consumption is significantly reduced when these power management methods are applied. The results clearly illustrate that the proposed methods are effective in reducing the ADC power consumption. Moreover, the design can be used universally at wide system clock ranges with reasonable amount of power consumption for multi-standard applications.

Table 5-2: ADC Power Measurement Results with Sampling Frequency Scaling Method.

Sampling Rate	*Power Consumption*
161.3 MHz	*69.4 mW*
32.3 MHz	*14.2 mW*
6.5 MHz	*3.4 mW*
1.3 MHz	*0.78 mW*
258 kHz	*0.16 mW*
52 kHz	*0.03 mW*

Table 5-3: ADC Power Measurement Results with and without Power Management Method.

System Clock Frequency	*With Frequency Adaptive Power Management*	*Without Power Management*
161.3 MHz	*73.2 mW*	*131.6 mW*
32.3 MHz	*15.7 mW*	*117.6 mW*
6.5 MHz	*3.7 mW*	*108.3 mW*
1.3 MHz	*0.8 mW*	*120.2 mW*
258 kHz	*0.17 mW*	*120.1 mW*
52 kHz	*0.03 mW*	*117.8 mW*

5.3 Size Optimization

Using polyimide flexible circuit boards and applying anisotropic conductive film (ACF) bonding to the miniature OCXO for further size optimization are discussed in this section. This work was mainly conducted by the JERG group.

5.3.1 Polyimide Flexible Circuit Board

A flexible circuit board **[56]** consists of copper conductor layer electroplated on thin polyimide film, and this technology is now used in wide variety of electronics manufacturing. Examples of flexible circuit applications are ink jet printer heads, digital and video cameras, cell phones, and disk drives. Using flexible circuits in these applications have number of advantages. Flexible circuit boards allow reduction in package size and weight since they utilize the thinnest dielectric substrates available. These features are essential in portable electronics where size and weight are important factors. The flexibility also allows this technique to be used widely for interconnection between moving parts such as printer heads and digital cameras. This can be further applied to build a three dimensional structure from two dimensional circuitries as shown in **Figure 5-14** to reduce the package size. Thus, applying the flexible circuit technique to the miniature OCXO can be useful for further size reduction. Also, since polyimide film has high heat resistance, it is safe to generate intensive heat inside the OCXO package.

Furthermore, the flexible circuit can be used as a heater. The heater can be implemented by repeating very narrow and long trace patterns on the flexible circuit board with one end connected to a current driver and the other end to an electrical ground. A miniature OCXO package or a resonator package can be heated with this flexible heater wrapped around itself.

To fabricate flexible circuits, patterns were directly printed on the copper layer of a flexible circuit board from a laser printer or a phaser printer. The toner/ink worked as an etch-resistant layer during the wet-etching process, which removes copper from the exposed area. Ferric chloride or sodium persulfate can be used for the copper etchant. The toner/ink patterns were removed with acetone after the etching process. Then the native copper oxide was removed and a layer of gold was deposited on copper using a electroless displacement gold-plating

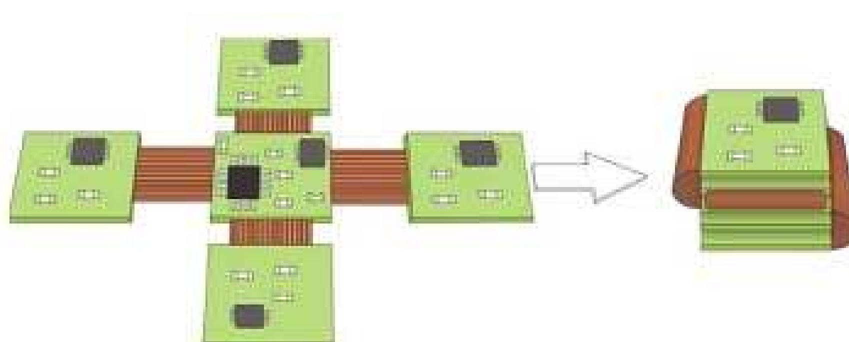

Figure 5-14: Building a 3-D structure from 2-D circuitries using flexible circuit boards **[56]**.

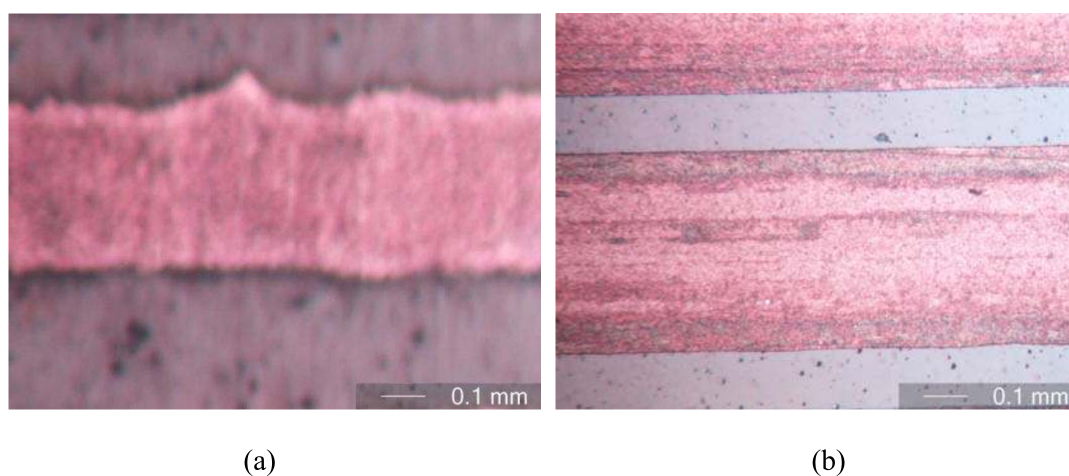

Figure 5-15: Comparison of two test patterns printed with (a) laser printer and (b) phaser printer on polyimide flexible boards.

solution. **Figure 5-15** shows two test boards fabricated by printing the patterns with a laser printer and a phaser printer. It clearly shows that the quality of the pattern is much better when it is printed with a phaser printer. The minimum line width and clearance distance achieved are both 130 μm.

5.3.2 Anisotropic Conductive Film

Anisotropic conductive film (ACF) **[57–59]** is an epoxy system that is used for electrical interconnection between bonding pads on a silicon wafer and electrical traces on a polyimide flex circuit board. In particular, ACF is widely used for high-density interconnection between liquid crystal display (LCD) panels and drive IC in the display industry. It is also used for the bonding of surface mounted devices where the soldering process is restricted. ACF is commonly composed of an adhesive resin and fine conductive fillers such as metallic particles or metal-coated polymer balls. Electrical connection between the interconnection areas is provided by the conductive fillers trapped between them when heat and pressure are applied. The adhesive layer is for electrical insulation, conductive particles protection from mechanical or chemical damage, and stable adhesion. The schematic of the bonding process showing adhesive and conductive particles is shown in **Figure 5-16**. The advantages of using an ACF include high density, fine pitch capability, low-temperature processing, environment friendly materials, and ability to bond to different substrates.

ACF can be applied to the miniature OCXO design to further minimize its size. By directly bonding the temperature controller chip onto the flexible board using ACF, wire bonding between the chip and PCB can be removed. This allows smaller form factor of the miniature OCXO since the wiring distance between mating bonding pads on the chip and the PCB can be minimized. Bonding wires can also act as a heat sink that absorb heat from the on chip heater and

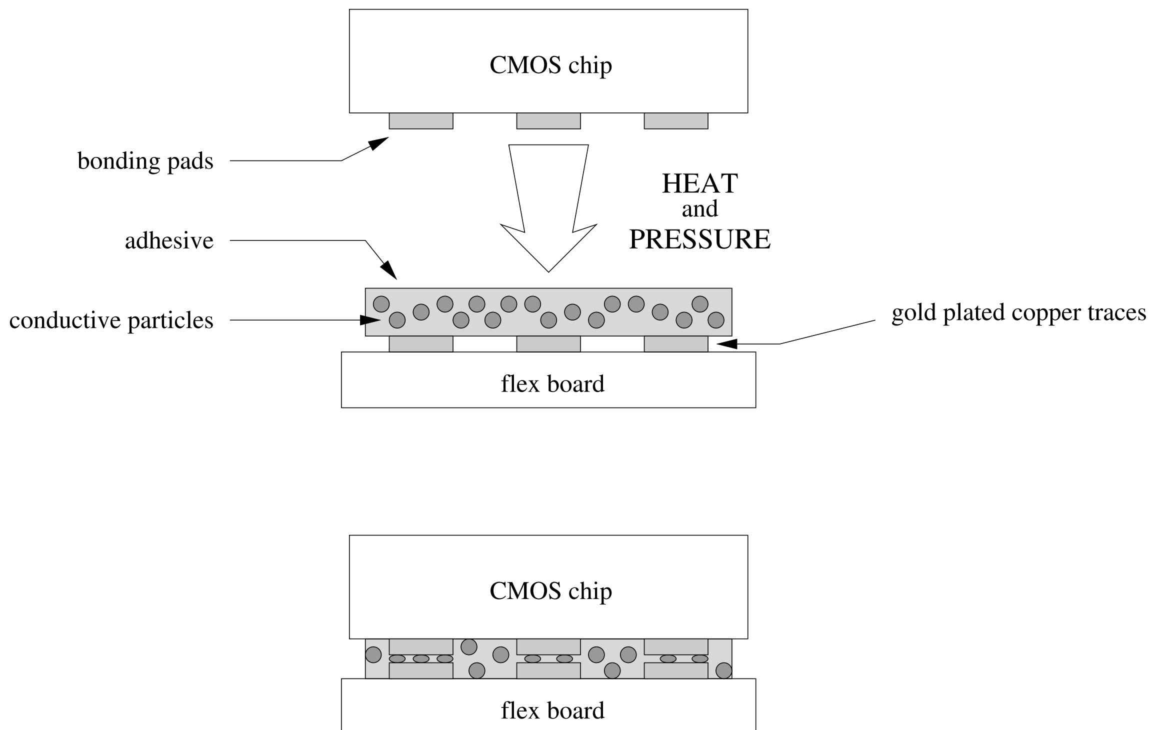

Figure 5-16: Schematic representation of an ACF bonding process.

dissipate into air or PCB. Thus removing bonding wires may lead to better heat efficiency that eventually results in lower power consumption.

Figure 5-17 shows a gold-platted flexible circuit board ACF-bonded on chromium electrodes. Heat of 160 °C and pressure of 190 psi were applied to ACF-bond the flexible circuit and the chromium electrodes together. Upon cooling down, the epoxy was fully cured and pressure was released, with the conductive particles forming a stable contact between the flexible circuit and the electrodes.

When ACF-bonding the flexible circuits and the miniature OCXO, precise alignment is necessary since the size of the bonding pads on the silicon chip are only 100 μm × 100 μm. Moreover, an excessive amount of pressure may damage the silicon chip during the bonding process.

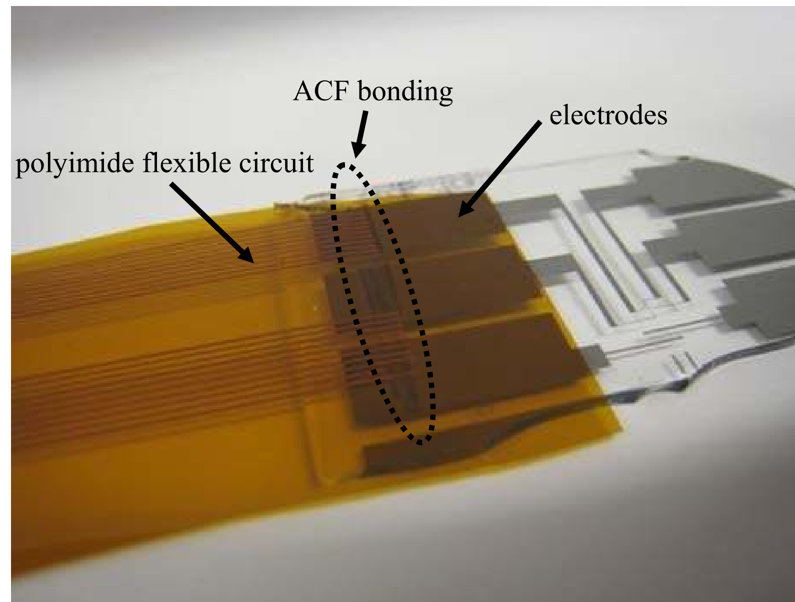

Figure 5-17: Photo of a flexible circuit sample ACF-bonded on chromium electrodes.

The flexible circuit board and the ACF-bonding techniques are not just limited to the miniature OCXO structure with the on-chip resonator. They can be also applied to miniaturizing an OCXO with a typical resonator package. **Figure 5-18** shows how it would look if these techniques were applied to a typical resonator package. The one-chip temperature controller that is ACF-bonded on a flexible circuit can be placed under the quartz resonator as in **Figure 5-18(a)**. Then the flexible heater is wrapped around the resonator package as in **Figure 5-18(b)**. Thus the resonator package itself is an oven that includes all the OCXO components. This structure can be again enclosed inside another package layer for better heat insulation.

(a) (b)

Figure 5-18: Miniaturizing an OCXO with a typical resonator by applying one-chip temperature control, flexible circuit, and ACF-bonding.

Chapter 6

Conclusion

Evaluation of the miniature OCXO performance and discussions about cost and size reduction are presented herein. Comparisons with other commercial OCXO and MEMS products are also presented. In addition, future research plans are also described.

6.1 Summary

A novel design of an ultra-compact and low-power oven controlled crystal oscillator (OCXO) design is presented for use in precision-timing applications. It has all the main components, such as a heater, temperature sensor, oscillator, resonator, and temperature control circuitry, on a single CMOS chip. This reduces the entire package size of an OCXO, as well as reducing power consumption and warm-up time, thus making OCXOs suitable for battery-powered mobile devices. **Table 6-1** is a comparison of our new design and some commercial high-frequency OCXOs. The results show that the performance of the proposed design is better or comparable to that of commercial products.

In addition to improving the performance of OCXOs, the cost of OCXOs can be reduced significantly. The cost of a typical commercial OCXO ranges from $100 to $500 **[60]**. This is mainly due to the use of an SC-cut crystal and its packaging issues. Although an SC-cut crystal has better frequency stability compared to that of an AT-cut crystal, the manufacturing costs of the former are high and it requires sophisticated packaging methods. The AT-cut crystal used in this project does not require separate packaging since it is directly mounted on the CMOS chip, and the crystal mounting process for mass manufacturing can be achieved inexpensively using

pick-and-place equipment. Moreover, all the circuitries used for driving the quartz crystal and controlling the temperature inside the package are implemented in a standard CMOS technology that also reduces the manufacturing costs. Thus, the cost of the proposed miniature OCXO can be projected to be that of a typical TCXO that ranges from $20 to $50 **[60]**. This is a cost reduction of more than a factor of ten.

In terms of the final form factor, since there is no need for separate packaging or PCB for the crystal resonator and temperature control circuitry, the miniature OCXO can be housed inside a small package such as a small outline package (SOP). With the aid of flexible circuit boards and ACF-bonding, the design can be further miniaturized. However, careful design of the heat insulation method will be required, as the smaller mass is more responsive to ambient temperature fluctuations.

To compare the proposed design with MEMS resonators, the frequency stability of two commercial MEMS resonators were measured **[61]**, **[62]**. The resonators were placed inside the temperature chamber, and at the constant temperature, their frequencies were recorded at every 10 seconds. The frequency of both resonators was 100 MHz, and the power supply voltage and chamber set temperature were 3.3 V and 60 °C respectively to meet the same conditions as those of the miniature OCXO. The frequency stabilities of the resonators were measured to be ±0.56 ppm and ±1.85 ppm. It can be clearly seen that the temperature stability of the miniature OCXO is superior compared to that of the commercial MEMS resonators. **Figure 6-1** is a temperature stability measurement plot of the MEMS resonators.

Table 6-1: Comparison Table of the Miniature OCXO and Commercial OCXOs.

Design	Frequency [MHz]	Stability [ppm]	Power [watt] (max/typical)	Warm-up Time [minute] (to 0.01 ppm)
proposed	100	±0.35	1.2 / 0.3	3
[63]	10 ~ 160	±0.25	2.5 / 1.0	2
[64]	40 ~ 80	±0.25	1.56 / NA	5
[65]	50 ~ 160	±0.5	2 / 0.15	0.4 (to 1 ppm)
[66]	~ 120	±0.25	2.5 / 0.7	15

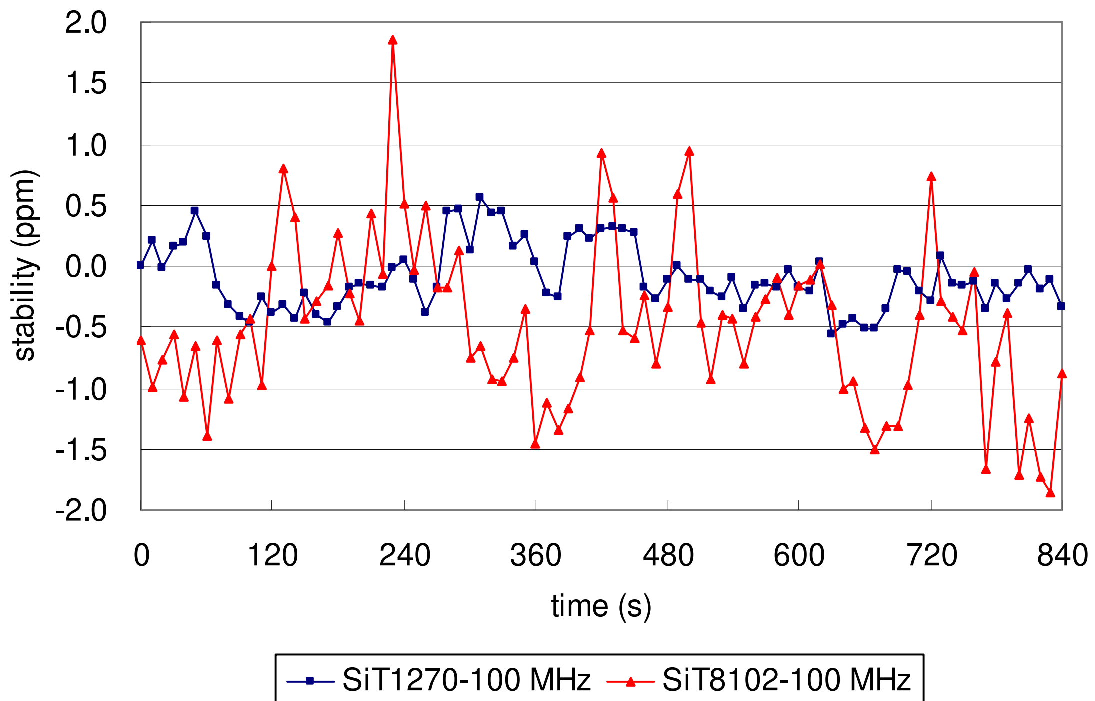

Figure 6-1: Frequency stability measurement plots of 100 MHz MEMS resonators.

From the comparison results, it can be concluded that the proposed miniature OCXO design is an effective method for reducing power consumption, warm-up time, manufacturing cost, and entire package size while maintaining superior frequency stability. Further, a chip-scale oscillator can be achieved using a quartz crystal resonator without MEMS technology that is not as mature as quartz technology. The power consumption at the steady state could be reduced further if the number of bonding wires on the chip is reduced. The bonding wires act as a heat sink on the chip, and many of them could be removed. The copper area on the PCB is also a heat sink; therefore, minimizing the copper area would reduce the amount of heat loss and lead to lower power consumption. Passive components such as the resistors and capacitors are not integrated in the chip at this point. Since the proper values of these components are collected after initial testing, they could be integrated on the chip and further reduce the final size of the package. It should also be noted that a temperature control with tighter controller circuitry may improve the frequency stability.

6.2 Future Work – Smart Clock Generating System

With the aid of an embedded microprocessor and a cubic compensation voltage generator, the miniature OCXO can be advanced to a smart clock generating system. For example, the device can be either a TCXO or an OCXO depending on how the system is configured. The device can even be a hybrid system that takes advantage of both the TCXO and the OCXO. The system can be programmed as a TCXO if power consumption is a more critical issue than frequency stability is for a certain application. On the other hand, if frequency stability is of the most importance, the system can be configured as an OCXO. If an application requires better frequency stability than that affordable by a TCXO, however, without an adequate power margin, the system can be programmed as an OCXO with a lower set temperature while the cubic

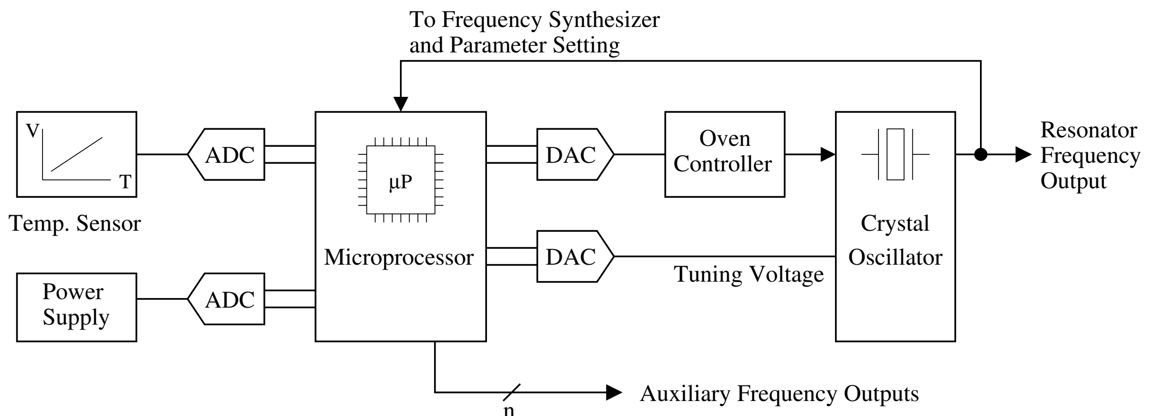

Figure 6-2: Miniature OCXO with an on-chip microprocessor.

frequency compensation technique is still applied.

The performance improvements and additional functionalities expected to accrue from integrating a microprocessor, ADC, and cubic compensation voltage generator are described in the following sections. **Figure 6-2** shows the miniature OCXO with an integrated microprocessor.

6.2.1 Frequency Compensation

A microprocessor can be used to improve both the short-term and long-term frequency stability of the chip-scale OCXO. Instead of using controller circuitry for temperature control, the embedded microprocessor can be used for frequency compensation against the temperature variation **[67]**. If the digitized value of the temperature sensor is monitored, the microprocessor can produce appropriate voltage for the oven controller to compensate for frequency variation caused by ambient temperature fluctuation. In addition, frequency stability can be improved by using the average value of the multiple measurements from the temperature sensor.

A variation in supply voltage also causes an instantaneous frequency fluctuation in the quartz resonator; on the other hand, at a constant temperature, the relationship between resonator frequency and supply voltage is nearly linear **[68]**. For the frequency compensation against the supply voltage variation, correction voltages should be stored in a microprocessor memory. The supply voltage converted into a digital value by the ADC can be used to look up the correction voltage in the memory. Then the analog value of the correction voltage converted by the DAC is sent to the crystal oscillator circuitry to tune the resonator frequency. However, due to the nature of the digital signals, the compensation voltages are not continuous, and this causes phase-jumping at the output frequency. Thus, a filter to smooth the level transition of the compensation voltages will be required in the oven controller.

In addition to the frequency compensation for short-term stability described above, long-term stability can be managed with the aid of a microprocessor. The aging behavior of a quartz oscillator can be modeled as the following equation **[69], [70]** with a few weeks of accumulated frequency data:

$$q(t) = q(t_0) + A \cdot \ln\left(1 + B(t - t_0)\right) \qquad \textbf{6.1}$$

where q is the frequency shift in a resonator due to aging, t is the time, t_0 is the starting time for the aging process, A and B are the material and device dependant constant coefficients respectively. The embedded microprocessor may use this equation to compensate for the resonator frequency caused by the oscillator aging. However, instead of using **Eq. 6.1**, the microprocessor can keep records of the resonator frequencies for a long enough time, for example ten days, to adjust for and control frequency drift; whenever a frequency drift is detected, the microprocessor can periodically tune the oscillator circuit parameter to correct the frequency.

6.2.2 Application and Operation Environment Adaptive System

An OCXO consumes high power because it is required to maintain the temperature inside the package at a high temperature of around 80 °C. However, with the aid of a microprocessor, an OCXO can be a system that adapts to different applications and operating environments, capable of reducing power consumption at the cost of slightly reduced frequency stability. Assuming the required operating temperature range for an OCXO is up to the temperature below area A in **Figure 6-3**, the oven temperature only need be maintained at area A. Thus, a miniature OCXO with an on-chip microprocessor can be reconfigured occasionally according to the system requirement variance. However, since area A's frequency-versus-temperature curve is not as flat as that of area B, the frequency stability in area A would deteriorate. On the contrary, the oven set temperature can be shifted to an even higher temperature for a wider operating range for a harsh environment at a cost of higher power consumption. **Table 6-2** is the table of power consumption comparison at different oven set temperatures. It shows that the total power consumption can be reduced by more than 50% if the oven set temperature can be lowered to 30 °C.

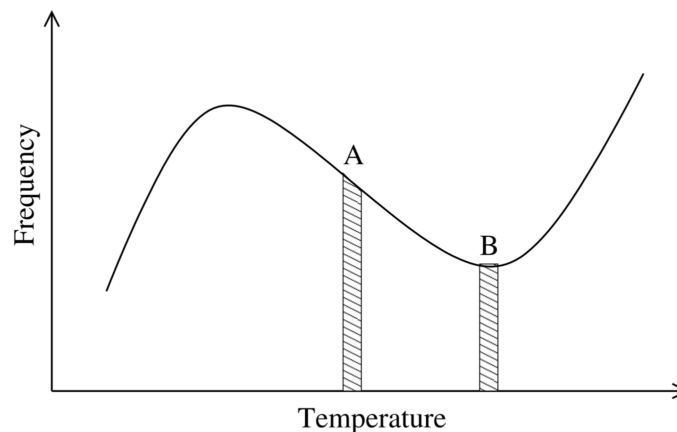

Figure 6-3: Quartz resonator f vs. T plot showing two different set temperature ranges.

Table 6-2: Power Consumption Comparison at Different Miniature OCXO Set Temperatures.

	Oven Set Temperature [°C]	Power Consumption [%]
	30	47.6
	40	63.5
below set temperature ↑	50	82.5
miniature OCXO set point →	60	100
above set temperature ↓	70	120.6
	80	141.3

6.2.3 Additional Functionalities

The embedded microprocessor can provide other useful operations. An automatic parameter setting can be a useful function. The quartz crystal oscillators are all likely to differ from each other slightly in regard to their respective frequency-versus-temperature curve. This is so even though they are cut at the same angle; it is the result of process variation in both resonator manufacturing and chip fabrication, especially at higher frequencies **[71]**, **[72]**. The microprocessor can be an effective tool for automatically performing a temperature sweep to establish the optimal set temperature at which the upper turning point of the quartz crystal is located. This can eliminate the need to manually tune each OCXO after it is fabricated.

Generating auxiliary clock signals, as well as the resonator fundamental frequency can be another example of a useful function. Many electronic systems require multiple clock signals for their operations, such as clock signals with different frequencies, phases, or pulse widths. By programming the microprocessor, it can generate different clock signals based on the resonator frequency by performing frequency division, multiplication, and pulse width modulation. Therefore, the work involved in designing a system that requires multiple frequencies can be reduced, as simply programming the microprocessor can generate the required clock signals.

6.3 Cubic Compensation

We expect that the frequency characteristics of the miniature OCXO can be further improved by applying the cubic frequency compensation voltage to the oscillator. Including a cubic compensation voltage generator inside the oven design may improve the warm-up time of the OCXO. As shown in Chapter 4, it takes about 3 minutes to achieve a stabilized resonator frequency after start-up. Simply using an SC-cut crystal resonator can reduce this time **[3]**, but this is a costly method. If a cubic compensation voltage generator compensates the resonator frequency until the oven temperature reaches the set temperature, the OCXO may produce a stable frequency faster than one without the compensation. In this case, we need a compensation voltage generator circuit that operates up to the set point temperature, which is normally between 60 °C and 80 °C.

Another idea is to compensate the resonator frequency above the set point temperature. As shown in **Figure 4-3**, the resonator frequency cannot be controlled above the oven set temperature as the ambient temperature is higher than the oven temperature. Increasing the maximum current flow through the on-chip heater can increase the operating temperature range. However, this will cause huge power consumption; it is, therefore, not suitable for mobile devices. If the frequency compensation above the set point of the OCXO is applied, the operation temperature range can be increased without large power consumption.

Bibliography

1. D. Salt, *Hy-Q handbook of Quartz Crystal Devices*, Van Nostrand Reinhold, 1987

2. M. E. Frerking, *Crystal Oscillator Design and Temperature Compensation*, New York: Van Nostrand Reinhold, 1978

3. J. A. Lichter, "Crystals and Oscillators," Tutorial, JL9113 Rev. B1, July 1991

4. C. T.-C. Nguyen, "MEMS Technology for Timing and Frequency Control," *IEEE Transactions on Ultrasound, Ferroelectrics, and Frequency Control*, vol. 54, no. 2, February 2007, pp. 251-270

5. W.-T. Hsu and P. Minfan, "The New Heart Beat of Electronics – Silicon MEMS Oscillators," *IEEE Proceedings of Electronic Components and Technology Conference*, 2007, pp. 1895-1899

6. M. Lutz, A. Partridge, P. Gupta, N. Buchan, E. Klaassen, J. McDonald, and K. Peterson, "MEMS Oscillators for High Volume Commercial Applications," *IEEE International Solid-State Sensors, Actuators, and Microsystems Conference*, 2007, pp. 49-52

7. W. C. Brown, "Understanding Ovenized Oscillators," Isotemp Research, Inc

8. J. Supadech, E. Ratanaudomphisut, C. Hruanun, and A. Poyai, "Characteristics of silicon thin film thermistors," *IEEE 5th International Conference on Electrical Engineering/Electronics, Computer, Telecommunication and Information Technology*, 2008, pp. 852-856

9. E. J. P. Santos and I. B. Vasconcelos, "RTD-based Smart Temperature Sensor: Process Development and Circuit Design," *IEEE 26th International Conference on Microelectronics*, 2008, pp. 333-336

10. D. Wobschall and W. S. Poh, "A Smart RTD Temperature Sensor with a Prototype IEEE 1451.2 Internet Interface," *Sensors for Industry Conference*, 2004, pp. 183-186

11. S. R. Chowdhury, C. Pramanik, and H. Saha, "ASIC Design of the Linearization Circuit of a PTC Thermistor," *IEEE International Conference on VLSI Design*, 2005, pp. 866-869

12. T. Nagai and M Itoh, "SiC Thin-Film Thermistors," *IEEE Transactions on Industry Application*, volume 26, issue 6, Nov.-Dec. 1990, pp. 1139-1143

13. L. Luh, J. Choma Jr., J. Draper, and H. Chiueh, "A High-Speed CMOS On-Chip Temperature Sensor," *Proceedings of the 25th European Solid-State circuit Conference*, 1999, pp. 290-293

14. M-C. Weng and J-C. Wu, "A Temperature Sensor in 0.6 µm CMOS Technology," *IEEE Asia Pacific Conference on ASICs*, 1999, pp. 116-119

15. T. Yasuda, "On-chip Temperature Sensor with High Tolerance for Process and Temperature Variation," *IEEE International Symposium on Circuit and Systems*, 2005, pp. 1024-1027

16. K. S. Szajda, C. G. Sodini, and H. F. Bowman, "A Low Noise, High Resolution Silicon Temperature Sensor," *IEEE Journal of Solid-State Circuits*, vol. 31, no. 9, September 1996, pp. 1308-1313

17. M. E. Frerking, "Fifty Years of Progress in Quartz Crystal Frequency Standards," *IEEE International Frequency Control Symposium*, 1996, pp. 33-46

18. J. R. Vig, "Introduction to Quartz Frequency Standards," Army Research Laboratory, October 1992

19. B. Long and G. Weaver, "Quartz Crystal Oscillators with Direct Resonator Heating," in *Proc. IEEE 45th Annual Frequency Control Symposium*, 1991, pp. 384-392

20. I. Abramzon, R. Boroditsky, and D. A. Cocuzzi, "Miniature OCXO Using DHR Technology," in *Proc. IEEE Annual Frequency Control Symposium*, May 1997, pp. 943-946

21. I Abramzon, "OCXO Design Using Composite-Heating of the Crystal Resonator," *IEEE Trans. Ultrasonics, Ferroelectrics, and Frequency Control*, vol. 41, no. 2, March 1994, pp. 284-287

22. K. Eda, T. Ogura, Y. Tomita, and Y. Taguchi, "One-Chip Quartz Crystal Oscillator Using a Direct-Bonding Technique of Quartz Crystal onto Silicon," *IEEE Proceedings of Ultrasonics Symposium,* Vol. 2, pp. 1045-1049, November 1994

23. S. V. Anastasyev, A. A. Volkov, Y. L. Vorokhovsky, and E. L. Kitanin, "New Design of Low Profile Precision OCXO for Time Keeping, Positioning And Telecom Applications," in *Proc. IEEE International Frequency Control Symposium*, 1998, pp. 346-348

24. T. Oita, M. Fukuda, A. Nakamura, T. Ishikawa, and K. Ono, "Dual Mode SC-Cut Crystal Oscillator," *IEEE International Frequency Control Symposium and Exposition*, 2004, pp. 436-442

25 Y. Watanabe, K. Ozake, S. Goka, and H. Sekimoto, "Ultra-Stable OCXO Using Dual-Mode Crystal Oscillator", *IEEE International Frequency Control Symposium and Exhibition*, 2000, pp. 459-462

26 H. Ascarrunz, F. L. Walls, E. S. Ferre-Pikal, D. Tsarapkin, and J. Vig, "Experimental Studies of Noise in a Dual Mode Oscillator," *IEEE International Frequency Control Symposium*, 1999, pp. 1163-1167

27. L. Frederic, W. Patrick, and A. J. Pierre, "A New Kind of View for a Double Oven Crystal Oscillator," in *Proc. IEEE International Frequency Control Symposium*, 2007, pp. 784-789

28. I. Abramzon and R. Boroditsky, "Short-Term Stability of Miniature Double Oven Crystal Oscillators Using Conventional and DHR Technology," in *Proc. IEEE International Frequency Control Symposium*, 2003, pp. 458-463

29. D. V. Bogomolov, "Two Crystals and Frequency Pulling in Precision 100 MHz OCXO," in *Proc. IEEE International Frequency Control Symposium*, June 2006, pp. 221-223

30. *High Frequency Crystal Resonator*, U.S. Patent No. 5,436,523, issued July 25. 1995, SaRonix

31. M. Tuthill, "A Switched-Current, Switched-Capacitor Temperature Sensor in 0.6-µm CMOS," *IEEE Journal of Solid-State Circuits*, vol. 33, no. 7, July, 1998, pp. 1117-1122

32. A. Golda and A. Kos, "Analysis and Design of PTAT Temperature Sensor in Digital CMOS VLSI Circuits," *IEEE Proceedings of the International Conference on Mixed Design of Integrated Circuits and System*, June, 2006, pp. 415-420

33. V. Szekely, C. Marta, Z. Kohari, and M. Rencz, "CMOS Sensors for On-Line Thermal Monitoring of VLSI Circuits," *IEEE Transactions on Very Large Scale Integration Systems*, vol. 5, no. 3, September 1997, pp. 270-276

34. F. Kocer and M. P. Flynn, "An RF-Powered, Wireless CMOS Temperature Sensor," *IEEE Sensors Journal*, vol. 6, no. 3, June 2006, pp. 557-564

35. M. A. P. Pertijs, G. C. M. Meijer, and J. H. Huijsing, "Precision Temperature Measurement Using CMOS Substrate PNP Transistors," *IEEE Sensors Journal*, vol. 4, no. 3, June 2004, pp. 294-300

36. I. M. Filanovsky and S.T. Lim, "Temperature Sensor Applications of Diode-Connected MOS Transistors," IEEE International Symposium on Circuits and Systems, vol. 2, May 2002, pp. 149-152

37. G. C. M. Meijer, G. Wang, and F. Fruett, "Temperature Sensors and Voltage References Implemented on CMOS Technology," IEEE Sensors Journal, vol. 1, no. 3, October 2001, pp. 225-234

38. R. J. Baker, *CMOS Circuit Design, Layout, and Simulation*, 2nd edition, IEEE Press Series on Microelectronic Systems, Wiley-Interscience, 2005

39. I. M. Filanovsky and S.T. Lim, "Interaction of Threshold Voltage and Mobility Temperature Dependencies Applied to Stabilization of Current and Voltage,"

Proceedings of the 43rd IEEE Midwest Symposium on Circuits and Systems, vol. 3, August 2000, pp. 1022-1025

40. *BSIM3v3.2.2 MOSFET Model Users' Manual*, Department of Electrical Engineering and Computer Sciences, University of California, Berkeley, 1999

41. M. Szermer and A. Napieralski, "The PTAT Sensor in CMOS Technology," IEEE International Semiconductor Conference, vol. 1, October 2005, pp. 197-200

42. JEDEC Standard, JEDEC Solid State Technology Association. Available: http://www.jedec.org/catalog/display.cfm

43. H. Kim, J. Lim, K. Choi, T. Jackson, and D. Kenny, "Direct Mounting of Quartz Crystal on a CMOS PLL Chip," in *IEEE International Ultrasonic, Ferroelectrics, and Frequency Control 50th Anniversary Joint Conference*, 2003, pp. 165-168

44. J. Lim, "Integrating Quartz Crystal on Chip for Ultra Compact and High Precision Clock Generation", *M.S. Thesis, the Pennsylvania State University*, December 2003

45. H. Kim, J. Lim, K. Choi, T. N. Jackson, and D. Kenny, "Frame Enclosed Resonator for Miniature Oven Controlled Crystal Oscillator," *IEEE International Frequency Control Symposium and Exposition*, 2006, pp. 491-49

46. R. Achenbach, et al., "A Digitally Temperature-Compensated Crystal Oscillator," *IEEE Journal of Solid State Circuits*, Vol. 35, No. 10, pp. 1502-1506, October 2000

47. K. Nemoto and K. Sato, "A 2.5 ppm Fully Integrated CMOS Analog TCXO," *IEEE International Frequency Control Symposium and PDA Exhibition*, pp. 740-743, June 2001

48. S. Kurogo, Y. Matsumoto, and T. Ohshima, “Analog TCXO Using Cubic Functional Voltage Generator,” *IEEE International Frequency Control Symposium*, pp. 484-492, June 1996

49. J. Lim, I. Kim, D. Kenny, and K. Choi, “A CMOS Cubic Compensation Voltage Generator for a Temperature Compensated Crystal Oscillator (TCXO),” *IEEE International Frequency Control Symposium*, 2008, pp. 550-553

50. C. Wu, C. Liu, and S. Liu, “A 2 GHz CMOS Variable-Gain Amplifier with 50 dB Linear-in-Magnitude Controlled Gain Range for 10GBase-LX4 Ethernet,” *IEEE International Solid-State Circuits Conference*, February 2004, pp. 484-541

51 J. Li, X. Zeng, L. Xie, J. Chen, J. Zhang, and Y. Guo, “A 1.8-V 22-mW 10-Bit 30-MS/s Pipelined CMOS ADC for Low-Power Subsampling Applications,” *IEEE Journal of Solid-State Circuits*, vol. 43, no. 2, February 2008, pp. 321-329

52. M. Wang, C.-I Chen, and S. Radhakrishnan, “Low-power 4-b 2.5-GSPS Piplined Flash Analog-to-Digital Converter in 130-nm CMOS,” *IEEE Transactions on Instrumentation and Measurement*, vol. 56, no. 3, June 2007, pp. 1064-1073

53. N. Verma and A. Chandrakasan, “An Ultra Low Energy 12-Bit Rate-Resolution Scalable SAR ADC for Wireless Sensor Nodes,” *IEEE Journal of Solid-State Circuits*, vol. 42, no. 6, June 2007, pp. 1196-1205

54. J. Yoo, K. Choi, and A. Tangel, “A 1-GSPS CMOS Flash Analog-to-Digital Converter for System-on-Chip Applications”, *IEEE Computer Society Workshop on VLSI*, pp. 135-139, 2001

55. I. Kim, J. Yoo, J. Kim, and K. Choi, "Highly Efficient Comparator Design Automation for TIQ Flash A/D Converter," *IEICE Transactions on Fundamentals of Electronics, Communications, and Computer Sciences*, vol. E91-A, no. 12, December 2008, pp. 3415-3422

56. J. Fjelstad, *Flexible Circuit Technology*, 3rd edition, BR Publishing, Inc., 2006

57. P. Misri and J. H. Constable, "Evaluation of Anisotropic Conductive film for a Flex to Silicon Interconnection," *IEEE Transaction on Components and Packaging Technologies*, vol. 29, no. 4, December 2006, pp. 809-817

58. M.-J. Yim and K.-W. Paik, "The Contact Resistance and Reliability of Anisotropically Conductive Film (ACF)," *IEEE Transactions on Advanced Packaging*, vol. 22, no. 2, May 1999, pp. 166-173

59. J. C. Jagt, "Reliability of Electrically Conductive Adhesive Joints for Surface Mount Applications: A Summary of the State of the Art," *IEEE Transaction on Components, Packaging, and Manufacturing Technology* – Part A, vol. 21, no. 2, June 1998, pp. 215-225

60. http://www.digikey.com (as of July 2009)

61. *SiT1 Fixed Frequency Oscillator Datasheet*, SiTime, Sunnyvale, CA, 2007

62. *SiT8102 High Performance Oscillator Datasheet*, SiTime, Sunnyvale, CA, 2009

63. *C440 Datasheet*, Vectron International, Hudson, NH, 2005

64. *CSOV3S3 Datasheet*, The Connor-Winfield Corp., Aurora, IL, 2004

65. *VFTH Series OCXO Datasheet*, Valpey Fisher Corp., Hopkinton, MA, 2006

66. *210 Series OCXO Datasheet*, MTI Miliren Technologies Inc., Newburyport, MA

67. M. F. Wacker and D. A. Villella, “Improvements in OCXO Performance by the Use of an On-Board Microprocessor,” *IEEE International Frequency Control Symposium*, 2008, pp. 159-164

68. T. Shoji and T. Adachi, “An Algebraic Formulation of Frequency Stability Against Supply Voltage Variation of Quartz Crystal Oscillator,” *Electronics and Communications in Japan* (Part II: Electronics), vol. 83, no. 5, April 2000, pp. 59-69

69. J. R. Vig and T. R. Meeker, “The Aging of Bulk Acoustic Wave Resonators, Filters, and Oscillators,” *IEEE 45th annual Symposium on Frequency Control*, 1991, pp. 77-101

70. R. L. Filler and J. R. Vig, “Long-Term Aging of Oscillators,” *IEEE Transactions on Ultrasonics, Ferroelectrics, and Frequency Control*, vol. 40, no. 4, July 1993, pp. 387-394

71. J. A. Kusters, “Improved Correlation Between Quartz Crystal Manufacturing and Oscillator Requirements,” *IEEE International Frequency Control Symposium and PDA Exhibition*, June 2001, pp. 376-380

72. J. Rabe, S. Buttgenbach, B. Zimmermann, and P. Hauptmann, “Design, Manufacturing, and Characterization of High-Frequency Thickness-Shear Mode Resonators,” *IEEE International Frequency Control Symposium and Exhibition*, June 2000, pp. 106-112

Appendix A

MOSIS Parametric Test Results for AMIS 0.5 µm CMOS Run

MOSIS WAFER ACCEPTANCE TESTS

RUN: T53Q VENDOR: AMIS

TECHNOLOGY: SCN05 FEATURE SIZE: 0.5 microns

INTRODUCTION: This report contains the lot average results obtained by MOSIS from measurements of MOSIS test structures on each wafer of this fabrication lot. SPICE parameters obtained from similar measurements on a selected wafer are also attached.

COMMENTS: American Microsystems, Inc. C5

TRANSISTOR PARAMETERS	W/L	N-CHANNEL	P-CHANNEL	UNITS
MINIMUM	3.0/0.6			
Vth		0.80	-0.92	volts
SHORT	20.0/0.6			
Idss		452	-245	uA/um
Vth		0.69	-0.90	volts
Vpt		10.0	-10.0	volts
WIDE	20.0/0.6			
Ids0		< 2.5	< 2.5	pA/um
LARGE	50/50			
Vth		0.72	-0.94	volts
Vjbkd		11.3	-11.7	volts

Ijlk	<50.0	<50.0	pA
Gamma	0.47	0.59	V^0.5
K' (Uo*Cox/2)	57.4	-18.5	uA/V^2
Low-field Mobility	465.44	150.01	cm^2/V*s

COMMENTS: Poly bias varies with design technology. To account for mask bias use the appropriate value for the parameter XL in your SPICE model card.

Design Technology	XL (um)	XW (um)
SCMOS_SUBM (lambda=0.30)	0.10	0.00
SCMOS (lambda=0.35)	0.00	0.20

FOX TRANSISTORS	GATE	N+ACTIVE	P+ACTIVE	UNITS
Vth	Poly	>15.0	<-15.0	volts

PROCESS PARAMETERS	N+	P+	POLY	PLY2_HR	POLY2	M1	M2	UNITS
Sheet Resistance	82.6	104.0	22.9	1028	41.8	0.10	0.09	ohms/sq
Contact Resistance	65.9	147.8	17.1		28.3		0.82	ohms
Gate Oxide Thickness	140							angstrom

PROCESS PARAMETERS	M3	N\PLY	N_W	UNITS
Sheet Resistance	0.05	839	828	ohms/sq
Contact Resistance	0.77			ohms

COMMENTS: N\POLY is N-well under polysilicon.

CAPACITANCE PARAMETERS	N+	P+	POLY	POLY2	M1	M2	M3	N_W	UNITS
Area (substrate)	428	728	88		32	17	11	39	aF/um^2
Area (N+active)			2460		36	17	12		aF/um^2
Area (P+active)			2356						aF/um^2

Area (poly)				875	54	16	10	aF/um^2
Area (poly2)					50			aF/um^2
Area (metal1)						36	14	aF/um^2
Area (metal2)							35	aF/um^2
Fringe (substrate)	321	259			77	59	41	aF/um
Fringe (poly)					66	40	29	aF/um
Fringe (metal1)						47	35	aF/um
Fringe (metal2)							56	aF/um
Overlap (N+active)			203					aF/um
Overlap (P+active)			257					aF/um

CIRCUIT PARAMETERS			UNITS
Inverters	K		
Vinv	1.0	2.04	volts
Vinv	1.5	2.29	volts
Vol (100 uA)	2.0	0.13	volts
Voh (100 uA)	2.0	4.86	volts
Vinv	2.0	2.47	volts
Gain	2.0	-19.79	
Ring Oscillator Freq.			
DIV256 (31-stg,5.0V)		92.19	MHz
D256_WIDE (31-stg,5.0V)		146.28	MHz
Ring Oscillator Power			
DIV256 (31-stg,5.0V)		0.48	uW/MHz/gate
D256_WIDE (31-stg,5.0V)		1.00	uW/MHz/gate

COMMENTS: SUBMICRON

T53Q SPICE BSIM3 VERSION 3.1 PARAMETERS

SPICE 3f5 Level 8, Star-HSPICE Level 49, UTMOST Level 8

```
* DATE: May 27/05
* LOT: T53Q                  WAF: 9102
* Temperature_parameters=Default
.MODEL CMOSN NMOS (                              LEVEL   = 49
+VERSION = 3.1              TNOM    = 27             TOX     = 1.4E-8
+XJ      = 1.5E-7           NCH     = 1.7E17         VTH0    = 0.6887474
+K1      = 0.7885764        K2      = -0.0715145     K3      = 30.3160775
+K3B     = -8.2734861       W0      = 1E-8           NLX     = 1E-9
+DVT0W   = 0                DVT1W   = 0              DVT2W   = 0
+DVT0    = 2.5182215        DVT1    = 0.3879398      DVT2    = -0.1385624
+U0      = 455.9346722      UA      = 1.010131E-13   UB      = 1.402093E-18
+UC      = 1.232252E-12     VSAT    = 1.583769E5     A0      = 0.5805947
+AGS     = 0.1141616        B0      = 2.69643E-6     B1      = 5E-6
+KETA    = -5.043353E-3     A1      = 2.876689E-4    A2      = 0.3794736
+RDSW    = 1.312263E3       PRWG    = 0.0508579      PRWB    = 0.041551
+WR      = 1                WINT    = 2.051785E-7    LINT    = 7.570428E-8
+XL      = 1E-7             XW      = 0              DWG     = 6.697045E-9
+DWB     = 3.826038E-8      VOFF    = -2.527988E-3   NFACTOR = 1.1541959
+CIT     = 0                CDSC    = 2.4E-4         CDSCD   = 0
+CDSCB   = 0                ETA0    = 2.85331E-3     ETAB    = -1.72447E-4
+DSUB    = 0.0920397        PCLM    = 2.4539683      PDIBLC1 = 0.9546662
+PDIBLC2 = 2.458492E-3      PDIBLCB = -0.0272306     DROUT   = 1.0330608
+PSCBE1  = 6.054456E8       PSCBE2  = 1.093818E-4    PVAG    = 0
+DELTA   = 0.01             RSH     = 82.6           MOBMOD  = 1
+PRT     = 0                UTE     = -1.5           KT1     = -0.11
+KT1L    = 0                KT2     = 0.022          UA1     = 4.31E-9
+UB1     = -7.61E-18        UC1     = -5.6E-11       AT      = 3.3E4
+WL      = 0                WLN     = 1              WW      = 0
+WWN     = 1                WWL     = 0              LL      = 0
+LLN     = 1                LW      = 0              LWN     = 1
+LWL     = 0                CAPMOD  = 2              XPART   = 0.5
+CGDO    = 2.03E-10         CGSO    = 2.03E-10       CGBO    = 1E-9
```

```
+CJ       = 4.264727E-4    PB       = 0.9024585      MJ       = 0.4274059
+CJSW     = 3.015232E-10   PBSW     = 0.8            MJSW     = 0.187618
+CJSWG    = 1.64E-10       PBSWG    = 0.8            MJSWG    = 0.187618
+CF       = 0              PVTH0    = -0.0273516     PRDSW    = 500
+PK2      = -0.0299581     WKETA    = -0.023493      LKETA    = 1.477551E-3     )
*
.MODEL CMOSP PMOS (                                  LEVEL    = 49
+VERSION = 3.1             TNOM     = 27             TOX      = 1.4E-8
+XJ       = 1.5E-7         NCH      = 1.7E17         VTH0     = -0.9259809
+K1       = 0.582786       K2       = 9.220197E-4    K3       = 11.8773186
+K3B      = -0.1110527     W0       = 1E-8           NLX      = 1E-9
+DVT0W    = 0              DVT1W    = 0              DVT2W    = 0
+DVT0     = 1.8284244      DVT1     = 0.4992527      DVT2     = -0.1557392
+U0       = 233.3971369    UA       = 3.511301E-9    UB       = 2.351723E-21
+UC       = -3.71663E-11   VSAT     = 2E5            A0       = 0.6279489
+AGS      = 0.0984829      B0       = 8.646629E-7    B1       = 5E-6
+KETA     = -0.0205689     A1       = 0              A2       = 0.7036371
+RDSW     = 3E3            PRWG     = -0.0472726     PRWB     = -0.0190586
+WR       = 1              WINT     = 2.652564E-7    LINT     = 9.143324E-8
+XL       = 1E-7           XW       = 0              DWG      = -1.608991E-8
+DWB      = 3.064067E-8    VOFF     = -0.0731955     NFACTOR = 0.8953604
+CIT      = 0              CDSC     = 2.4E-4         CDSCD    = 0
+CDSCB    = 0              ETA0     = 7.19185E-4     ETAB     = -2.607733E-3
+DSUB     = 0.013517       PCLM     = 2.4964083      PDIBLC1 = 0.3307859
+PDIBLC2 = 8.161165E-4     PDIBLCB = -0.1           DROUT    = 0.4369184
+PSCBE1   = 5.297294E9     PSCBE2   = 5E-10          PVAG     = 4.6976655
+DELTA    = 0.01           RSH      = 104            MOBMOD   = 1
+PRT      = 0              UTE      = -1.5           KT1      = -0.11
+KT1L     = 0              KT2      = 0.022          UA1      = 4.31E-9
+UB1      = -7.61E-18      UC1      = -5.6E-11       AT       = 3.3E4
+WL       = 0              WLN      = 1              WW       = 0
+WWN      = 1              WWL      = 0              LL       = 0
+LLN      = 1              LW       = 0              LWN      = 1
+LWL      = 0              CAPMOD   = 2              XPART    = 0.5
+CGDO     = 2.57E-10       CGSO     = 2.57E-10       CGBO     = 1E-9
+CJ       = 7.209355E-4    PB       = 0.943403       MJ       = 0.4955242
```

```
+CJSW     = 2.713757E-10   PBSW     = 0.99           MJSW     = 0.2915465
+CJSWG    = 6.4E-11        PBSWG    = 0.99           MJSWG    = 0.2915465
+CF       = 0              PVTH0    = 0.0368158      PRDSW    = 500
+PK2      = 3.434377E-4    WKETA    = 2.503164E-3    LKETA    = 0.0246002      )
*
```

Appendix B

MOSIS Parametric Test Results for TSMC 0.35 μm CMOS Run

MOSIS WAFER ACCEPTANCE TESTS

RUN: T59N (MM_EPI) VENDOR: TSMC

TECHNOLOGY: SCN035 FEATURE SIZE: 0.35 microns

Run type: SKD

INTRODUCTION: This report contains the lot average results obtained by MOSIS from measurements of MOSIS test structures on each wafer of this fabrication lot. SPICE parameters obtained from similar measurements on a selected wafer are also attached.

COMMENTS: TSMC 035

TRANSISTOR PARAMETERS	W/L	N-CHANNEL	P-CHANNEL	UNITS
MINIMUM	0.6/0.4			
Vth		0.55	-0.76	volts
SHORT	20.0/0.4			
Idss		495	-213	uA/um
Vth		0.58	-0.75	volts
Vpt		9.0	-10.0	volts
WIDE	20.0/0.4			
Ids0		< 2.5	< 2.5	pA/um
LARGE	50/50			
Vth		0.52	-0.74	volts

Vjbkd	8.7	-8.4	volts
Ijlk	<50.0	<50.0	pA
Gamma	0.60	0.36	V^0.5
K' (Uo*Cox/2)	92.3	-31.6	uA/V^2
Low-field Mobility	416.99	142.76	cm^2/V*s

COMMENTS: Poly bias varies with design technology. To account for mask bias use the appropriate value for the parameter XL in your SPICE model card.

Design Technology		XL (um)	XW (um)
SCMOS_SUBM	(lambda=0.20)	-0.05	0.15
	thick oxide	-0.10	0.15
SCMOS	(lambda=0.25)	-0.15	0.15
	thick oxide	-0.25	0.15

FOX TRANSISTORS	GATE	N+ACTIVE	P+ACTIVE	UNITS
Vth	Poly	>10.0	<-10.0	volts

PROCESS PARAMETERS	N+	P+	POLY	POLY2	POLY2_ME	M1	M2	UNITS
Sheet Resistance	79.4	157.4	8.4	47.8	47.8	0.07	0.07	ohms/sq
Contact Resistance	69.2		6.9					ohms
Gate Oxide Thickness	78							angstrom

PROCESS PARAMETERS	M3	M4	N_W	N\PLY	UNITS
Sheet Resistance	0.07	0.04	998	1045	ohms/sq
Contact Resistance	2.22	3.42			ohms

COMMENTS: N\POLY is N-well under polysilicon.

CAPACITANCE PARAMETERS	N+	P+	POLY	POLY2	M1	M2	M3	M4	N_W	UNITS
Area (substrate)	895	1401	100		18	9			98	aF/um^2
Area (N+active)			4447			17	12	10		aF/um^2
Area (P+active)			4513							aF/um^2
Area (poly)				909	46	15	9	6		aF/um^2
Area (poly2)					45					aF/um^2
Area (metal1)						39	14	8		aF/um^2
Area (metal2)							36	14		aF/um^2
Area (metal3)								36		aF/um^2
Fringe (substrate)	268	305			35		---	---		aF/um
Fringe (poly)					67	39	29	23		aF/um
Fringe (metal1)						48	34	28		aF/um
Fringe (metal2)								36		aF/um
Fringe (metal3)								58		aF/um
Overlap (N+active)			339							aF/um
Overlap (P+active)			273							aF/um

CIRCUIT PARAMETERS			UNITS
Inverters	K		
Vinv	1.0	1.21	volts
Vinv	1.5	1.34	volts
Vol (100 uA)	2.0	0.21	volts
Voh (100 uA)	2.0	2.88	volts
Vinv	2.0	1.44	volts
Gain	2.0	-18.60	
Ring Oscillator Freq.			
DIV256 (31-stg,3.3V)		171.27	MHz
D256_THK (31-stg,5.0V)		110.17	MHz
Ring Oscillator Power			
DIV256 (31-stg,3.3V)		0.15	uW/MHz/gate
D256_THK (31-stg,5.0V)		0.31	uW/MHz/gate

COMMENTS: SUBMICRON

T59N SPICE BSIM3 VERSION 3.1 PARAMETERS

SPICE 3f5 Level 8, Star-HSPICE Level 49, UTMOST Level 8

```
* DATE: Nov 14/05
* LOT: T59N                  WAF: 4011
* Temperature_parameters=Default
.MODEL CMOSN NMOS (                              LEVEL   = 49
+VERSION = 3.1            TNOM    = 27            TOX     = 7.8E-9
+XJ      = 1E-7           NCH     = 2.2E17        VTH0    = 0.4767602
+K1      = 0.6042685      K2      = 2.656925E-3   K3      = 95.531891
+K3B     = -7.9422223     W0      = 3.00304E-5    NLX     = 2.395007E-7
+DVT0W   = 0              DVT1W   = 0             DVT2W   = 0
+DVT0    = 2.6980828      DVT1    = 0.8741343     DVT2    = -0.3
+U0      = 371.1868341    UA      = -7.11437E-10  UB      = 2.336545E-18
+UC      = 4.188714E-11   VSAT    = 1.430328E5    A0      = 1.1847102
+AGS     = 0.1818798      B0      = 7.96536E-7    B1      = 5E-6
+KETA    = 1.61741E-3     A1      = 0             A2      = 0.4894048
+RDSW    = 1.253871E3     PRWG    = -0.1011577    PRWB    = -0.0796206
+WR      = 1              WINT    = 1.46129E-7    LINT    = 0
+XL      = -5E-8          XW      = 1.5E-7        DWG     = -6.013971E-9
+DWB     = 5.100427E-9    VOFF    = -0.0873021    NFACTOR = 1.4484509
+CIT     = 0              CDSC    = 2.4E-4        CDSCD   = 0
+CDSCB   = 0              ETA0    = 0.8414784     ETAB    = 0.0191725
+DSUB    = 0.789704       PCLM    = 1.5954936     PDIBLC1 = 1.702944E-3
+PDIBLC2 = 6.278521E-4    PDIBLCB = 0.0447528     DROUT   = 0
+PSCBE1  = 7.257077E8     PSCBE2  = 8.256183E-4   PVAG    = 5.267274E-3
+DELTA   = 0.01           RSH     = 79.4          MOBMOD  = 1
+PRT     = 0              UTE     = -1.5          KT1     = -0.11
+KT1L    = 0              KT2     = 0.022         UA1     = 4.31E-9
+UB1     = -7.61E-18      UC1     = -5.6E-11      AT      = 3.3E4
+WL      = 0              WLN     = 1             WW      = 0
+WWN     = 1              WWL     = 0             LL      = 0
+LLN     = 1              LW      = 0             LWN     = 1
+LWL     = 0              CAPMOD  = 2             XPART   = 0.5
+CGDO    = 3.39E-10       CGSO    = 3.39E-10      CGBO    = 1E-12
```

```
+CJ      = 8.934754E-4    PB       = 0.8            MJ       = 0.3537542
+CJSW    = 2.494734E-10   PBSW     = 0.99           MJSW     = 0.1684982
+CJSWG   = 1.82E-10       PBSWG    = 0.99           MJSWG    = 0.1684982
+CF      = 0              PVTH0    = -0.0282376     PRDSW    = -132.9940525
+PK2     = 3.337368E-3    WKETA    = -1.165546E-3   LKETA    = 9.809282E-5     )
*
.MODEL CMOSP PMOS (                                 LEVEL    = 49
+VERSION = 3.1            TNOM     = 27             TOX      = 7.8E-9
+XJ      = 1E-7           NCH      = 8.52E16        VTH0     = -0.6951561
+K1      = 0.4117413      K2       = -5.100951E-3   K3       = 79.8101303
+K3B     = -5             W0       = 6.972381E-6    NLX      = 2.641821E-7
+DVT0W   = 0              DVT1W    = 0              DVT2W    = 0
+DVT0    = 1.3525593      DVT1     = 0.5482948      DVT2     = -3.164227E-4
+U0      = 151.5095134    UA       = 1.426454E-10   UB       = 1.877729E-18
+UC      = -1.62077E-11   VSAT     = 1.17586E5      A0       = 1.1998654
+AGS     = 0.3882402      B0       = 2.792458E-6    B1       = 5E-6
+KETA    = -5.340598E-3   A1       = 8.014984E-5    A2       = 0.3701981
+RDSW    = 4E3            PRWG     = -0.1013569     PRWB     = 0.2184207
+WR      = 1              WINT     = 1.456993E-7    LINT     = 0
+XL      = -5E-8          XW       = 1.5E-7         DWG      = -1.861432E-8
+DWB     = 1.182633E-8    VOFF     = -0.1360309     NFACTOR  = 1.9154977
+CIT     = 0              CDSC     = 2.4E-4         CDSCD    = 0
+CDSCB   = 0              ETA0     = 0.0154526      ETAB     = 0.0450199
+DSUB    = 0.2981307      PCLM     = 2.5713934      PDIBLC1  = 3.026574E-3
+PDIBLC2 = 1.211565E-3    PDIBLCB  = -9.590996E-4   DROUT    = 0.0105271
+PSCBE1  = 7.995031E10    PSCBE2   = 5.016924E-10   PVAG     = 0.029256
+DELTA   = 0.01           RSH      = 157.4          MOBMOD   = 1
+PRT     = 0              UTE      = -1.5           KT1      = -0.11
+KT1L    = 0              KT2      = 0.022          UA1      = 4.31E-9
+UB1     = -7.61E-18      UC1      = -5.6E-11       AT       = 3.3E4
+WL      = 0              WLN      = 1              WW       = 0
+WWN     = 1              WWL      = 0              LL       = 0
+LLN     = 1              LW       = 0              LWN      = 1
+LWL     = 0              CAPMOD   = 2              XPART    = 0.5
+CGDO    = 2.73E-10       CGSO     = 2.73E-10       CGBO     = 1E-12
+CJ      = 1.418474E-3    PB       = 0.99           MJ       = 0.558493
```

```
+CJSW    = 2.804744E-10   PBSW    = 0.99          MJSW    = 0.4048991
+CJSWG   = 4.42E-11       PBSWG   = 0.99          MJSWG   = 0.4048991
+CF      = 0              PVTH0   = 8.635732E-3   PRDSW   = 2.3117328
+PK2     = 2.046602E-3    WKETA   = 9.940692E-4   LKETA   = -0.0100893      )
*
```

Appendix C

MOSIS Parametric Test Results for TSMC 0.18 µm CMOS Run

MOSIS WAFER ACCEPTANCE TESTS

RUN: T77A (MM_NON-EPI) VENDOR: TSMC

TECHNOLOGY: SCN018 FEATURE SIZE: 0.18 microns

Run type: SKD

INTRODUCTION: This report contains the lot average results obtained by MOSIS from measurements of MOSIS test structures on each wafer of this fabrication lot. SPICE parameters obtained from similar measurements on a selected wafer are also attached.

COMMENTS: DSCN6M018_TSMC

TRANSISTOR PARAMETERS	W/L	N-CHANNEL	P-CHANNEL	UNITS
MINIMUM	0.27/0.18			
Vth		0.51	-0.50	volts
SHORT	20.0/0.18			
Idss		565	-259	uA/um
Vth		0.51	-0.50	volts
Vpt		4.8	-5.4	volts
WIDE	20.0/0.18			
Ids0		15.2	-8.9	pA/um
LARGE	50/50			
Vth		0.43	-0.42	volts

Vjbkd	3.2	-4.3	volts
Ijlk	<50.0	<50.0	pA
K' (Uo*Cox/2)	171.6	-35.2	uA/V^2
Low-field Mobility	407.50	83.59	cm^2/V*s

COMMENTS: Poly bias varies with design technology. To account for mask bias use the appropriate value for the parameters XL and XW in your SPICE model card.

Design Technology	XL (um)	XW (um)
SCN6M_DEEP (lambda=0.09)	0.00	-0.01
thick oxide	0.00	-0.01
SCN6M_SUBM (lambda=0.10)	-0.02	0.00
thick oxide	-0.02	0.00

FOX TRANSISTORS	GATE	N+ACTIVE	P+ACTIVE	UNITS
Vth	Poly	>6.6	<-6.6	volts

PROCESS PARAMETERS	N+	P+	POLY	N+BLK	PLY+BLK	M1	M2	UNITS
Sheet Resistance	6.8	7.5	7.9	61.7	331.5	0.08	0.08	ohms/sq
Contact Resistance	10.4	10.8	9.7				5.05	ohms
Gate Oxide Thickness	41							angstrom

PROCESS PARAMETERS	M3	POLY_HRI	M4	M5	M6	N_W	UNITS
Sheet Resistance	0.08	1098.8	0.08	0.07	0.03	950	ohms/sq
Contact Resistance	10.75		15.87	20.15	22.15		ohms

COMMENTS: BLK is silicide block.

CAPACITANCE PARAMETERS	N+	P+	POLY	M1	M2	M3	M4	M5	M6	R_W	D_N_W	M5P	N_W	UNITS

Area (substrate)	938	1187	99	33	14	8	6	5	3		119		119	aF/um^2
Area (N+active)			8364	52	19	13	10	9	8					aF/um^2
Area (P+active)			8093											aF/um^2
Area (poly)				63	17	10	7	5	4					aF/um^2
Area (metal1)					36	14	9	6	5					aF/um^2
Area (metal2)						36	14	9	6					aF/um^2
Area (metal3)							37	15	9					aF/um^2
Area (metal4)								36	14					aF/um^2
Area (metal5)									36			1027		aF/um^2
Area (r well)	925													aF/um^2
Area (d well)										564				aF/um^2
Area (no well)	130													aF/um^2
Fringe (substrate)	197	222		40	35	29	21	14	15					aF/um
Fringe (poly)				63	39	29	23	20	17					aF/um
Fringe (metal1)					54	34		22	19					aF/um
Fringe (metal2)						51	35	27	22					aF/um
Fringe (metal3)							54	34	28					aF/um
Fringe (metal4)								58	35					aF/um
Fringe (metal5)									54					aF/um
Overlap (N+active)			828											aF/um
Overlap (P+active)			779											aF/um

CIRCUIT PARAMETERS			UNITS
Inverters	K		
Vinv	1.0	0.75	volts
Vinv	1.5	0.79	volts
Vol (100 uA)	2.0	0.09	volts
Voh (100 uA)	2.0	1.62	volts
Vinv	2.0	0.83	volts
Gain	2.0	-25.26	
Ring Oscillator Freq.			
D1024_THK (31-stg,3.3V)		292.38	MHz
DIV1024 (31-stg,1.8V)		351.70	MHz
Ring Oscillator Power			

```
  D1024_THK (31-stg,3.3V)            0.07  uW/MHz/gate
  DIV1024 (31-stg,1.8V)              0.02  uW/MHz/gate

COMMENTS: DEEP_SUBMICRON
```

T77A SPICE BSIM3 VERSION 3.1 PARAMETERS

SPICE 3f5 Level 8, Star-HSPICE Level 49, UTMOST Level 8

```
* DATE: Oct  3/07
* LOT: T77A                  WAF: 1003
* Temperature_parameters=Default
.MODEL CMOSN NMOS (                                LEVEL   = 49
+VERSION = 3.1            TNOM    = 27             TOX     = 4.1E-9
+XJ      = 1E-7           NCH     = 2.3549E17      VTH0    = 0.3647749
+K1      = 0.5815814      K2      = 6.025001E-3    K3      = 1E-3
+K3B     = 1.4745568      W0      = 1E-7           NLX     = 1.632187E-7
+DVT0W   = 0              DVT1W   = 0              DVT2W   = 0
+DVT0    = 1.4728771      DVT1    = 0.4373426      DVT2    = 0.0213359
+U0      = 265.6444712    UA      = -1.423009E-9   UB      = 2.335093E-18
+UC      = 5.245012E-11   VSAT    = 9.412881E4     A0      = 1.8428561
+AGS     = 0.4038804      B0      = 5.524599E-7    B1      = 5E-6
+KETA    = -7.935044E-3   A1      = 0.8            A2      = 0.8804594
+RDSW    = 105            PRWG    = 0.4944853      PRWB    = -0.2
+WR      = 1              WINT    = 2.60605E-9     LINT    = 1.939129E-8
+XL      = 0              XW      = -1E-8          DWG     = -2.843075E-9
+DWB     = 2.865387E-9    VOFF    = -0.0894361     NFACTOR = 2.3051876
+CIT     = 0              CDSC    = 2.4E-4         CDSCD   = 0
+CDSCB   = 0              ETA0    = 2.398164E-3    ETAB    = 3.392679E-5
+DSUB    = 8.234246E-3    PCLM    = 0.7444877      PDIBLC1 = 0.185852
+PDIBLC2 = 3.274134E-3    PDIBLCB = -0.1           DROUT   = 0.7550884
+PSCBE1  = 8E10           PSCBE2  = 1.726969E-9    PVAG    = 1.068222E-3
+DELTA   = 0.01           RSH     = 6.8            MOBMOD  = 1
+PRT     = 0              UTE     = -1.5           KT1     = -0.11
+KT1L    = 0              KT2     = 0.022          UA1     = 4.31E-9
+UB1     = -7.61E-18      UC1     = -5.6E-11       AT      = 3.3E4
+WL      = 0              WLN     = 1              WW      = 0
+WWN     = 1              WWL     = 0              LL      = 0
+LLN     = 1              LW      = 0              LWN     = 1
+LWL     = 0              CAPMOD  = 2              XPART   = 0.5
+CGDO    = 8.28E-10       CGSO    = 8.28E-10       CGBO    = 1E-12
```

```
+CJ      = 9.427065E-4    PB      = 0.8            MJ      = 0.3709737
+CJSW    = 1.928292E-10   PBSW    = 0.7            MJSW    = 0.1902367
+CJSWG   = 3.3E-10        PBSWG   = 0.7            MJSWG   = 0.1902367
+CF      = 0              PVTH0   = 3.643308E-5    PRDSW   = -0.8968745
+PK2     = 3.285774E-4    WKETA   = -5.791315E-4   LKETA   = -0.0101627
+PU0     = 10.0548745     PUA     = 1.901573E-11   PUB     = 1.831424E-24
+PVSAT   = 1.433548E3     PETA0   = 5.358064E-5    PKETA   = 1.519426E-3     )
*
.MODEL CMOSP PMOS (                                LEVEL   = 49
+VERSION = 3.1            TNOM    = 27             TOX     = 4.1E-9
+XJ      = 1E-7           NCH     = 4.1589E17      VTH0    = -0.3887191
+K1      = 0.5899188      K2      = 0.0207529      K3      = 0.0996803
+K3B     = 4.9079533      W0      = 1E-6           NLX     = 7.820782E-8
+DVT0W   = 0              DVT1W   = 0              DVT2W   = 0
+DVT0    = 0.5500873      DVT1    = 0.3455653      DVT2    = 0.1
+U0      = 109.7547017    UA      = 1.381876E-9    UB      = 1.115366E-21
+UC      = -1E-10         VSAT    = 1.558387E5     A0      = 1.8416644
+AGS     = 0.404121       B0      = 2.986627E-7    B1      = 5.817037E-7
+KETA    = 0.0173044      A1      = 0.4159329      A2      = 0.4467425
+RDSW    = 224.0543155    PRWG    = 0.5            PRWB    = -0.0577039
+WR      = 1              WINT    = 0              LINT    = 2.948671E-8
+XL      = 0              XW      = -1E-8          DWG     = -2.393677E-8
+DWB     = -9.12926E-10   VOFF    = -0.086012      NFACTOR = 2
+CIT     = 0              CDSC    = 2.4E-4         CDSCD   = 0
+CDSCB   = 0              ETA0    = 0.1514642      ETAB    = -0.0631443
+DSUB    = 1.0119856      PCLM    = 0.6710126      PDIBLC1 = 1.052378E-3
+PDIBLC2 = 0.016329       PDIBLCB = -1E-3          DROUT   = 9.803072E-4
+PSCBE1  = 1.718561E9     PSCBE2  = 5E-10          PVAG    = 14.8638824
+DELTA   = 0.01           RSH     = 7.5            MOBMOD  = 1
+PRT     = 0              UTE     = -1.5           KT1     = -0.11
+KT1L    = 0              KT2     = 0.022          UA1     = 4.31E-9
+UB1     = -7.61E-18      UC1     = -5.6E-11       AT      = 3.3E4
+WL      = 0              WLN     = 1              WW      = 0
+WWN     = 1              WWL     = 0              LL      = 0
+LLN     = 1              LW      = 0              LWN     = 1
+LWL     = 0              CAPMOD  = 2              XPART   = 0.5
```

```
+CGDO    = 7.79E-10       CGSO    = 7.79E-10       CGBO    = 1E-12
+CJ      = 1.17722E-3     PB      = 0.8611654      MJ      = 0.4184273
+CJSW    = 1.924705E-10   PBSW    = 0.9275508      MJSW    = 0.3248627
+CJSWG   = 4.22E-10       PBSWG   = 0.9275508      MJSWG   = 0.3248627
+CF      = 0              PVTH0   = 2.665377E-3    PRDSW   = 9.5152385
+PK2     = 2.387138E-3    WKETA   = 0.0143424      LKETA   = -3.279135E-3
+PU0     = -2.0258474     PUA     = -7.30986E-11   PUB     = 1.973019E-22
+PVSAT   = 50             PETA0   = 1E-4           PKETA   = -5.502283E-4    )
*
```

VITA

Jaehyun Lim

Jaehyun Lim was born in Seoul, Korea, on April 2, 1977. He received a B.S. degree in electrical engineering from Korea University, Seoul, Korea, in February, 2001. He received an M.S. degree in electrical engineering from the Pennsylvania State University in December, 2003, and a Ph.D. degree in computer science and engineering from the Pennsylvania State University in August 2009. His research interests include high-precision frequency control devices and CMOS mixed-signal circuit design.